The Pennsylvania State University

The Graduate School

Chemistry Department

CATALYTIC SYSTEMS USED FOR POLYMERIZATION, BIOMASS CONVERSION, AND ENHANCING DIFFUSION

A Dissertation in

Chemistry

by

Frances Pong

Submitted in Partial Fulfillment
of the Requirements
for the Degree of

Doctor of Philosophy

May 2016

The dissertation of Frances Pong was reviewed and approved* by the following:

Ayusman Sen
Distinguished Professor of Chemistry
Dissertation Adviser
Chair of Committee

Benjamin Lear
Professor of Chemistry

Alexander Radosevich
Professor of Chemistry

T.C. Mike Chung
Professor of Materials Science and Engineering

Ken Feldman
Professor of Chemistry
Graduate Program Chair

*Signatures are on file in the Graduate School.

Abstract

A significant amount of research has been dedicated towards the study and improvement of catalysts. A better understanding of how catalysts work can lead to developing more cost-efficient catalytic systems for a variety of applications. My research is focuses on catalytic systems used in three different fields, which are (i) organometallic polymerization catalysts, (ii) molecular motors and (iii) biomass conversion.

Researchers have long studied and modified organometallic catalysts for use in the direct co- and homopolymerization of monomers with polar functional groups. The ability to add polar moieties to polymers, which can potentially yield materials with a wider range of physical properties, is highly desirable. In this study (i), a series of naphthoxyimine palladium(II) catalysts – in which the naphthyl backbone had been functionalized with different moieties – were synthesized and systematically studied to determine the ligand structure's impact on catalytic activity. The study showed that slight modifications of the naphthyl backbone led to significant changes in the polymer's molecular weight and polydispersity index. The catalysts were also displayed some ability to co-polymerize ethylene and functionalized norbornene. These positive results suggest that further exploration of naphthoxyimine palladium (II) catalysts may be fundamentally interesting.

The effect of active, motile particles at the nanoscale has been vigorously researched during the past decade. By understanding how such active suspensions behave, researchers can gain new insights which can potentially provide new applications in many fields. Here (ii) the momentum transfer of active catalysts (Grubbs' 2nd generation catalyst with a hydrodynamic radius of 6Å) to their immediate surroundings is observed in an organic suspension. This

phenomenon, which has been coined “enhanced diffusion,” has not been well studied at the angström scale until now. Diffusion-NMR spectroscopy surprisingly revealed that these angström sized catalysts nearly double the speed of diffusion of passive molecular tracers in their immediate surroundings. This result is particularly intriguing because in this size regime, the viscosity of the surroundings is expected to completely overcome the inertial forces of these catalysts. This study has prompted further diffusion-NMR studies of molecular catalysts and enzymes as molecular motors.

Catalytic systems play a crucial role in the conversion of renewable biomasses into energy and useful materials. This field of research has become increasingly important and lucrative as fossil fuel sources continue to decline/destabilize in the face of increased worldwide demand for more resources. In this work (iii), the efficacy of a hydrogen-pressurized, biphasic catalytic system to convert linear sugar polyols to iodoalkanes was examined. These iodoalkanes can easily be converted to 1-alkenes which can then be used for the synthesis of low density polyethylene. The results indicated that the system products were relatively pure and that the catalytic layer had a degree of recyclability, hinting that such a system may be viable for industrial use.

TABLE OF CONTENTS

List of Schemes

List of Figures

List of Tables

Preface

The research detailed in this dissertation was carried out between May 2010 to December 2015 under the direction of Professor Ayusman Sen. All projects involved some degree of collaboration; the studies performed on Grubbs catalyst, in particular, involved a number of contributors.

For Chapter 2, which details the synthesis and characterization of organometallic polymerization catalysts, Dr. Sukhendu Mandal ran XRD on the catalysts collected and generated the ORTEP figures/crystallography data.

Chapter 3, which focuses on the Diffusion NMR measurements of active solutions of Grubbs catalyst, is primarily a joint effort between Dr. Krishna Kanti Dey and I, started by Dr. Ryan Pavlick. We collaborated extensively on the analysis of the data collected; Dr. Dey was responsible for collection of the much of the viscosity data. Dr. Jens Breffke performed picosecond laser spectroscopy measurements on our samples in order to obtain local viscosity data. Our NMR staff, Doctors Emmanuel Hatzakis and Carlos Pacheco, helped with interpretation of the NMR data.

Chapters 4 and 5 started as a collaboration with Doctors Ryan Pavlick and Weiran Yang respectively. The work in Chapter 4, organometallic pumps, has become a collaboration between I and my colleague, Scott Biltek.

Acknowledgments

The completion of this thesis would not have been possible without the help, support, and guidance of many teachers, colleagues, friends, and family.

First and foremost, I am incredibly grateful to Professor Ayusman Sen, for his support – both financial and intellectual – during my graduate career. Without the opportunities and guidance he has provided me, I would not be the scientist I am today. I would also like to thank my committee members – Professors Mike T.C. Chung, Alexander Radosevich, Benjamin Lear, and Gong Chen - for their helpful insights regarding my research. Additionally, I thank the NMR Facility– Dr. Emmanuel Hatzakis, Dr. Carlos Pacheco, and Dr. Wenbin Luo - for their consistent support and their willingness to share their expertise with me.

I have had the great privilege of working with many excellent colleagues during my time in the Sen Group, in which we've supported one another through our failures and frustrations and also celebrated one another's successes and accomplishments. In particular - Flory Wong, Dr. Krishna Kanti Dey, Dr. Chandrani Chatterjee, Dr. Weiran Yang, Scott Biltek, Alex Chertok - made the lab for me a wonderful place to work and to learn. I am also grateful for friendships and great science discussions I have had with many of my fellow chemists in the department, namely Jennifer Tan, Dr. Jenny Axe, Dr. Jens Breffke, and my significant other, Dr. Matthew Bradley.

Last, but not least, I am indebted to my family, who have always encouraged and stood by me during the many challenges I have faced during my graduate career.

Chapter 1. Thesis Overview

As a result, a generous portion of both academic and industrial research is dedicated towards the discovery and engineering of more efficient and robust catalysts for thousands of commercial applications, such as the production of platform chemicals and new types of polymers. Robust and effective catalysts can significantly increase reaction efficiency, thereby minimizing waste production and enabling better production cost efficiency, particularly in industrial scale processes.[1–3] In my dissertation, I will focus primarily on catalysts used for polymerization and for enhancing the diffusion of a system via catalytic turnover, and will briefly cover research I have performed for biomass conversion.

In Chapter 2, I discuss the synthesis and characterization of palladium (II) catalysts. These late transition catalysts have some ability to withstand the polar functional groups the metal center is exposed to during polymerization reactions. Catalyst characterization includes both XRD and NMR solution studies. The study explores the ability of these catalysts to co- and homopolymerize ethene and functionalized norbornene and the changes in the ligand structure of the catalyst are correlated with subsequent effects on the resultant polymer. Additional information for this chapter is included in Appendix A.

The following two chapters focus on how active catalysts can enhance diffusion at the small scale. I examine the effects of active Grubbs catalyst on the diffusion of their immediate surroundings first as a molecular motor and secondly as a pump. Chapter 3 focuses on the catalyst in solution where it acts as a molecular motor. Soluble molecular passive tracers, which have been added to the solution, can be monitored via diffusion NMR to observe the transfer of the catalysts' momentum and energy to their immediate surroundings. In chapter 4, the catalyst is affixed to a bead, thereby becoming a pump which can move relatively large amounts of

surrounding fluid when exposed to a reactant. The activity of these catalytic pumps can be visually detected using a microscope by following the movement of glass tracer beads. Additional information for Chapter 3 is included in Appendix B.

In Chapter 5, I discuss the use of a biphasic catalytic system to convert sugar alcohols to useful platform chemical precursors. By using this biphasic liquid catalytic system, which couples hydriodic acid with a metal catalyst, the polyols can be converted into iodoalkanes in relatively high purity and yield. Additionally, by using a metal catalyst, it is possible to regenerate the hydriodic acid consumed in the reaction thereby prolonging the lifetime of the catalytic acidic layer.

1.1 References

(1) Chatterjee, C.; Pong, F.; Sen, A. Chemical Conversion Pathways for Carbohydrates. *Green Chem.* **2015**, *17*, 40–71.

(2) Tanabe, K.; Hölderich, W. F. Industrial Application of Solid Acid–base Catalysts. *Appl. Catal. Gen.* **1999**, *181*, 399–434.

(3) Flaris, V.; Singh, G. Recent Developments in Biopolymers. *J. Vinyl Addit. Technol.* **2009**, 15, 1–11.

Chapter 2. Steric and Electronic Effects in Ethene/Norbornene Copolymerization by Neutral Salicylaldiminato-Ligated Palladium (II) Catalysts

2.1. Introduction

Polymers, which have a wide range of chemical and structural properties, are used for a diverse array of applications. One of long-standing challenges in this field is the incorporation of functional groups containing polar moieties into polymers. Such polymers are desirable because the added functionality imparts useful qualities to the polymer (e.g. adhesive ability, ease of further functionalization). The polar moieties of the monomers, however, often poison the catalyst and stop the reaction, thereby preventing the polymers from reaching useful molecular weight and polydispersity index.

Late transition metal catalysts have been researched extensively for both homo- and co-polymerization of polar monomers.[1–4] Several groups of ligands have been studied, some of the most popular being diimine and phosphine-sulfonate ligands.[5–7] In order to make catalysts that are more robust in the presence of polar functional groups, researchers have used a combination of late transition metal catalysts such as nickel, palladium and cobalt and specially synthesized ligands to ensure sustained activity in the presence of polar functional groups.

Phenoxyimine (FI)/salicylaldiminato ligands are another family of ligands that are particularly useful in homo- and copolymerization of polar monomers.[8–10] Although phenoxyimine catalysts were studied as early as the 1960's – FI ligands were largely ignored until Grubbs' 1999 publication.[11,12] Grubbs et al. synthesized a FI-nickel catalyst which, notably and impressively, was not only capable of incorporating high amounts of functionalized norbornene derivatives into the polyethene chain, but was also able to maintain the polymer's

high molecular weight (MW) and low polydispersity index (PDI).[13, i] Another advantage of FI ligands is that they can be synthesized in a simple, one-step Schiff base condensation reaction. A wide variety of both salicylaldehyde and aniline derivatives are available commercially, thereby facilitating the synthesis of different FI ligands. The straightforward synthesis of the FI ligands allows researchers to study the effect of different functional groups on catalyst behavior (Scheme 2-1).[14–22] Unsurprisingly, FI-ligands have garnered much more attention in the past decade. Researchers have recently focused attention on naphthoxyimine ligands – a small subset of FI ligands that have the rigid naphthalene backbone (Figure 2-1).[18,23]

Modifications of the functional group on the C8 of the naphthalene backbone significantly influence the polymerization behavior of the catalyst. Thus far, several studies of the naphthoxyimine ligand have been conducted with nickel, with intriguing results. In one example, Song et al. placed bulky groups such as R = norbornyl, phenyl, at the C8 of the naphthalene backbone, which resulted in greater yields of higher molecular weight polyethene than observed for catalysts with less sterically hindering groups (Figure 2-2).[18] In our study, we decided to study the effects of naphthoxyimine ligands, with different C8 functional groups, on the polymerization activity of the Pd(II) center. Our group has studied Pd(II) catalysts extensively because of their ability to tolerate polar functional groups in monomers.[4,23–28] The primary advantage that palladium catalysts offer over their nickel counterparts are increased air/water stability, thereby making them more robust and considerably easier to handle.[29]

While FI-ligated nickel catalysts have been studied broadly, their palladium analogs have remained relatively unexplored.[9] Chen et al. synthesized a Pd(II) catalyst ligated with an asymmetric naphthoxyimine ligand (Scheme 2-2, Catalyst **B**, R = -OH) which was capable of

[i] DFT studies, conducted in 2000, by Michalak and Zeigler, have shown that phenoxyimine group 10 catalysts are particularly well-suited for direct copolymerization of polar norbornene derivatives and ethene because the π-coordination to the metal center is more stable and favored over the σ-coordination of the polar monomer.

incorporating significant amounts of norbornene/5-*n*-butyl-2-norbornene (up to 50%) and polar-functionalized norbornene (32–34%) into an ethene copolymer without the aid of a co-catalyst.[23] In this study, the effects of different functional groups on the C8 of the naphthoxyimine ligand was further investigated by synthesizing two additional catalysts in which the hydroxyl group on the naphthol 8-carbon was replaced with a hydrogen (Catalyst **A**) or a methoxy group (Catalyst **C**).

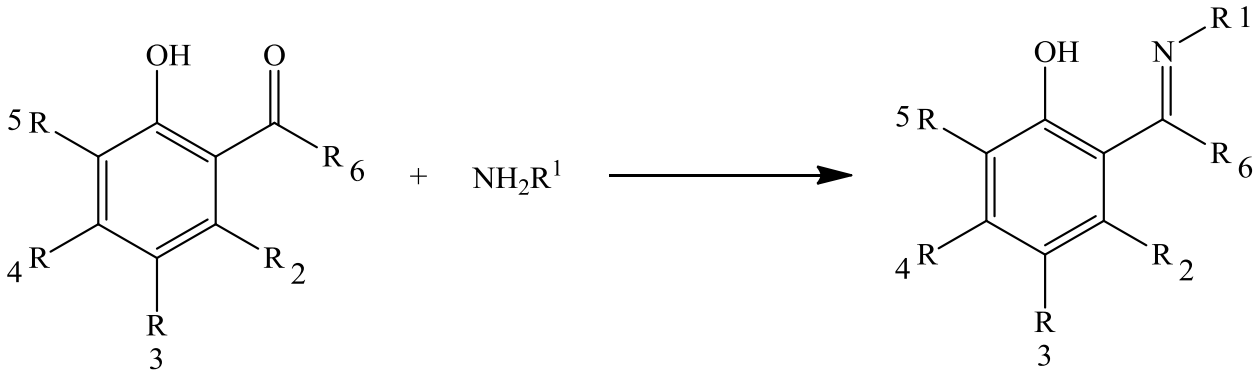

Scheme 2-1. General synthesis of FI ligands.

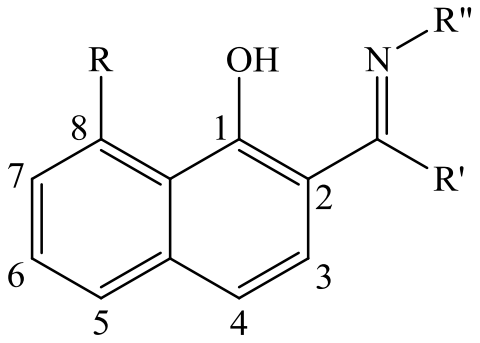

Figure 2-1. Naphthoxyimine ligand.

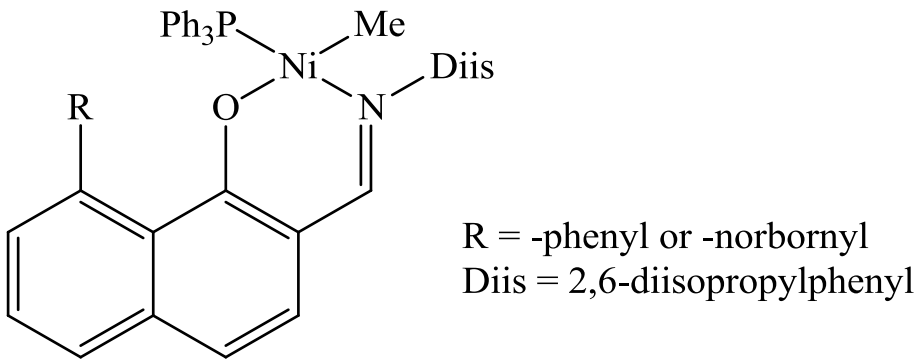

Figure 2-2. Song's asymmetric nickel catalysts ligated with naphthoxyimine ligands.[18]

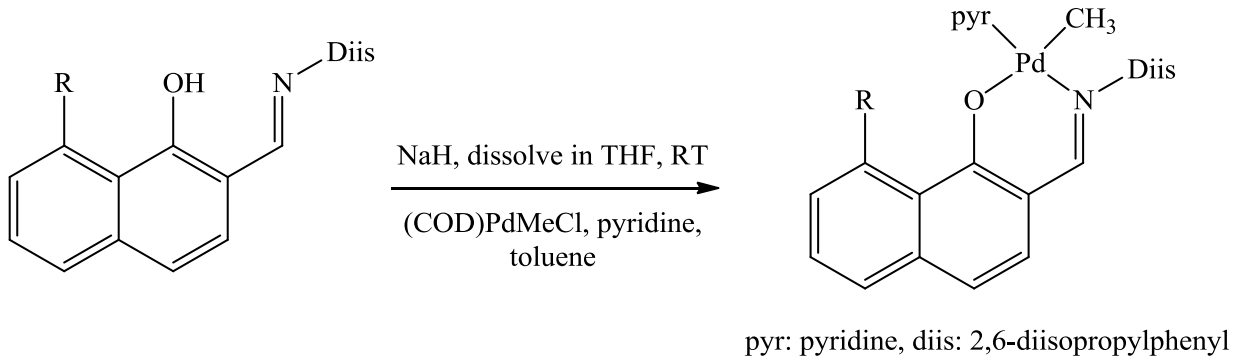

pyr: pyridine, diis: 2,6-diisopropylphenyl

Ligand A: R = H
Ligand B: R = OH
Ligand C: R = OCH_3

Catalyst A: R = H
Catalyst B: R = OH
Catalyst C: R = OCH_3

Scheme 2-2. Using Ligands 1-3 to synthesize Catalysts A-C.

2.2. Results and Discussion

For context, Catalyst **A**, where R = H, was considered to be the "control" catalyst where there was no functionality on the 8-carbon. Catalyst **B**, with R = OH, exhibited hydrogen bonding between the two phenolic oxygens. Electronically, Catalyst **C** (R = OCH_3) is similar to Catalyst **B**; however, there is no hydrogen bonding in Catalyst **C**. X-ray crystallography reveals that the functionality on the 8-carbon has a significant effect on the crystal structure, and this has a large effect on the polymerization activity of the respective catalysts. The data for Catalyst **B** has been taken from Chen's previous study.[23]

2.2.1. ORTEP Plots

Crystals of **A** and **C**, suitable for X-ray crystallography, were grown from slowly evaporating toluene. Selected bond angles and lengths for Catalysts **A**, **B**, and **C** are listed in Table 2-1 and the ORTEP plots are shown in Figures 2-4 to 2-5. As expected for Pd(II) complexes, **A**, **B**, and **C** are square planar and diamagnetic.[30] The pyridine and imine nitrogen are coordinated to the metal center in a trans arrangement. Catalyst **B** has the longest Pd-C(Me) bond (2.030Å) thereby facilitating alkene insertion. All three catalysts have similar Pd(1)-N(2) bond lengths, although the bond length of Catalyst **A** appears to be slightly lengthened to 2.049 Å. Data for Catalyst **B** and Ligand **2** (Figure 3) are taken from Chen et al.[23]

The possible H-bonding interactions are marked in Figures 2-4 and 2-6 for Catalyst **B** and Ligand **2**, respectively, by dotted lines. The relevant bond lengths and bond angles for hydrogen bonding in case of Catalyst **B** and Ligand **2** are presented in Table 2-2. In Catalyst **B**, the close proximity of the O(1) and OH group on C(8) may be responsible for possible intramolecular

hydrogen-bonding (Figure 2-4).[31, ii] According to Rozas et al., a distance between H(2) and O(1) shorter than 2.09 Å and an angle for ∠O(2)–H(2)•••O(1) between 120°–180° is sufficient for the formation of a hydrogen bond between both oxygen atoms.[32, iii] Bond lengths and bond angles for both Catalyst **B** and its corresponding ligand, Ligand **2**, show that both compounds fulfill the given intramolecular hydrogen bonding structural requirements; the distance between O(2)H(2)•••O(1) is 1.773 Å and the bond angle of ∠O(2)–H(2)•••O(1) is 148° (Figure 2-4, Table 2-2). The hydrogen bond elongates the Pd(1)–O(1) and O(1)–C(2) bonds and further distorts the highly puckered chelate ring. **A** and **C** have bond lengths of ~1.28 Å for O(1)–C(2) and ~2.08Å for Pd(1)–O(1), while the corresponding bond lengths in **B** are elongated to ~1.32 Å and ~2.11 Å. In an earlier work, Delferro et al. also observed that intramolecular hydrogen bonding of the benzylic alcohol to the metal center also the a lengthened the metal-oxygen bond from 1.900 Å to 1.925 Å (Figure 2-7, Catalysts **D** and **E**).[33]

[ii] 1,8-naphthalenediols are well known for their intramolecular-hydrogen bonding (IMHB) abilities. The IMHB qualities of naphthanediols have been studied in detail, particularly their ability to stabilize internal radicals, by Foti et al.

[iii] Results from Delferro et al.'s study indicate that this H-bonding effect leads to increased electrophilicity at the nickel center, and results in a 2.5x increase in the yield of polyethylene.

Table 2-1. **Bonds and angles of interest in Catalysts A, B, and C.** [a] Ref 23.

Bonds of Interest	**Catalyst A (Å)**	**[a] Catalyst B (Å)**	**Catalyst C (Å)**
Pd(1)-O(1)	2.0851(1)	2.108	2.0820(2)
Pd(1)-C(1)	2.019(2)	2.030(6)	2.017(3)
Pd(1)-N(2)	2.0493(2)	2.040(5)	2.040(2)
Pd(1)-N(1)	2.0230(2)	2.018(5)	2.012(2)
O(1)-C(2)	1.280	1.318	1.276

Angles of interest	**Catalyst A (Å)**	**[a] Catalyst B (Å)**	**Catalyst C (Å)**
N(1)-Pd(1)-O(1)	91.30(6)	90.73	90.75(9)
N(2)-Pd(1)-O(1)	85.95(6)	86.75	88.05(8)
C(1)-Pd(1)-N(2)	89.31(8)	90.1	88.66(12)
C(1)-Pd(1)-N(1)	93.66(8)	92.7	93.04(12)
C(1)-Pd(1)-O(1)	174.69(8)	176.1	173.98(12)
N(1)-Pd(1)-N(2)	173.29(7)	173.7	174.01(9)
C(12)-N(1)-Pd(1)	122.66(1)	122.8	122.8(2)
C(2)-O(1)-Pd(1)	126.71(13)	127.1	128.79(18)

Table 2-2. Selected bond lengths and angles from Catalyst B and Ligand 2.

Bonds of Interest	Catalyst B (Å)	Ligand 2 (Å)
O(2)-H(2)	0.82	0.819
O(1)…H(2)	1.773	1.782

Angles of Interest	Catalyst B (°)	Ligand 2 (°)
C(8)-O(2)-H(2)	109.4	109.5
O(1)-H(2)-O(2)	148.2	148.7

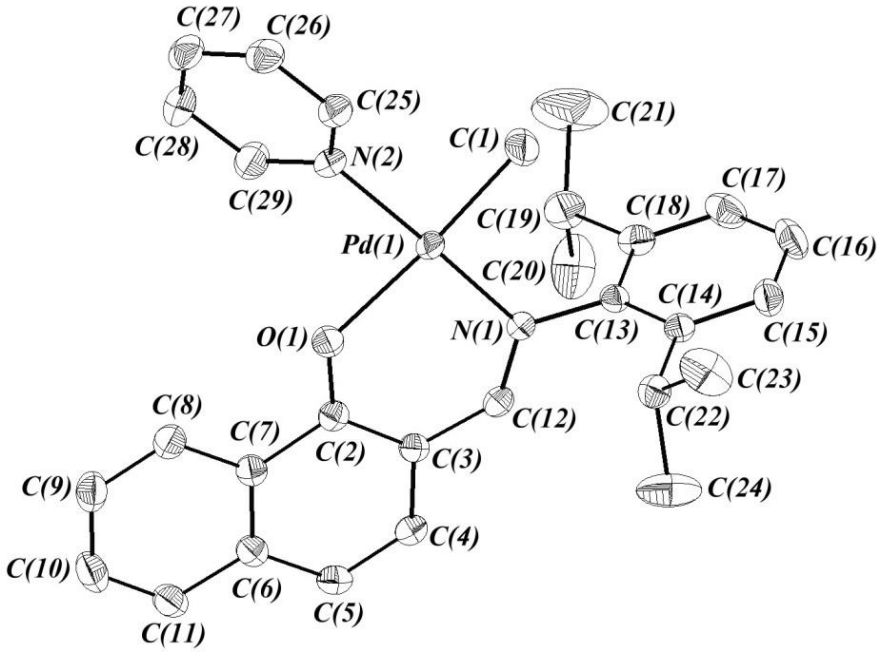

Figure 2-3. **ORTEP plot of Catalyst A.** Hydrogen atoms have been omitted for clarity.

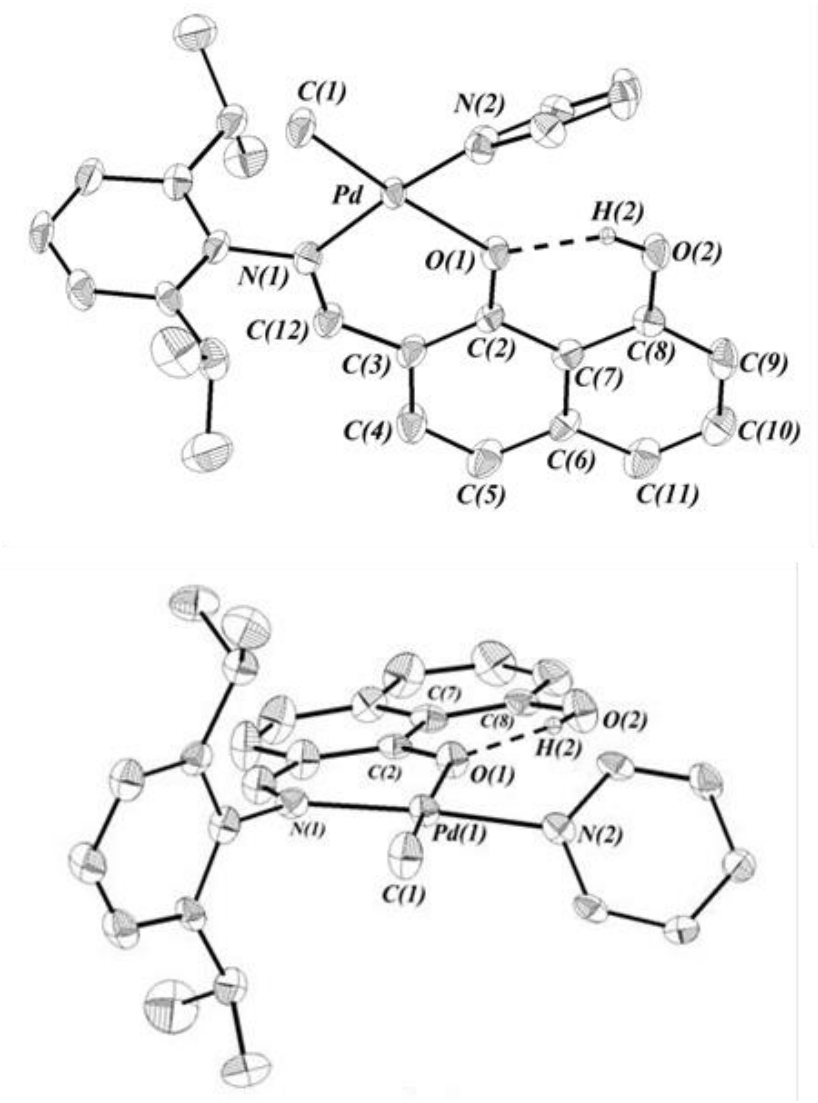

Figure 2-4. ORTEP plots of Catalyst B (above) perpendicular to the molecular plane and (below) in line with the molecular plane. All hydrogens have been omitted for clarity with the exception of H(2) which participates in hydrogen bonding between O(2) and O(1).

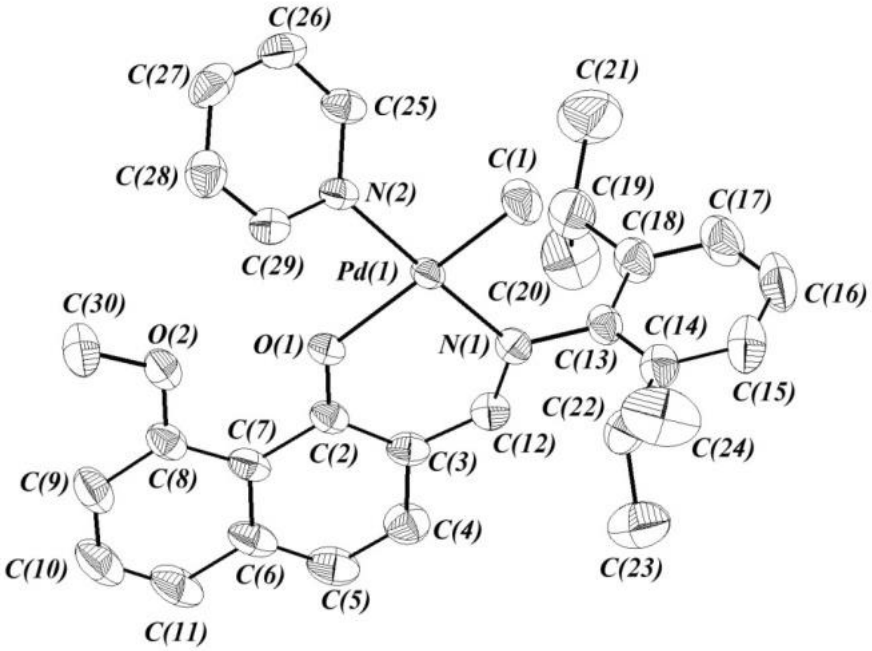

Figure 2-5. **ORTEP Plot of Catalyst C.** Hydrogen atoms have been omitted for clarity.

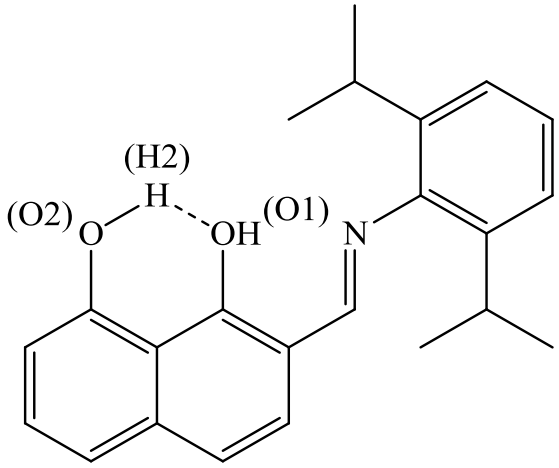

Figure 2-6. Intramolecular hydrogen bonding in Ligand 2.

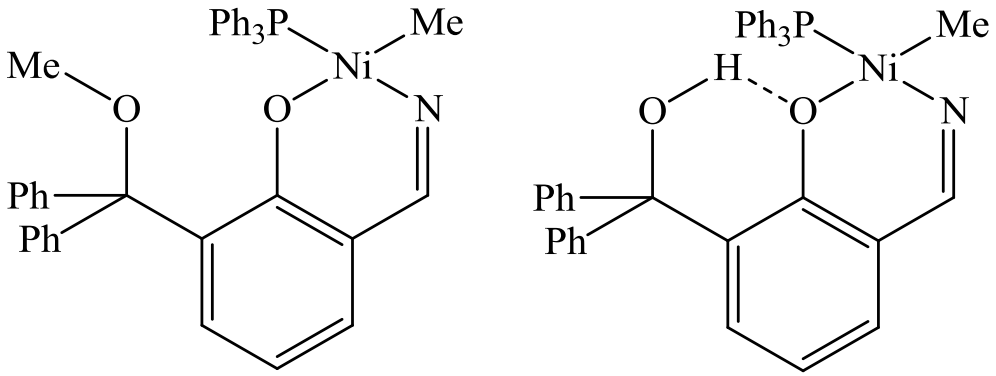

D **E**

Figure 2-7. H-bonding effects observed. Catalyst **D** (left) serves as a control catalyst for Catalyst **E** (right). Delferro et al. observed that the activity of Catalyst **D** was 50 kg polyethene/mmol[Ni]•h as compared to 150 kg polyethene/mmol [Ni]•h for Catalyst E. The presence of the -OH group lengthens the Ni-O bond in E.[33]

2.2.2. 2D NOESY Experiments.

In order to confirm the persistence of Catalyst **B**'s hydrogen bond in solution, NOESY experiments were performed in dichloromethane (see Appendix 6.3). NOESY showed that the naphtholic hydrogen (13.25 ppm) interacts with 2,6-hydrogens on the pyridine ligand (8.82 ppm). This suggests the survival of the hydrogen bond in solution. Additional NMR spectra, detailing the identification of the pyridine hydrogens of Catalyst **B** have been included in Appendix 6.3.

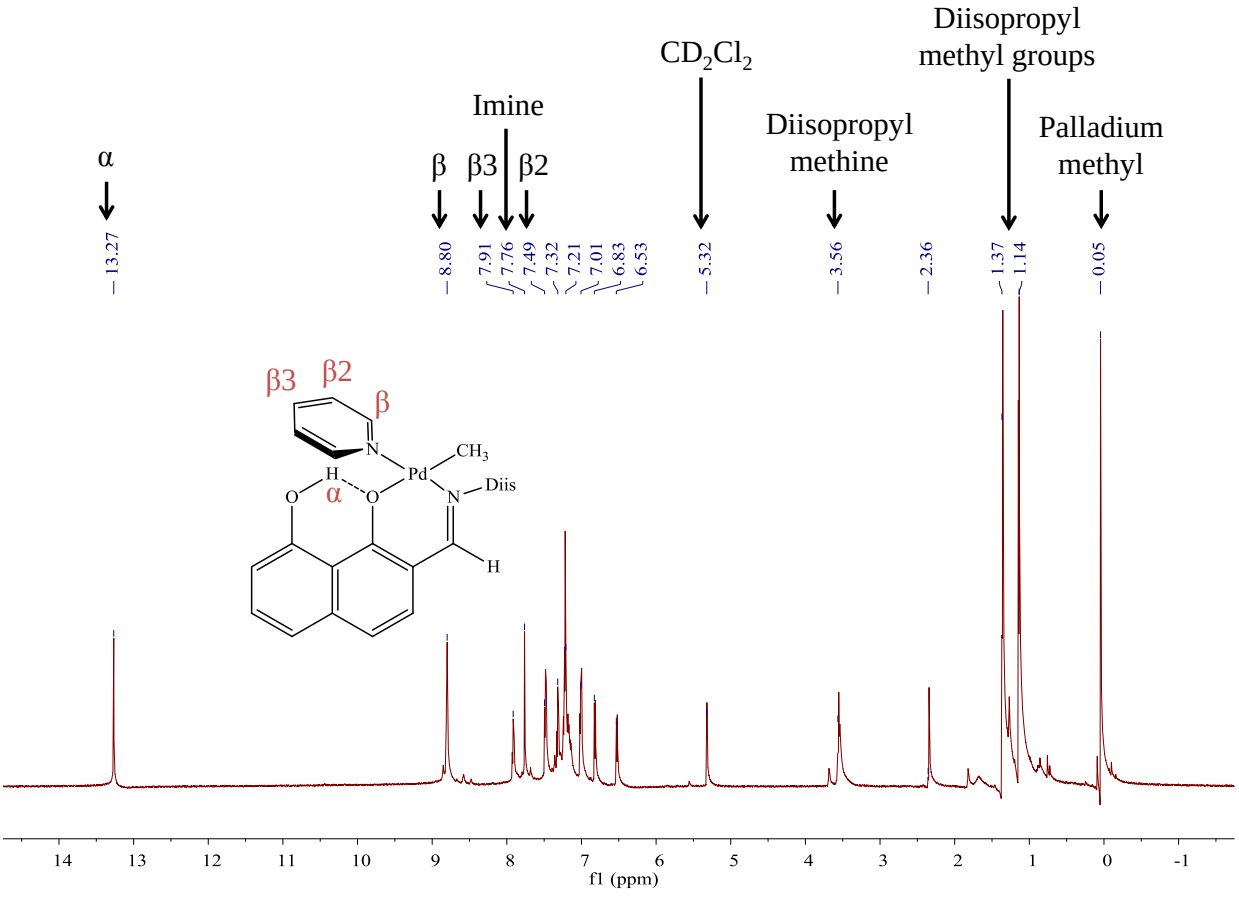

Figure 2-8. 1D ^{1}H spectrum of Catalyst B in dichloromethane. Sample conditions: CD_2Cl_2, 298 K, 600 MHz. Acquisition parameters: 1 scan, 1 second relaxation delay, 32k points acquired. Select peaks denoted; unmarked aromatic peaks attributed to hydrogens found in naphthyl ligand, aniline ring, and toluene.

2.2.3. Ethene and norbornene homopolymerizations.

All three catalysts – **A**, **B**, and **C** – are incapable of homopolymerizing ethene and norbornene at 30°C. Even when the temperature was increased to 90°C, a negligible amount of polymer (<10 mg, with 2 g of norbornene) was produced. The catalysts were observed to undergo decomposition in the presence of pure ethene, producing low molecular weight ethene oligomers; typically, black solid or a metallic sheen was left on the sides of the glass liner in the autoclave after the reaction was stopped at 2 hours.

Catalysts **A** – **C** in ethene/5-*n*-hexyl-2-norbornene and ethene/5-norbornene-*tert*-butyl-2-carboxylate copolymerizations. Catalysts **A**, **B**, and **C** are all capable of copolymerizing ethene and 5-*n*-hexyl-2-norbornene (NB-$(CH_2)_5CH_3$) with low polydispersity (PDI = 1.1-1.2) as noted in Table 2-3. All three catalysts incorporate fairly high amounts of NB-$(CH_2)_5CH_3$; however, the molar percentage norbornene derivative incorporated into each copolymer differs. Catalyst **C** (R = -OCH_3) incorporated the least amount of the norbornene derivative (39%), while Catalyst **A** (R = -H) incorporated the most (58%), showing that different functional groups on the C8 position of the naphthyl backbone influences polymer composition.

Catalysts A and B produce polymers of similar composition and in similar yields; A does produce polymer with slightly more norbornene units, thereby leading to a significantly higher molecular weight polymer. There was a marked preference for insertion of the exo monomer into the polymer chain for all three catalysts.[34] Catalyst **A** particularly favored the insertion of the *exo* isomer over the *endo* isomer –the amount of *exo* isomer dropped from 22% to only 6% (Table 2-3, entry 1). In comparison, Catalyst **B** consumed *exo* isomer less readily, although **B** consumed nearly the same total amount of norbornene as did **A**; 12 % of the exo isomer remains after the reaction was terminated (Table 2-3, entry 2). Interestingly, the addition of the non-

coordinating proton sponge, 2,6-*di*-*tert*-butyl-pyridine had little effect on the polymerization activities of **A** and **B** (Table 2-3). Only a slight decrease in molecular weight and norbornene incorporation was observed.

A and **B** produced significantly more polymer (1.7 and 1.6 g, respectively) than Catalyst **C** (0.8 g), and both were also able to copolymerize respectable amounts of ethene and 5-norbornene-*tert*-butyl-2-carboxylate NB-($COOC(CH_3)_3$) (Table 2-4). Regarding Catalysts **B** and **C**, it is fascinating that the replacement of the hydroxyl group with a methoxy group drastically decreases polymer yield (a 50% decrease was observed, Table 2-3, entries 2 and 3) and completely stops the palladium(II) center from copolymerizing ethene and NB-$COOC(CH_3)_3$ (Table 2-4). This behavior does hearken back to Delferro et al.'s study (Figure 2-7) in which the authors observed that the removal of the intramolecular hydrogen bond also decreased polyethylene yields of a nickel (II) catalyst by a considerable amount (~66%).

Table 2-3. **Copolymerizations of ethene and 5-n-hexyl-2-norbornene using Catalysts A, B, and C.**[a]

Entry	Catalyst	M_n	PDI	NB incorp. (mol%)[b]	NB conv. (%)[c]	*exo/endo* (before)[c]	*exo/endo* (after)[c]	Yield (g)[d]
1	**A**	53000	1.2	58%	74%	22/78	6/93	1.7
2	**B**	39000	1.1	52%	73%	21/79	12/88	1.7
3	**C**	28000	1.1	39%	30%	21/79	14/86	0.8
[e]4	**A**	49000	1.2	61%	69%	22/78	9/91	1.5
[e]5	**B**	37000	1.1	56%	69%	21/79	13/87	1.6

[a] Conditions: Catalyst (0.03 mmol), 5-*n*-hexyl-2-norbornene (2 g), toluene (5 mL), 100 psi ethene, 2 h reaction at 30°C. [b] Determined by ^{13}C-NMR. [c] Determined using GC. [d] Yield calculated from norbornene incorporation and norbornene consumption. [e] Sample contained 2,6-*di-tert*-butyl-pyridine (1:1 molar ratio of pyridine to catalyst).

Table 2-4. **Copolymerization of 5-norbornene-tert-butyl-2-carboxylate with ethene using Catalysts A, B, and C.**[a]

Ent.	Cat.	yield (g)	*exo*/ *endo* (bef.)	*exo*/ *endo* (after)	NB inc. mol%
1	**A**	1.3	20/80	15/85	31%
2[b]	**B**	1.2	40/60	31/69	33%
3	**C**	0	--	--	--

[a] Conditions: 0.03 mmol catalyst, 5 mL toluene, 300 psi ethene, 2 g of 5-norbornene-*tert*-butyl-2-carboxylate, 2 hours, 90°C. [b] From Chen, 2010, Ref. 23.

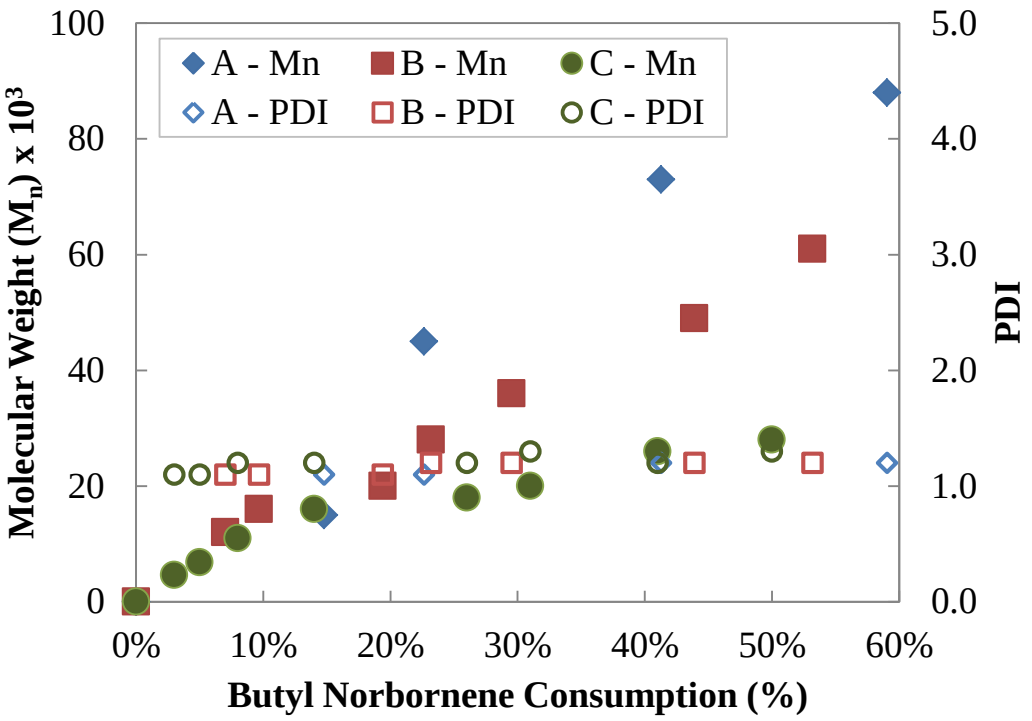

Figure 2-9. Tracking the molecular weight and PDI of the ethene/5-*n*-butyl-2-norbornene polymer chain. Conditions: 0.071 mM catalyst and 31.6 mM 2-n-butyl-5-norbornene were dissolved in toluene. The reaction was run under 1 atm ethene pressure at 30°C. Molecular weights and PDI were determined using GPC; norbornene consumption was determined using GC.

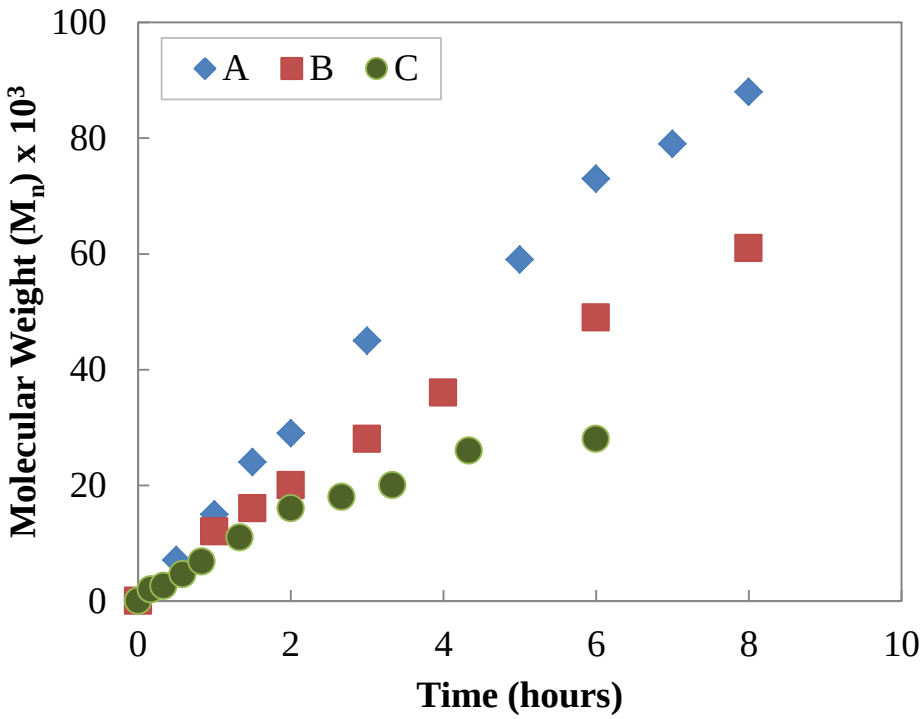

Figure 2-10. Increase in molecular weight of the ethene/5-*n*-butyl-2-norbornene polymer chain over time. Conditions noted previously in Figure 2-9.

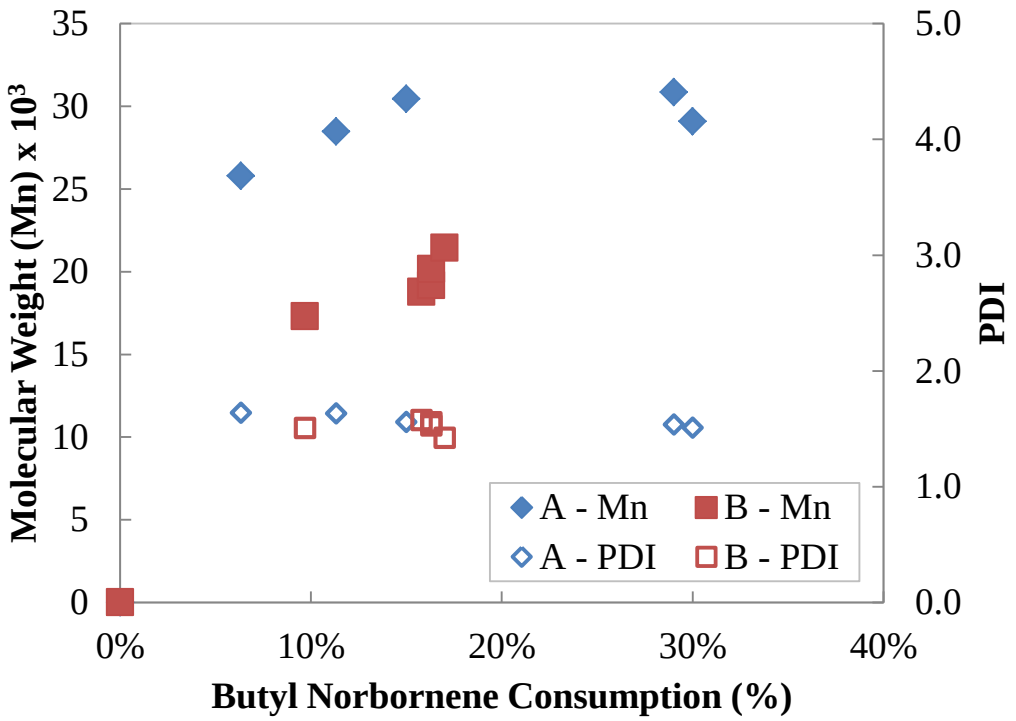

Figure 2-11. Tracking the molecular weight and PDI of the ethene/5-norbornene-*tert*-butyl-2-carboxylate polymer chain. Conditions: 0.071 mM catalyst and 31.6 mM 5-norbornene-*tert*-butyl-2-carboxylate were dissolved in toluene. The reaction was run under 4 atm ethene pressure at 90°C in autoclaves. Molecular weights and PDI were determined using GPC; norbornene consumption was determined using GC.

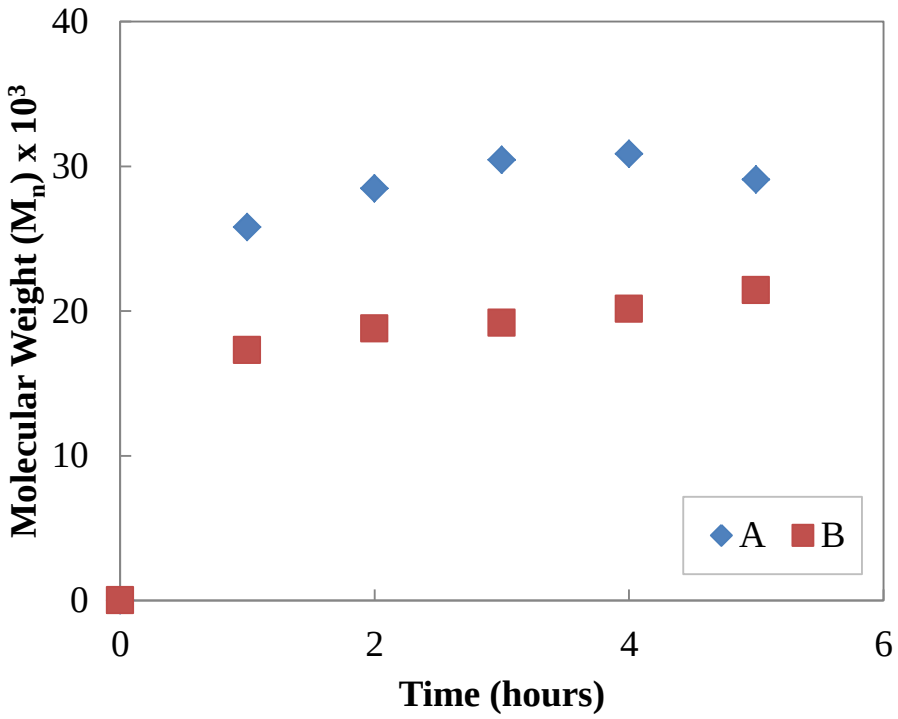

Figure 2-12. Increase in molecular weight of the ethene/5-norbornene-*tert*-butyl-2-carboxylate polymer chain over time. Conditions noted previously in Figure 2-11.

2.2.4. Evidence of living polymerization for ethene/2-n-butyl-5-norbornene

Catalysts **A**, **B**, and **C**, all display characteristics of a quasi-living polymerization. As displayed in Figure 2-9, for the copolymerization of 2-*n*-butyl-5-norbornene (NB-$(CH_2)_3CH_3$) with ethene, the M_n increased relatively linearly and the PDI remains between 1.1-1.3 as a function of the norbornene uptake.[34] The molecular weight also grew linearly over time, as shown in Figure 2-10. The rate of monomer conversion and increase in Mn was faster for Catalyst **A** (R = H) compared to either Catalyst **B** (-OH) or Catalyst **C** (-OCH_3). For example, at the 120 minute mark, for **A**, M_n = 29000 (29% norbornene consumption), for **B**, M_n = 20000 (28%), and for **C**, M_n = 16000 (14%) were observed. Although not displayed in Figure 2-9, past the eight-hour mark, the M_n plateaued and the PDI increased. This behavior suggests that the propensity towards chain termination by β-H elimination[15] increases with higher ethene to norbornene feed ratios (the ethene pressure was held constant while the amount of 2-*n*-butyl-5-norbornene decreased with time). Hypothetically, if the initial concentration of 2-*n*-butyl-5-norbornene was maintained, both catalyst activity and polymer chain growth would persist for a longer period of time.

The copolymerization of ethene and 5-norbornene-*tert*-butyl-2-carboxylate does not proceed in a living manner. Polymerizations involving NB-$COOC(CH_3)_3$ could not be performed at low ethene pressures because little polymerization occurs under this condition. Under atmospheric ethene pressure, Catalyst **A** and **B** produced polymers of only $M_n \sim 1000$ after an hour, and the molecular weight did not increase over the next four hours. A higher ethene pressure of 4 atm was successfully used to promote faster and more easily observable polymer chain growth (Figure 2-11). However, while rapid chain growth was observed in the first hour of the reaction for both Catalysts **A** and **B**, the molecular weight plateaued after that

first hour of the reaction (Figure 2-12). The PDI was also much higher than those observed in the ethene/NB-$(CH_2)_3CH_3$ living polymerization; the PDI for the ethene/NB-$COOC(CH_3)_3$ copolymerizations was ~1.5-1.6. Additionally, catalyst decomposition is observed for both Catalyst A and B; Pd(0) began precipitating even after the first hour of the reaction. **A** again copolymerizes ethene and norbornene derivative more rapidly than **B**. Polymerization was not attempted Catalyst **C**; earlier tests showed that **C** decomposed rapidly in the presence of ethene and carboxylate monomer and failed to produce any polymer (Table 2-4, entry 3).

2.3. Experimental Section

2.3.1. Materials

All materials were obtained from Sigma-Aldrich or Fisher Scientific unless otherwise noted. Solvents, which had been dried and degassed, were used in the glove box without further purification. Norbornene derivatives, 5-*n*-butyl-2-norbornene (Promerus) and 5-norbornene-*tert*-butyl-2-carboxylate, were dried over molecular sieves, degassed, and stored in the glove box prior to use. 1,5-Cyclooctadiene palladium(II) methyl chloride, (COD)PdMeCl, Ligand **2**, and Catalyst **B** were synthesized according to literature procedures.[23, 36–39] All manipulations of air-sensitive materials were performed under nitrogen.

2.3.2. Ligand and Catalyst Synthesis

^{1}H-NMR and ^{13}C-NMR spectra were recorded using the Bruker 300-DPX, 400-DRX, and 500-AV-III spectrometers. Gas chromatography analysis was performed on an Agilent 5890 Series II GC using a RTX-5 split capillary column (Restek) connected to an FID detector. The GC column specifications were as follows: 5% diphenyl/95% dimethyl polysiloxane, 30 m, 0.25 mm i.d. (internal diameter), 0.5 μm d.f. (film thickness).[40] The column temperature was increased at a rate of 15°C/min, from 40°C to 250°C. For GC analyses, 0.20 mL of test solution and 50 μL of chlorobenzene – an internal standard – were combined. Molecular weights and the polydispersity index (PDI) were determined on a Hewlett-Packard HP 1090 gel permeation chromatograph (GPC) equipped with an HP-1047A refractive index detector, American Polymer Standards AM gel 10 mm and AM gel 10 mm 104 Å columns, and calibrated versus polystyrene standards (Polysciences). The ethene/norbornene derivative copolymers were run at 40 °C with a 0.1 wt % solution of tetra-*n*-butylammonium nitrate (Sigma-Aldrich) in tetrahydrofuran. Analysis was performed using Cirrus GPC Offline software, v. 3.0 (©2006, Varian, Inc.).

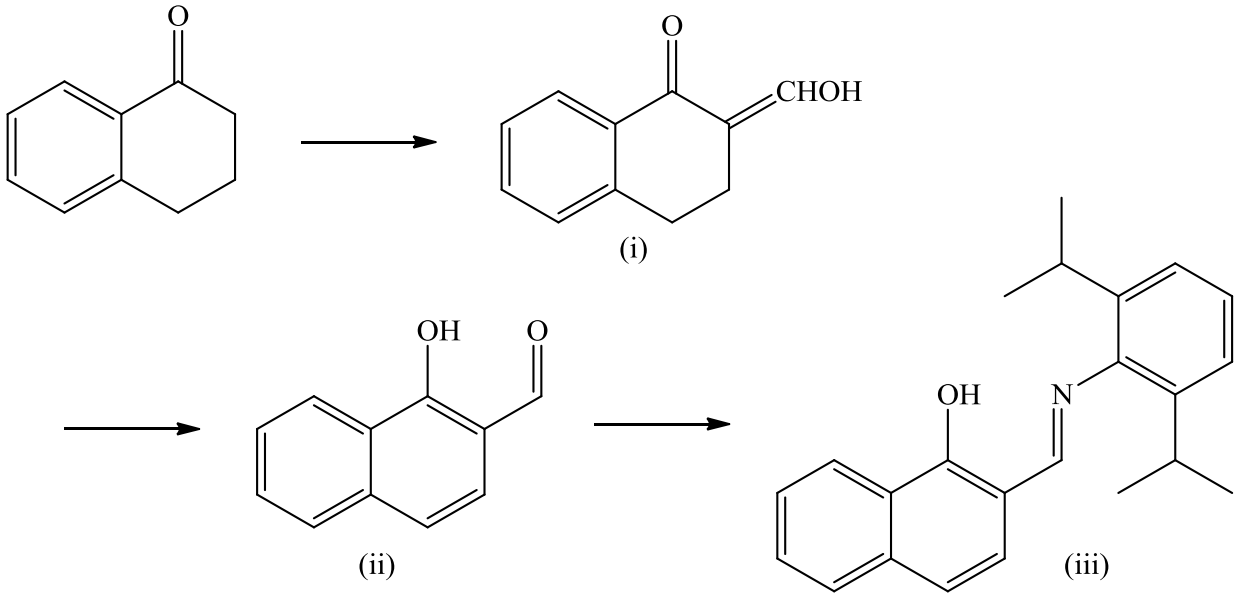

Scheme 2-3. Synthesis of Ligand 1.

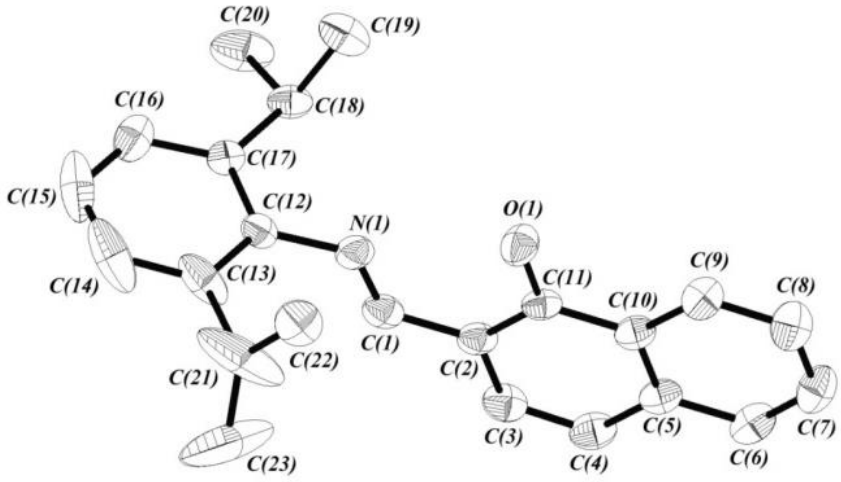

Figure 2-13. ORTEP plot of Ligand 1.

*Synthesis of 2-(2,6-diisopropylphenyl)-imino-1-naphthol (Ligand **1**, Scheme 2-3, Figure 2-13).* 2-formyl-1-naphthol (2.35 g, 10.9 mmol) and 2,6-diisopropylaniline (90% purity, 10.86 mmol, 2.27 mL) were dissolved in CH_2Cl_2 (150 mL). A drop of formic acid was added and the sample was refluxed for 6 hours under N_2(g). CH_2Cl_2 was removed via rotary evaporation, leaving a fluffy, yellow solid. The crude product was purified on a silica column (5% EtOAc/hexanes) to remove unreacted aniline. (Yield = 92%) ^{1}H-NMR, 300 MHz, ($CDCl_3$, 25°C, ppm): 14.64 (s, 1H, -OH), 8.52 (s, 1H, -HC=N-), 8.49–7.19 (9H, aromatic), 3.11 (m, 2H, -$CH(CH_3)_2$), 1.24 (d, 12H, -$CH(CH_3)_2$).

*Synthesis of 2-(2,6-diisopropylphenyl)-imino-8-methoxy-1-naphthol (Ligand **3**).* Synthesis of the immediate precursor of Ligand **3**, 8-methoxy-2-formyl-1-naphthol, is detailed by Bilger et al.[37] This precursor was subsequently reacted under the same conditions as 2-formyl-1-naphthol (Scheme 3, ii), giving rise to Ligand **3**. The ligand was purified on a 20% CH2Cl2/hexane column, to yield a bright yellow solid. (Yield = 80%), ^{1}H-NMR, 300 MHz, (CDCl3, 25°C, ppm): 8.40 (s, 1H, -HC=N-), 7.54–6.9 (8H, aromatic), 4.11 (s, 3H, -OCH_3), 3.18–3.12 (m, 2H, -$CH(CH_3)_2$), 1.33-1.22 (d, 12H, -$CH(CH_3)_2$).

*Synthesis of 2-(2,6-diisopropylphenyl)-imino-1-naphtholate sodium salt (**1-Na**).* NaH (240 mg, 10 mmol) was added to a solution of Ligand **1** (331 mg, 1 mmol in 10 mL THF). The solution was allowed to stir under N_2(g) for 2 hours, and was then syringe-filtered (PTFE, 0.45 μm). The filtrate was collected, and under low pressure, the solvent was removed, leaving a bright yellow solid. This salt was immediately used for the synthesis of Catalyst **A**. (yield = 80%). ^{1}H-NMR, 300 MHz, (THF-d6, 25°C, ppm): 8.38 (s, 1H, -HC=N-), 7.50–6.38 (9H, aromatic), 3.15 (m, 2H, -$CH(CH_3)_2$), 1.13 (d, 12H, -$CH(CH_3)_2$).

*Synthesis of 2-(2,6-diisopropylphenyl)-imino-1-naphtholate sodium salt (**3-Na**).* **3-Na** was synthesized using the same conditions as the synthesis of **1-Na**. After the solvent was removed, a bright yellow powder was obtained. (Yield = 80%). ^{1}H-NMR, 300 MHz, (THF-d6, 25°C, ppm): 8.16 (s, 1H, -HC=N-), 7.54–6.9 (3d, 2m, 8H, aromatic), 4.11 (s, 3H, -OCH_3), 3.18–3.12 (m, 2H, -$CH(CH_3)_2$), 1.33-1.22 (d, 12H, -$CH(CH_3)_2$).

*Synthesis of Catalyst **A***. Pyridine (80 mg, 1 mmol), and (COD)PdMeCl (265 mg, 1 mmol) were added to a solution of **1-Na** dissolved in toluene (10 mL). The solution was allowed to stir overnight, and was then filtered through celite and a syringe filter (PTFE, 0.45 μm). Toluene was removed at 30°C under vacuum, leaving a viscous oil. The oil rapidly crystallized into golden crystals at room temperature. (Yield = 80%). ^{1}H-NMR, 300 MHz, ($CDCl_3$, 25°C, ppm): 9–6.8 (14 H, aromatic), 7.81 (s, 1H, -HC=N-), 3.70–3.61 (m, 2H, -$CH(CH_3)_2$), 1.39–1.15 (2d, 12H, -$CH(CH_3)_2$), 0.08 (s, 3H, Pd-CH_3).

*Synthesis of Catalyst **C**.* Catalyst **C** was synthesized under the same conditions as Catalyst **A**. Removal of toluene yielded a viscous, dark yellow oil. When left standing at room temperature, the oil rapidly formed dark, red crystals. (Yield = 80%). ^{1}H-NMR, 300 MHz, ($CDCl_3$, 25°C, ppm): 9.02–6.70 (13H, aromatic), 7.70 (s, 1H, -HC=N-), 3.75 (s, 3H, -OCH_3), 3.68–3.61 (m, 2H, -$CH(CH_3)_2$), 1.33-1.11 (2d, 12H, -$CH(CH_3)_2$), 0.06 (s, 3H, Pd-CH_3).

2.3.3. Polymerization conditions for ethene/5-*n*-butyl-norbornene and ethene/5-*n*-hexyl-norbornene copolymers

Polymerizations were conducted in Parr high-pressure autoclaves. The glass liner inserts and autoclave parts were cleaned thoroughly, dried at 120°C overnight, and were allowed to cool to room temperature, under vacuum, before use. Reaction contents – including toluene,

norbornene derivatives, catalyst, and a stir bar – were added to the glass liner inserts and the contents were thoroughly stirred. Before the autoclave and its contents were assembled, 300 mg of solution was extracted for GC analysis. The autoclaves were then assembled and sealed. After being removed from the glove box, the autoclaves were pressurized with the appropriate amount of ethene. The autoclaves were then heated in oil baths at the desired temperature (30°C) for 2 hours. At the two-hour mark, the autoclaves were removed from the oil baths, and immediately depressurized. Another 300 mg sample was immediately extracted for GC analysis.

In order to isolate polymer for NMR studies, the reaction contents were immediately added to HCl/MeOH (10:90 v/v) in a centrifuge tube, and a gel-like polymer immediately phase-segregated from the solution. The sample was centrifuged at 10,000 rpm for 10 minutes; a gelatinous pellet of polymer formed at the bottom of the tube. The supernatant was discarded, the pellet was dissolved in THF, precipitated again in MeOH, and centrifuged once more. The process of polymer dissolution and precipitation was repeated several times to ensure the removal of any remaining monomer. The isolated polymer was finally collected in a pre-weighed round bottom flask, dried under rotary evaporation, and then placed under high vacuum overnight to remove trace solvent. Typically, between 0.8 – 1.3 grams of polymer was isolated.

Polymerization conditions for ethene and norbornene homooligomers. Ethene homooligomerizations were performed under the same conditions as the ethene/norbornene derivative copolymerizations. Norbornene homooligomerizations were allowed to run for 16 hours. When exposed to acidic methanol, the ethene oligomers formed a yellow, viscous liquid; norbornene oligomers precipitated as a white solid.

2.3.4. NMR spectra collection conditions and sample preparation

The copolymers (100-150 mg) were easily dissolved in $CDCl_3$ with chromium (III) acetylacetonate (0.025M). Cr(III)acac, a paramagnetic agent, was used to reduce the long relaxation delay times for carbon nuclei.[40] In order to obtain accurate ^{13}C-NMR integrations, an inverse-gated decoupling pulse program was employed. Program parameters were as follows: a relaxation delay (D1) of 10 seconds; sample points (td) at 64k; a spectrum width (sw) of 240 ppm; and a spectrum center position (o1p) of 100 ppm. A range of 1k – 4k scans for each sample was collected. All spectra were collected at room temperature. An example of an ethene/5-*n*-hexyl-2-norbornene copolymer is shown below in Figure 2-14.

Calculations for the norbornene content (mol % of NB in the polymer) varies depending on the type of norbornene derivative present in the copolymer. For each copolymer, a single carbon from the norbornene derivative was identified and used as an internal standard. In order to clearly identify the terminal methyl carbon in the ^{13}C-NMR spectra for ethene/5-*n*-butyl-2-norbornene and ethene/5-*n*-hexyl-2-norbornene copolymers, ^{13}C-DEPT spectra of the copolymers were collected (Figure 2-14, b). The terminal methyl carbons appear at 23.0 ppm and 14.2 ppm, respectively. For the ethene/5-norbornene-*tert*-butyl-2-carboxylate copolymer, the carbonyl carbon (175.9 – 174.5 ppm) was used as the internal calibration standard. The portions of the spectra containing the carbon peaks attributed to the copolymer (C_{TOT}) were integrated. For both ethene/butyl norbornene and ethene/hexyl norbornene copolymers, C_{TOT} was obtained by integrating 50–13 ppm region of the ^{13}C-NMR spectrum; for ethene/carboxylate copolymers, C_{TOT} was determined by integrating the regions 177 – 173, 81 – 79.5, and 55 – 20 ppm. To determine the mole percent of norbornene present in the copolymer, where C_{NB} is the

integration of the carbons attributed to the norbornene derivative, the following general equation was employed:

$$NB(mol\ \%) = \frac{C_{NB}}{C_{NB} + ((C_{TOT} - C_{NB})(\#C\ in\ ethene))}$$

The number of carbons in the NB derivative (# C in NB deriv.) varies depending on the identity of the NB derivative. The number of carbons in ethene (# C in ethene) is always set to 2.

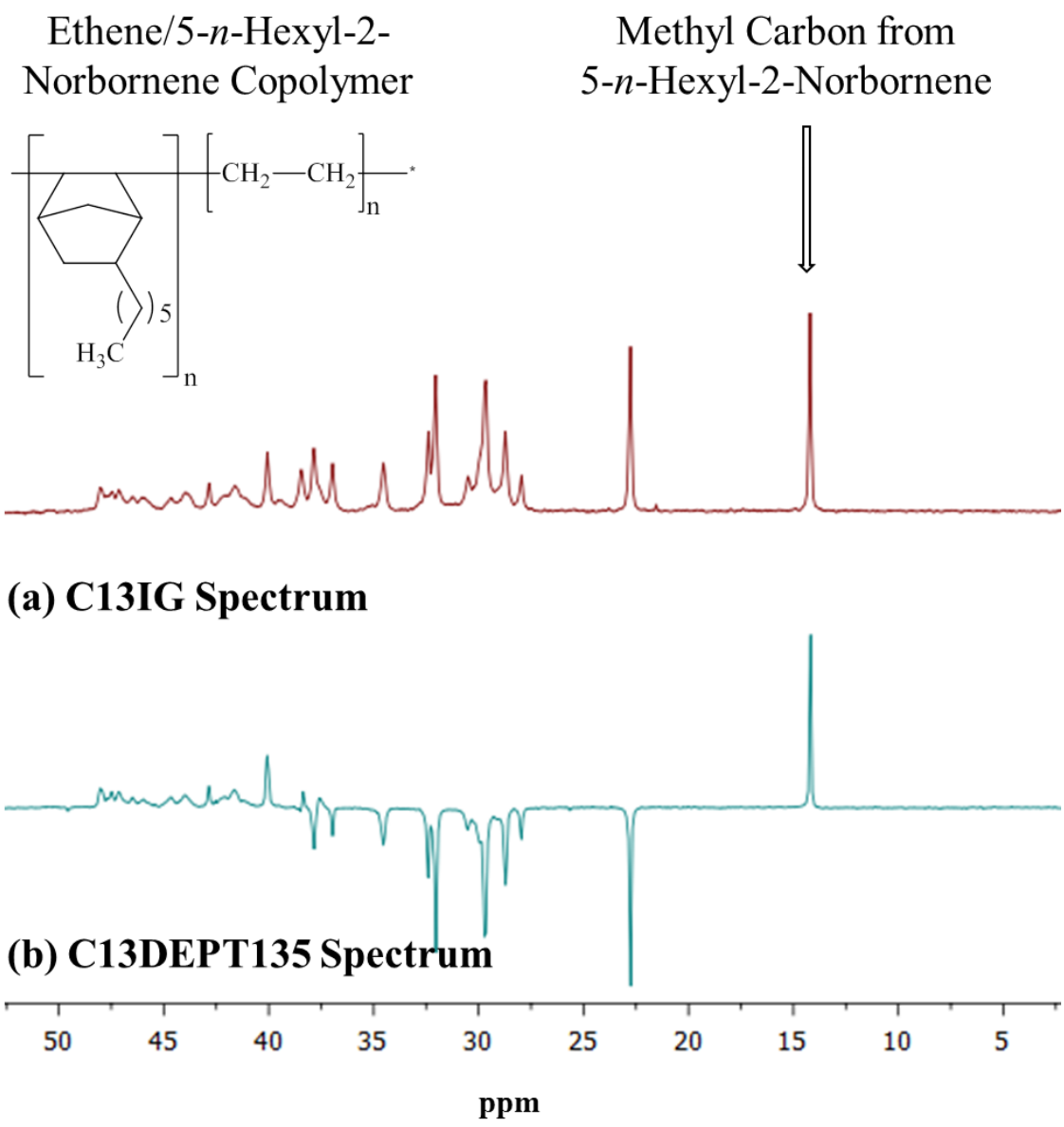

Figure 2-14. ^{13}C spectra of ethene/5-*n*-hexyl-2-norbornene copolymer. Conditions: $CDCl_3$, 298 K, 500 MHz. A C13DEPT135 spectrum of the polymer was obtained in order to identify the methyl group.

2.3.5. Conditions for living polymerizations

For Catalysts **A** and **B**, living polymerizations of ethene/5-*n*-butyl-2-norbornene and ethene/5-norbornene-*tert*-butyl-2-carboxylate were performed and monitored. In the glove box, 0.0225 mmol catalyst, a 445:1 mol: mol ratio of the norbornene derivative to catalyst, and 30 mL toluene were combined in a round bottom flask. The solution was then removed from the glove box, and stirred under constant ethene pressure (1 atm). At designated times, 0.5 – 1.0 mL of solution was extracted for GPC and GC analyses. In order to record monomer consumption over time in living polymerizations, 0.2 mL of sample was combined with 50 μL of chlorobenzene, and immediately injected into the GC. To prepare samples for molecular weight analyses, samples were dried down via rotary evaporation, dissolved in THF, and pushed through 0.45 μm Teflon filters to remove any undissolved polymer/particles. The filtrate was then analyzed using the GPC.

2.3.6. X-ray Crystallography

Single crystals for Ligand **1**, Catalyst **A**, and Catalyst **C** were selected under a polarizing microscope and mounted on a loop using paratone oil. The crystal was cooled to 120 K by a Rigaku X-stream 2000 cryo-system. The single-crystal diffraction data were collected on a Bruker-AXS diffractometer with a SMART APEX CCD area detector. The X-ray generator was operated at 50 kV and 32 mA using Mo Kα (λ = 0.71073 Å) radiation. Data were collected with a ω scan width of 0.3°. A total of 600, 430, 235, and 50 frames were collected in four different settings of φ (0°, 90°, 180°, 270°), keeping the sample-to-detector distance fixed at 5.8 cm and the detector position (2θ) fixed at −25°. The data were reduced using SAINTPLUS,[iv] and an

[iv] SMART (V 5.628), SAINT (V 6.45a), XPREP, SHELXTL; Bruker AXS Inc.: Madison, WI, 2004.

empirical absorption correction was applied using the SADABS program.[v] The crystal structure was solved by direct methods using SHELXS97 and refined using SHELXL97 present in the SHELXTL V6.14 package.[vi] All non-hydrogen atoms were easily determined from the differential Fourier maps and were refined anisotropically. For the final refinement, the hydrogen atoms were placed in geometrically ideal positions and refined using the riding mode. The last cycles of the refinement included atomic positions, anisotropic thermal parameters for all the non-hydrogen atoms, and isotropic thermal parameters for all the hydrogen atoms. Full-matrix least-squares structure refinement against F2 was carried out using the SHELXTL V6.14 package of programs.[vii]

[v] Sheldrick, G. M. Siemens Area Correction Absorption Correction Program; University of Göttingen: Göttingen, Germany, 1994.

[vi] Sheldrick, G. M. SHELXL-97, Program for Crystal Structure Solution and Refinement; University of Göttingen: Göttingen, Germany, 1997.

[vii] CCDC 904834 and 904835 contain the supplementary crystallographic data for Catalysts **A** and **C**, respectively. These data can be obtained free of charge from The Cambridge Crystallographic Data Centre (CCDC) via www.ccdc.cam.ac.uk/data_request/cif.

Table 2-5. Crystallographic parameters.[v–vi, a]

Compound	Catalyst A	Catalyst C
Empirical Formula	$C_{29}H_{32}N_2OPd$	$C_{30}H_{34}N_2O_2Pd$
Formula weight (g/mol)	530.97	560.99
Space group	*P b c a* (no. 61)	*P* -1 (no. 2)
a (Å)	23.108(3)	9.3297(14)
b (Å)	8.3660(10)	10.5642(16)
c (Å)	26.211(3)	14.770(2)
a (°)	90	101.590(2)
β (°)	90	91.832(2)
γ (°)	90	104.375(2)
Volume ($Å^3$)	5067.1(11)	1376.3(3)
Z	8	2
Size (mm^3)	0.32 x 0.18 x 0.10	0.20 x 0.10 x 0.08
ρcalc (g cm^{-3})	1.395	1.354
θ range (°)	1.55 to 28.31	2.04 to 28.37
Reflections collected	44740	13323
Unique reflections	6223	6703
Number of parameters	303	322
Goodness of fit (S)	1.052	1.142
[b] Final R indices [I>2sigma(I)]	R_1 = 0.0350, wR_2 = 0.0851	R_1 = 0.0456, wR_2 = 0.0954
[b] R (all data)	R_1=0.0409, wR_2=0.0881	R_1=0.0526, wR_2= 0.0985

[a] For crystallography data for Catalyst **B**, please see reference 23. [b] Formulas for variables R1 and wR1: R1 = Σ|| Fo | - | Fc || / Σ | Fo |; wR2 = {Σ [w (Fo2 – Fc2)]/Σ [w (Fo2) 2]} 1/2. w = 1/[ρ2(Fo)2+(aP)2+bP]. P = [max (Fo, O)+2(Fc) 2]/3, where a = 0.0373 and b = 3.8451 for Catalyst **A**, a = 0.0449 and b = 0.2966 for Catalyst **C**, respectively.

2.4. Conclusion

Naphthyl-ligated Pd(II) catalysts remain relatively rare; these results shed some more light on how the functionalization of the 8-carbon on the naphthyl backbone affects the palladium center. Comparing Catalysts **B** and **C**, hydrogen-bonding had a significantly positive effect on the polymerization ability of the catalyst, increasing polymer yield dramatically, as well as copolymerization ability of ethene and polar monomers.

The findings in this and the previous studies provide a platform to further explore the effects of H-bonding in naphthyl compounds by modifying of the functional group on the 8-carbon. One particularly interesting variable to investigate is varying the acidity of the –OH group on the 8-carbon. Foti et al. has shown that the presence of the –OH group on the 5-carbon can increase the acidity of the C8 hydroxyl hydrogen considerably.[32] The compounds should also be monitored using FTIR to confirm the presence of the hydrogen bond.

2.5. Abbreviations

Phenoxyimine or salicylaldiminato, FI; 5-*n*-butyl-2-norbornene, butyl norbornene or NB-$(CH_2)_3CH_3$; 5-*n*-hexyl-2-norbornene, hexyl norbornene or NB-$(CH_2)_5CH_3$; 5-norbornene-*tert*-butyl-2-carboxylate, NB-$COOC(CH_3)_3$; 2,6-diisopropylphenyl, Diis; sodium hydride, NaH; (1,5-cyclooctadiene)palladium(II) methyl chloride, (COD)PdMeCl; Cr(III)acac, chromium(III) acetylacetonate.

2.6. References

(1) Popeney, C. S.; Camacho, D. H.; Guan, Z. Efficient Incorporation of Polar Comonomers in Copolymerizations with Ethylene Using a Cyclophane-Based Pd(II) Alpha-Diimine Catalyst. *J. Am. Chem. Soc.* **2007**, *129*, 10062 – 10063.

(2) Popeney, C.; Guan, Z. Ligand Electronic Effects on Late Transition Metal Polymerization Catalysts. *Organometallics* **2005**, *24*, 1145–1155.

(3) Ittel, S. D.; Johnson, L. K.; Brookhart, M. Late-Metal Catalysts for Ethylene Homo- and Copolymerization. *Chem. Rev.* **2000**, *100*, 1169–1203.

(4) Nakamura, A.; Anselment, T. M. J.; Claverie, J.; Goodall, B.; Jordan, R. F.; Mecking, S.; Rieger, B.; Sen, A.; van Leeuwen, P. W. N. M.; Nozaki, K. Ortho-Phosphinobenzenesulfonate: A Superb Ligand for Palladium-Catalyzed Coordination–Insertion Copolymerization of Polar Vinyl Monomers. *Acc. Chem. Res.* **2013**, *46*, 1438–1449.

(5) Borkar, S.; Sen, A. Controlled Copolymerization of Vinyl Acetate with 1-Alkenes and Their Fluoro Derivatives by Degenerative Transfer. *J. Polym. Sci. Part -Polym. Chem.* **2005**, *43*, 3728–3736.

(6) Hearley, A. K.; Nowack, R. A. J.; Rieger, B. New Single-Site Palladium Catalysts for the Nonalternating Copolymerization of Ethylene and Carbon Monoxide. *Organometallics* **2005**, *24*, 2755–2763.

(7) Kochi, T.; Nakamura, A.; Ida, H.; Nozaki, K. Alternating Copolymerization of Vinyl Acetate with Carbon Monoxide. *J. Am. Chem. Soc.* **2007**, *129*, 7770 – 7771.

(8) Nakamura, A.; Ito, S.; Nozaki, K. Coordination−Insertion Copolymerization of Fundamental Polar Monomers. *Chem. Rev.* **2009**, *109*, 5215–5244.

(9) Makio, H.; Terao, H.; Iwashita, A.; Fujita, T. FI Catalysts for Olefin Polymerization-A Comprehensive Treatment. *Chem. Rev.* **2011**, *111*, 2363–2449.

(10) Blank, F.; Janiak, C. Metal Catalysts for the Vinyl/Addition Polymerization of Norbornene. *Coord. Chem. Rev.* **2009**, *253*, 827–861.

(11) Taylor, K. J. Catalysts for the Low Temperature Polymerization of Ethylene. *Polymer* **1964**, *5*, 207–211.

(12) Younkin, T. R.; Connor, E. F.; Henderson, J. I.; Friedrich, S. K.; Grubbs, R. H.; Bansleben, D. A. Neutral, Single-Component Nickel (II) Polyolefin Catalysts That Tolerate Heteroatoms. *Science* **2000**, *287*, 460–462.

(13) Michalak, A.; Ziegler, T. DFT Studies on the Copolymerization of A-Olefins with Polar Monomers: Comonomer Binding by Nickel- and Palladium-Based Catalysts with Brookhart and Grubbs Ligands. *Organometallics* **2001**, *20*, 1521–1532.

(14) Mu, H.-L.; Ye, W.-P.; Song, D.-P.; Li, Y.-S. Highly Active Single-Component Neutral Nickel Ethylene Polymerization Catalysts: The Influence of Electronic Effects and Spectator Ligands. *Organometallics* **2010**, *29*, 6282–6290.

(15) Chan, M. S. W.; Deng, L. Q.; Ziegler, T. Density Functional Study of Neutral Salicylaldiminato nickel(II) Complexes as Olefin Polymerization Catalysts. *Organometallics* **2000**, *19*, 2741–2750.

(16) Crabtree, R. H. *The Organometallic Chemistry of Transition Metals*; 4th ed.; John Wiley & Sons: Hoboken, 2005.

(17) Hu, T.; Li, Y. G.; Li, Y. S.; Hu, N. H. Novel Highly Active Binuclear Neutral Nickel and Palladium Complexes as Precatalysts for Norbornene Polymerization. *J. Mol. Catal. Chem.* **2006**, *253*, 155–164.
(18) Song, D.-P.; Wang, Y.-X.; Mu, H.-L.; Li, B.-X.; Li, Y.-S.. Observations and Mechanistic Insights on Unusual Stability of Neutral Nickel Complexes with a Sterically Crowded Metal Center. *Organometallics* **2011**, *30*, 925–934.
(19) Salata, M. R.; Marks, T. J. Synthesis, Characterization, and Marked Polymerization Selectivity Characteristics of Binuclear Phenoxyiminato Organozirconium Catalysts. *J. Am. Chem. Soc.* **2008**, *130*, 12 – 13.
(20) Stephenson, C. J.; McInnis, J. P.; Chen, C.; Weberski, M. P.; Motta, A.; Delferro, M.; Marks, T. J. Ni(II) Phenoxyiminato Olefin Polymerization Catalysis: Striking Coordinative Modulation of Hyperbranched Polymer Microstructure and Stability by a Proximate Sulfonyl Group. *ACS Catal.* **2014**, *4*, 999–1003.
(21) Carrow, B. P.; Nozaki, K. Transition-Metal-Catalyzed Functional Polyolefin Synthesis: Effecting Control through Chelating Ancillary Ligand Design and Mechanistic Insights. *Macromolecules* **2014**.
(22) Weberski, M. P.; Chen, C.; Delferro, M.; Marks, T. J. Ligand Steric and Fluoroalkyl Substituent Effects on Enchainment Cooperativity and Stability in Bimetallic Nickel(II) Polymerization Catalysts. *Chem. Eur. J.* **2012**, *18*, 10715–10732.
(23) Chen, Y.; Mandal, S.; Sen, A. Synthesis of (N-O)-Ligated Palladium(II) Complexes and Their Use in Ethene Homopolymerization and Norbornene Copolymerizations. *Organometallics* **2010**, *29*, 3160–3168.
(24) Chung, T. C. *Functionalization of Polyolefins*; 1st ed.; Academic Press, 2002.
(25) Liu, S.; Borkar, S.; Newsham, D.; Yennawar, H.; Sen, A. Synthesis of Palladium Complexes with an Anionic P~O Chelate and Their Use in Copolymerization of Ethene with Functionalized Norbornene Derivatives: Unusual Functionality Tolerance. *Organometallics* **2007**, *26*, 210–216.
(26) Kang, M.; Sen, A. Reaction of Palladium 1,5-Cyclooctadiene Alkyl Chloride with Norbornene Derivatives: Relevance to Metal-Catalyzed Addition Polymerization of Functionalized Norbornenes. *Organometallics* **2004**, *23*, 5396–5398.
(27) Kacker, S.; Kim, J. S.; Sen, A. Insertion of Imines into Palladium-Acyl Bonds: Towards Metal-Catalyzed Alternating Copolymerization of Imines with Carbon Monoxide to Form Polypeptides. *Angew. Chem. Int. Ed.* **1998**, *37*, 1251–1253.
(28) Sen, A.; Borkar, S. Perspective on Metal-Mediated Polar Monomer/Alkene Copolymerization. *One-Electron Organomet. React.* **2007**, *692*, 3291–3299.
(29) Heyndrickx, W.; Occhipinti, G.; Bultinck, P.; Jensen, V. R. Striking a Compromise: Polar Functional Group Tolerance versus Insertion Barrier Height for Olefin Polymerization Catalysts. *Organometallics* **2012**, *31*, 6022–6031.
(30) Lee, J. D. *Concise Organic Chemistry*; 5th ed.; Blackwell Science: Oxford, 2006.
(31) Foti, M. C.; Johnson, E. R.; Vinqvist, M. R.; Wright, J. S.; Barclay, L. R. C.; Ingold, K. U. Naphthalene Diols: A New Class of Antioxidants Intramolecular Hydrogen Bonding in Catechols, Naphthalene Diols, and Their Aryloxyl Radicals. *J Org. Chem.* **2002**, *67*, 5190–5196.
(32) Rozas, I.; Alkorta, I.; Elguero, J. Inverse Hydrogen-Bonded Complexes. *J. Phys. Chem. A* **1997**, *101*, 4236–4244.

(32) Delferro, M.; McInnis, J. P.; Marks, T. J. Ethylene Polymerization Characteristics of an Electron-Deficient Nickel(II) Phenoxyiminato Catalyst Modulated by Non-Innocent Intramolecular Hydrogen Bonding. *Organometallics* **2010**, *29*, 5040–5049.
(34) Funk, J. K.; Andes, C. E.; Sen, A. Addition Polymerization of Functionalized Norbornenes: The Effect of Size, Stereochemistry, and Coordinating Ability of the Substituent. *Organometallics* **2004**, *23*, 1680–1683.
(34) Young, R. J.; Lovell, P. A. *Introduction to Polymers, Second Edition*; Taylor & Francis, 1991.
(35) Ladipo, F. T.; Anderson, G. K. Convenient Method for the Synthesis of Chloro-Bridged Methylpalladium and Acetylpalladium(II) Dimers. *Organometallics* **1994**, *13*, 303–306.
(36) Rulke, R. E.; Ernsting, J. M.; Spek, A. L.; Elsevier, C. J.; Vanleeuwen, P. W. N. M.; Vrieze, K. NMR-Study on the Coordination Behavior of Dissymmetric Terdentate Trinitrogen Ligands on Methylpalladium(II) Compounds. *Inorg. Chem.* **1993**, *32*, 5769–5778.
(37) Bilger, C.; Demerseman, P.; Royer, R. Research on Nitro-Derivatives of Biological Interest .44. Synthesis of 2-Nitro-naphtho[1,2-B]furans Monomethoxylated on the External Homocycle. *Eur. J Med. Chem.* **1987**, *22*, 363–365.
(39) Cowell, D. B.; Mathieson, D. W. Synthetic Analogues of Adrenal Cortical Hormones - Some 6-7-8-9-Tetrahydro-4-5-Benzindanes. *J Pharm. Pharmacol.* **1957**, *9*, 549–557.
(40) SGE Analytical Science. Documents & Support: Capillary Column Selection Guide. Accessed August 27, 2013.
(41) Zhou, Z.; Kümmerle, R.; Qiu, X.; Redwine, D.; Cong, R.; Taha, A.; Baugh, D.; Winniford, B. A New Decoupling Method for Accurate Quantification of Polyethylene Copolymer Composition and Triad Sequence Distribution with 13C NMR. *J. Magn. Reson.* **2007**, *187*, 225–233.

Chapter 3. Dynamic Coupling at the Ångström Scale

3.1. Introduction

Research on active, self-powered systems has undergone grown tremendously in the past decade.[1-4] Work has focused on both improving and/or designing new, autonomous functional systems an on understanding the behaviors of active particles in response to both external stimuli and in situ perturbations. Typically, these systems involve microscale active particles that autonomously move and interact with each other, forming reversible assemblies in the presence of localized triggers.[5-8] An important aspect of the dynamics of such active assemblies is their effect on their immediate surroundings. These effects were previously thought to be insignificant, especially at smaller length scales, because viscosity overcomes inertial forces of active particles when in the low Reynold's number regime. However, studies conducted on micron-scale organisms and catalytic particles show that such active assemblies exert considerable influence over the motion of their surroundings.[9-16] Diffusion of inert tracer particles dispersed in a suspension of micron-scale swimmers is dependent upon the total activity of a system; the higher the total activity of the system, greater is the diffusion enhancement of the tracers.[10-12] The enhancement appears to be independent of swimming patterns and mechanisms, signifying the generic role of hydrodynamic coupling among the swimmers and their surroundings. This phenomenon is termed momentum transfer, in which the active particles enhances the diffusion of its environment.[11]

While much research has been conducted with micron-scale swimmers, little work has been performed on molecular, soluble swimmers. Recently, it was theorized that the advection effects induced by active molecular catalysts should also result in significant enhancement of diffusion of passive molecules present in solution.[17] In order to address this research gap, we

measured the diffusion of molecular tracers in a solution of Grubbs second generation catalysts non-invasively using diffusion-ordered nuclear magnetic resonance spectroscopy (DOSY-NMR).[18-21] In order to investigate momentum transfer at the angström level, we elected to study the ring closing metathesis (RCM) reaction of diethyl diallylmalonate (DDM) catalyzed by Grubbs second generation catalyst (hydrodynamic radius RH = 6 Å [22]). The reaction is well-understood, robust, and is easy to monitor via NMR over a reasonable time-scale, making it an acceptable model system. Upon metathesis, DDM is converted into the cyclic compound, 3-cyclopentene-1,1-diethylmalonate, and one molecule of ethene (Scheme 3-1). We had earlier demonstrated that substrate turnover at room temperature can substantially enhance the motion of Grubbs catalyst molecules in solution.[22] This observation is consistent with the recent proposal that angström-scale chemically-powered motors are capable of moving in a self-generated concentration gradient.[23] Our previous observation, coupled with the recent theoretical suggestion,[17] prompted us to quantify the collective effect of these molecular swimmers on their surroundings during catalysis. In our experiments, tetramethylsilane (TMS) and benzene were used as passive tracer particles (Scheme 3-1) and their diffusion was measured in the presence and absence of substrate turnover.

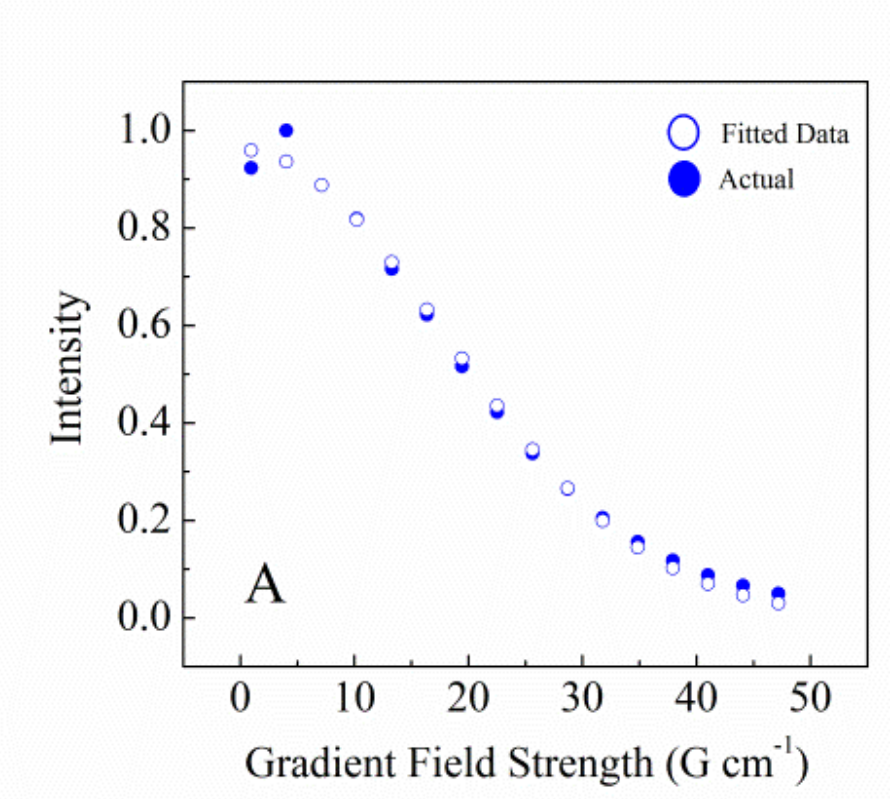

Figure 3-1. Typical curve-fitting for Diffusion NMR data

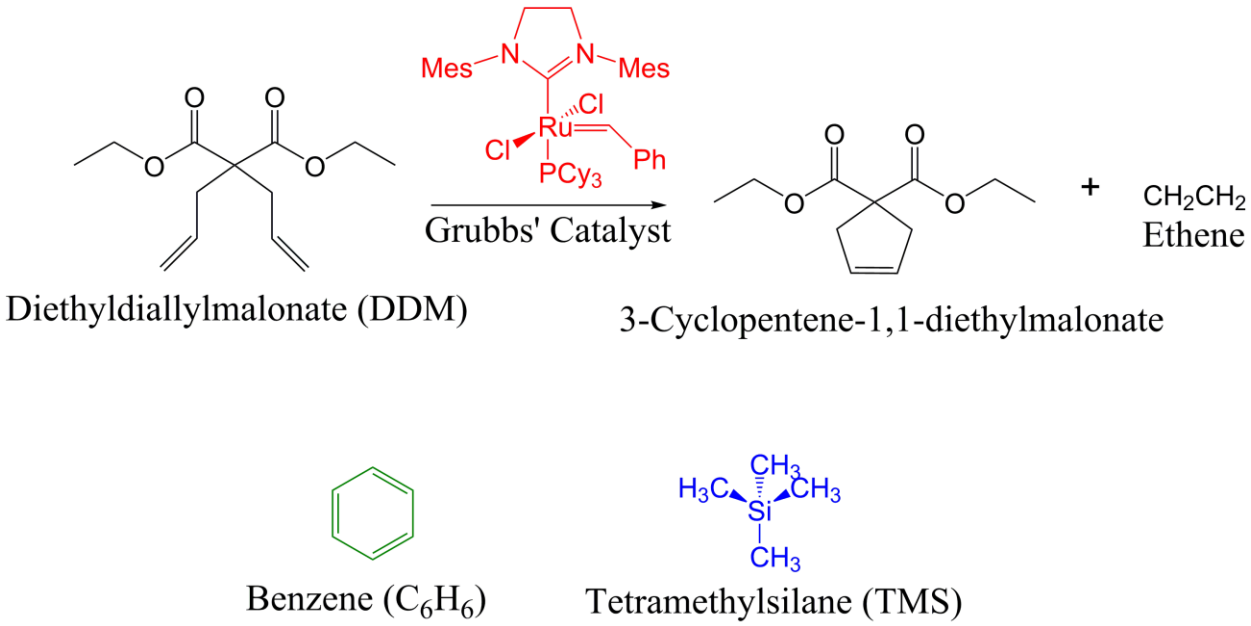

Scheme 3-1. Schematic of ring closing metathesis reaction of DDM by Grubbs 2nd generation catalysts. Upon metathesis, DDM is converted into the cyclic compound, 3-cyclopentene-1,1-diethylmalonate, and one molecule of ethene. Momentum transfer from active catalytic sites upon substrate turnover was quantified by measuring the diffusion of TMS and benzene in a solution of Grubbs catalyst at different DDM concentrations.

3.2. Results and Discussion

3.2.1. DOSY-NMR

The principle of DOSY-NMR spectroscopy has already been well-reviewed.[18-21] While the sample is in a static magnetic field of the spectrometer, it is subjected to a series of radio frequency gradient pulses of increasing strength. The gradient pulse effectively phase encodes (i.e. labels) the nuclear spins according to a molecule's position in solution. After the encoding gradient has been applied, molecules can freely diffuse through the solution for a specified period of time which is referred to as the diffusion delay time (Δ). A decoding gradient pulse is then applied for a set time (δ) to reverse the phase change applied by the encoding gradient. Molecules that diffuse to a different region of the sample during the delay time will not have their phase encoding (introduced by the first gradient pulse) reversed by the decoding gradient. As a result, the intensity I of the resonances of the molecule detected by the spectrometer will be attenuated. The stronger the gradient, the weaker the signal becomes. This decrease in intensity, or the degree of attenuation, is a function of the magnetic gradient pulse amplitude (G) and occurs at a rate proportional to the diffusion coefficient (D) of the molecule, as shown in Equation 3-1 below:

(Equation 3-1) $$\boldsymbol{I = I_o exp[-D(G\delta\gamma)^2(\Delta - \frac{\delta}{3})]}$$

Here, δ is the signal intensity in the absence of the gradient pulse and γ is the magnetogyric ratio of the nucleus of interest. The typical curve fit which is used to estimate the diffusion coefficient of tracers is shown in Figure 3-1.

3.2.2. Estimation of Tracer Radii and Diffusion Speed

The diffusion of the tracers of interest – TMS and benzene – can be estimated using the Stokes-Einstein equation:

Equation 3-2 $$\boldsymbol{D = \frac{kT}{6\pi\eta R}}$$

Here, D is the diffusion, T is the temperature, r is the hydrodynamic radius, η is the viscosity, and R is the hydrodynamic radius.

1) Hydrodynamic radii:
    a. The TMS radius was estimated to be 2.46×10^{-10} m via simulations using Gaussian 03 software, basis set B3LYP/6—31G(d).
    b. Benzene (C_6H_6) radius approximated to 1.33×10^{-10} m, taking into account carbon-carbon bond length to be 1.39×10^{-10} m ($R = \frac{6\times1.39\times10^{-10}\,\text{m}}{2\pi} = 1.33\times10^{-10}\,\text{m}$).
2) Calculating diffusion of tracers in a solution where no reaction takes place:

$$D_{\text{TMS}} = \frac{kT}{6\pi\eta R} = \frac{1.38\times10^{-23}\ \text{JK}^{-1}\times298\ \text{K}}{6\pi\times8.39\times10^{-4}\ \text{Pa.s}\times2.46\times10^{-10}\ \text{m}} = 1.06\times10^{-9}\ \text{m}^2/\text{s}$$

$$D_{\text{Benzene}} = \frac{kT}{6\pi\eta R} = \frac{1.38\times10^{-23}\ \text{JK}^{-1}\times298\ \text{K}}{6\pi\times8.39\times10^{-4}\ \text{Pa.s}\times1.33\times10^{-10}\ \text{m}} = 1.96\times10^{-9}\ \text{m}^2/\text{s}$$

3.2.3. Viscosity Measurements

Viscosity did not contribute to the changes in diffusion observed in the experimental samples in which catalytic turnover took place. To confirm our observation, we measured the viscosity of the Grubbs catalyst solution both as a function of substrate concentration and as function of time. The addition of 3 mM catalyst to the substrate solution did not change its viscosity significantly ($(8.68 \pm 0.27) \times 10^{-4}$ Pa.s without catalyst compared to $(8.39 \pm 0.28) \times 10^{-4}$ Pa.s with catalyst). Furthermore, when observed for a period of nearly 30 min, the viscosity of reacted mixture was approximately the same as that of the unreacted solution, signifying that the conversion of reactant to product does not influence the solution viscosity at any point during the reaction. Additional details of the viscosity measurements are provided in Appendix 7.1. Picosecond fluorescence anisotropy decay measurements were used to examine the rotational dynamics of a tracer fluorophore, allowing us to monitor changes in the local viscosity of a sample during the course of the reaction.[24] No significant changes in viscosity were observed in the measurements, as seen in Figure 3-2.

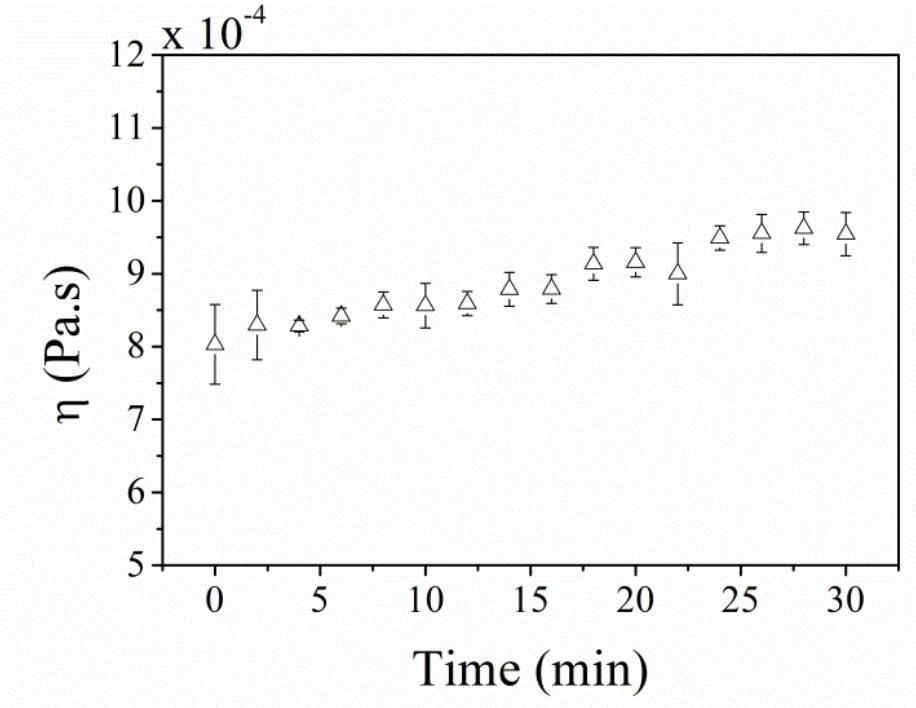

Figure 3-2. **Time dependent viscosity measurement of the experimental solution (3 mM catalyst + 1 M DDM) performed at constant shear rate 200 s^{-1}.** The error bars represent standard deviations corresponding to three independent set of measurements.

3.2.4. Ethene Measurements

To minimize the effect of convection due to possible solvent evaporation or escape of ethene, the experiments were performed in high-pressure, screw-capped NMR tubes. However, as shown in Figures 3-3 & 3-4, for the substrate concentration range used in the experiments, the diffusion coefficients were nearly the same in the closed and open systems. In addition, contrary to our observations, convection due to an ethene gradient should have resulted in similar enhancements in diffusion for both tracers and catalyst molecules.

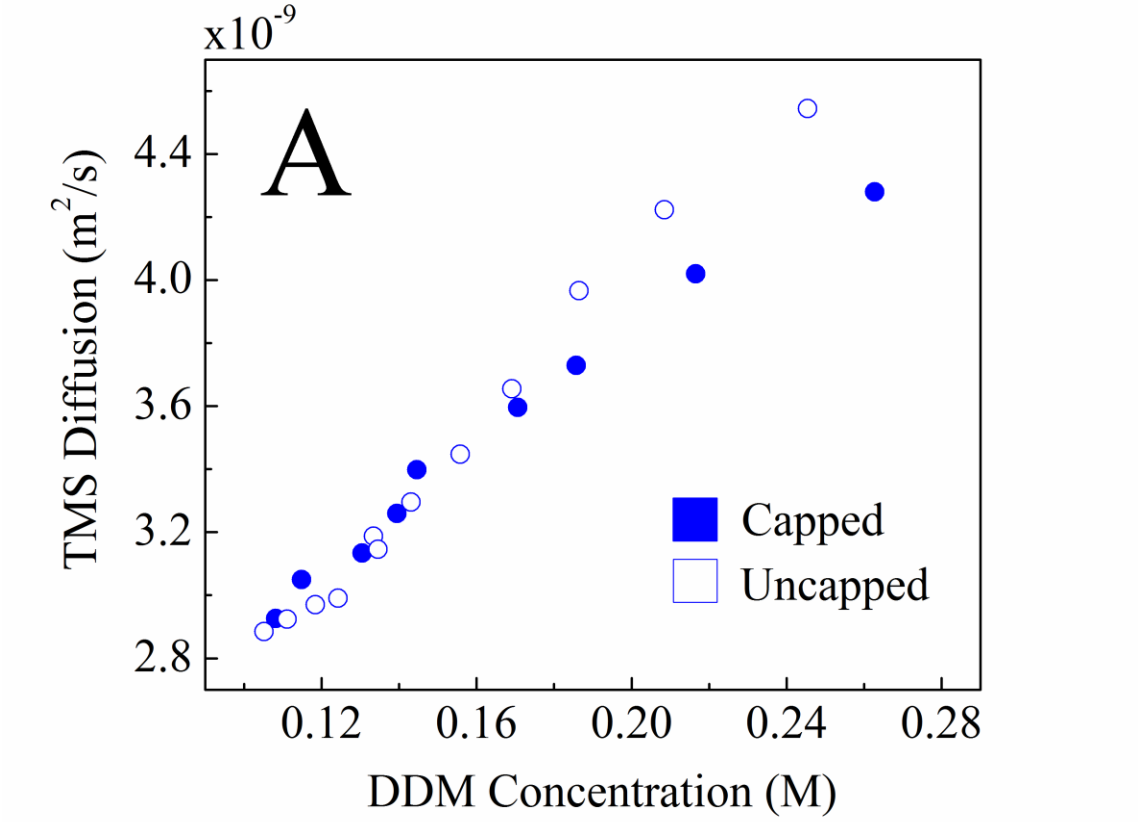

Figure 3-3. Diffusion of TMS measured in capped and open uncapped NMR tubes in the presence of 3 mM catalyst and 1 M DDM. For the substrate concentration range used in experiments, the diffusion coefficients were nearly the same under these two conditions. However at higher substrate concentrations, the diffusion of tracers measured in uncapped NMR tubes were significantly higher compared to that measured in the capped – signifying the effect of convection arising from the escape of ethene.

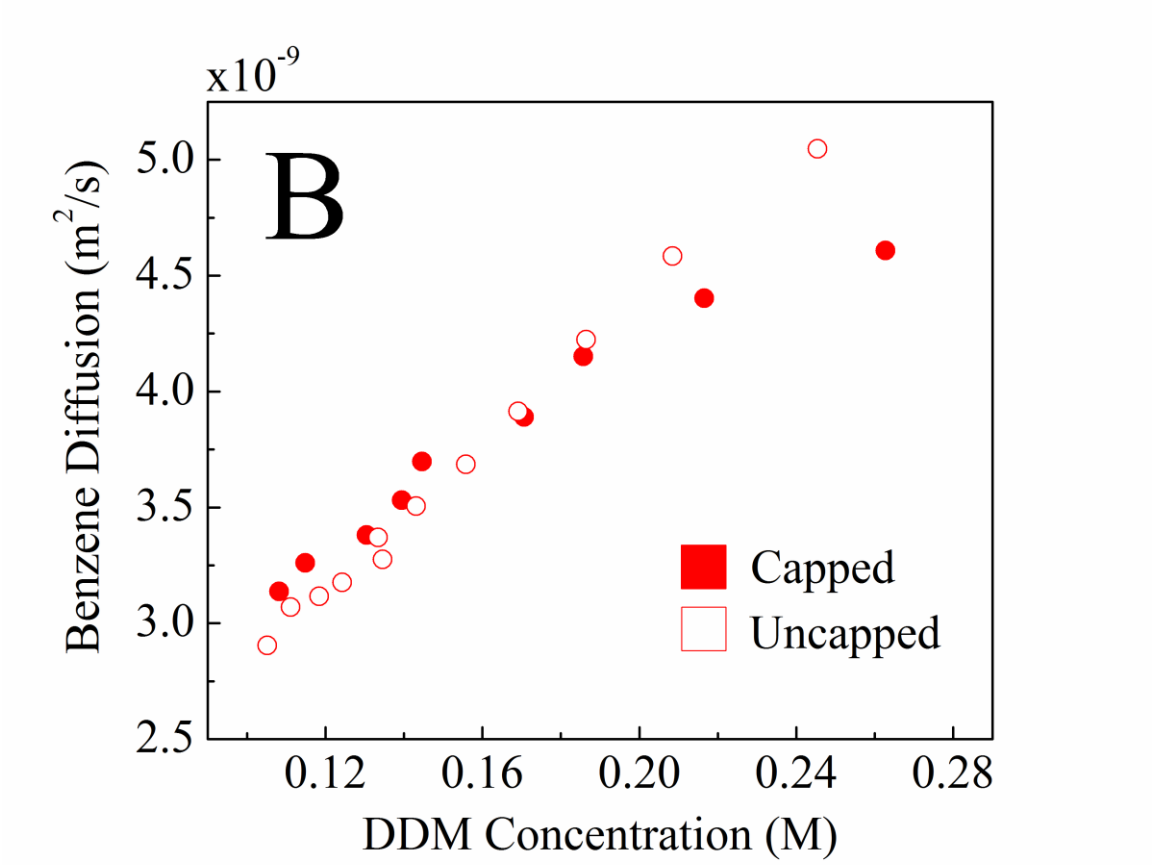

Figure 3-4. Diffusion of benzene measured in capped and open uncapped NMR tubes in the presence of 3 mM catalyst and 1 M DDM. For the substrate concentration range used in experiments, the diffusion coefficients were nearly the same under these two conditions. However at higher substrate concentrations, the diffusion of tracers measured in uncapped NMR tubes were significantly higher compared to that measured in the capped – signifying the effect of convection arising from the escape of ethene.

3.2.5. DOSY Measurements

The diffusion of both TMS and benzene measured in a suspension solution containing 3 mM Grubbs catalyst and various concentrations of DDM is shown in Figure 3-5. DDM concentrations were calculated using 1D ^{1}H-NMR spectroscopy, while tracer diffusions were simultaneously measured using 2D DOSY-NMR. In the absence of reaction, the diffusion coefficients of the tracers remained constant over time (D_{TMS} = (2.46 ± 0.01) × 10^{-9} m^2/s and $D_{Benzene}$ = (2.68 ± 0.02) × 10^{-9} m^2/s) and were comparable with the values estimated using the Stokes-Einstein equation in a previous section, 3.2.2. In contrast, in the presence of a reaction, the diffusion increased significantly. The reaction rate increases as a function of the substrate concentration, which in turn enhances tracer diffusion. Additionally, when an active sample containing catalyst and substrate was monitored for an extended period of time (> 5h), the tracers gradually returned to their Brownian (or base) diffusion values as the substrate was exhausted (Figure 3-6). These results strongly suggest that substrate turnover is responsible for the observed enhancement in tracer diffusion in our systems.

In addition to the passive tracers, we also measured the diffusion of the catalyst molecules under identical experimental conditions to quantify the diffusion enhancement of the swimmers themselves in the presence of reaction. In an active suspension solution, the catalyst molecules also behave as tracers for each other, because the motion of each molecule is influenced by its active neighbors. Figure 3-7 shows the diffusion of Grubbs catalysts measured at 3 mM catalyst and different DDM concentrations. Like the tracers, the diffusion of the catalysts at first increases significantly and then approaches the base value as the reaction progresses toward completion (Figure 3-8).

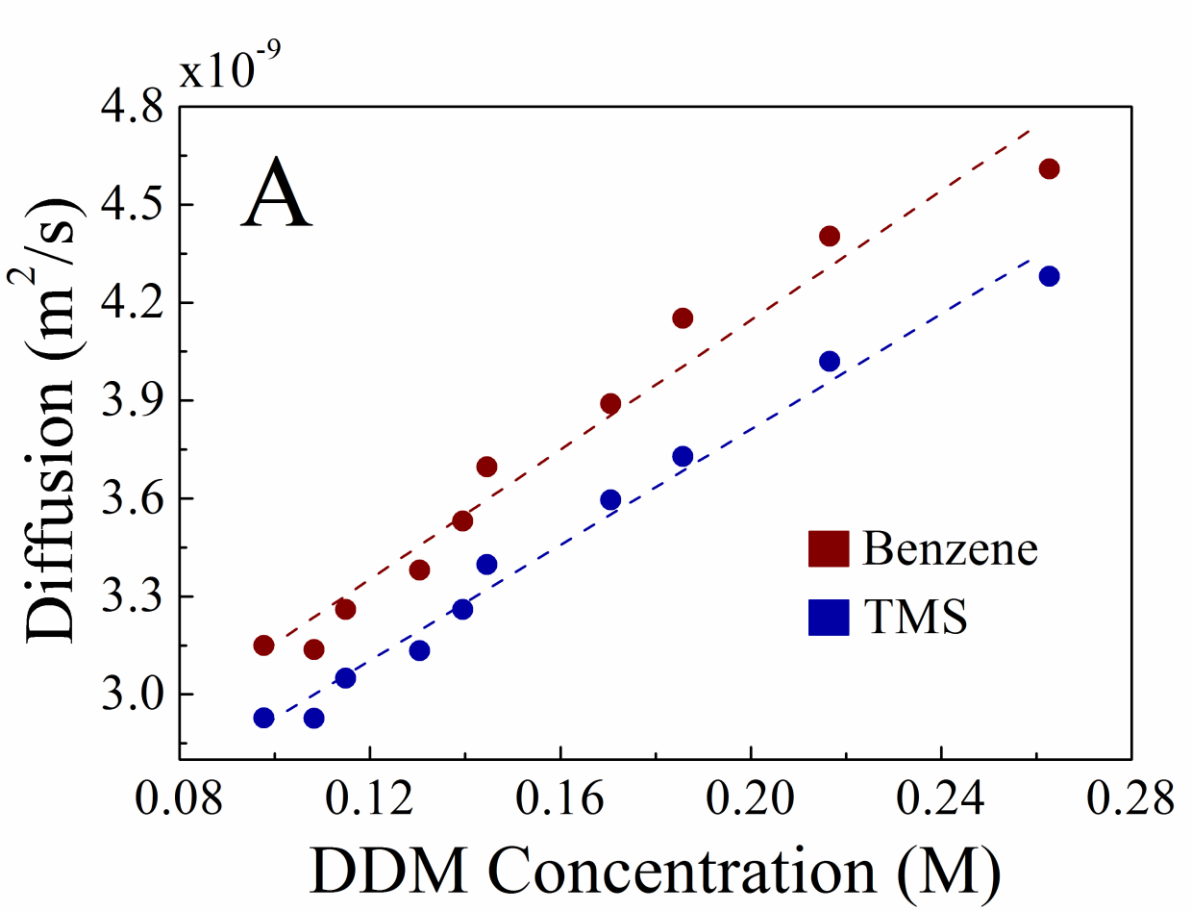

Figure 3-5. Measured diffusion of TMS and benzene as a function of substrate concentration. Diffusion coefficients of TMS and benzene measured in a solution containing 3 mM Grubbs catalyst plotted against changing DDM concentrations At higher concentrations of DDM, both the reaction rate and tracer diffusion increase significantly. The data presented are the average of three independent measurements with a maximum standard deviation of 2.78×10^{-10} m^2/s and 4.08×10^{-10} m^2/s, for TMS and benzene respectively.

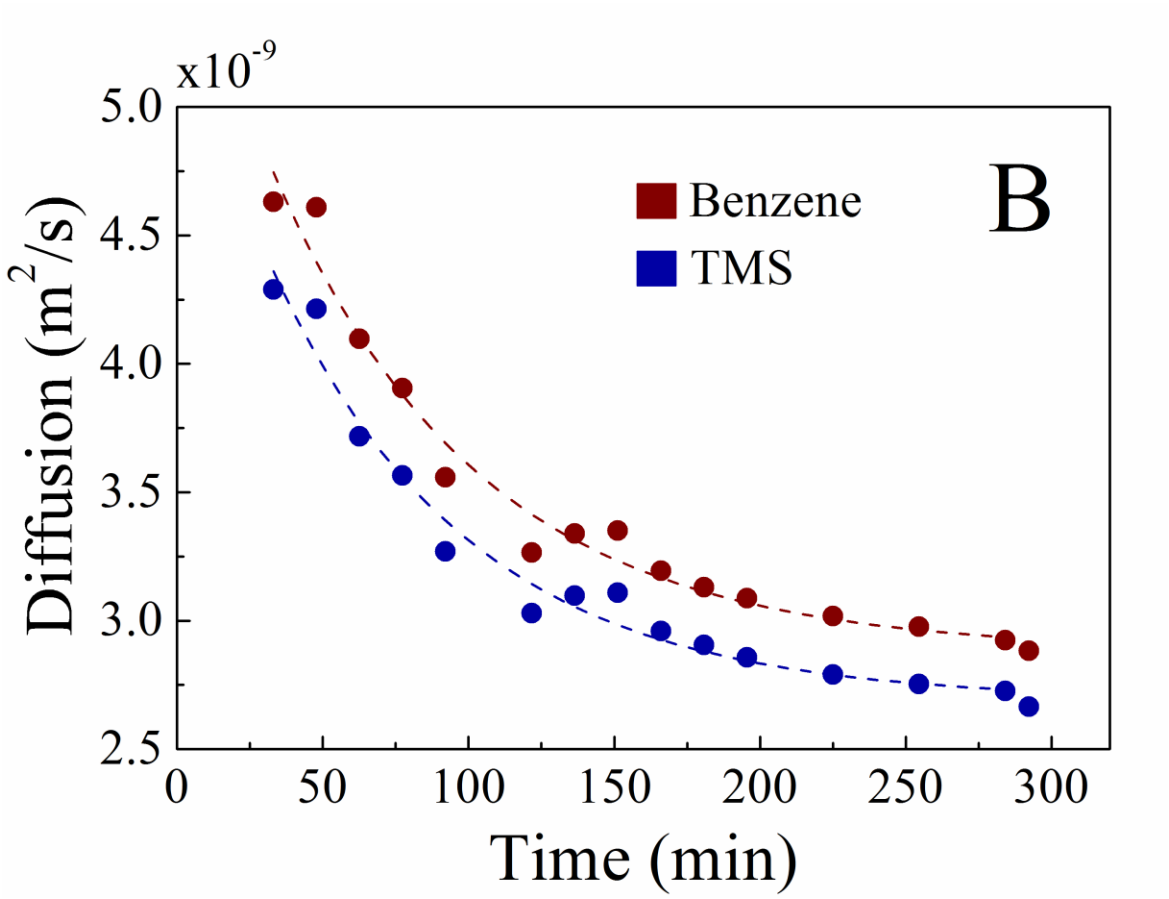

Figure 3-6. Measured diffusion of TMS and benzene as a function of substrate time. Time dependent decrease in diffusion of TMS and benzene in a solution of 3 mM Grubbs catalyst and 1 M DDM, monitored over an extended period of time. Upon completion of reaction, the diffusion values returns to base values, which are close to those measured in the absence of any reaction. The data presented are the average of three independent measurements with a maximum standard deviation of 2.62×10^{-10} m^2/s and 3.78×10^{-10} m^2/s, for TMS and benzene respectively.

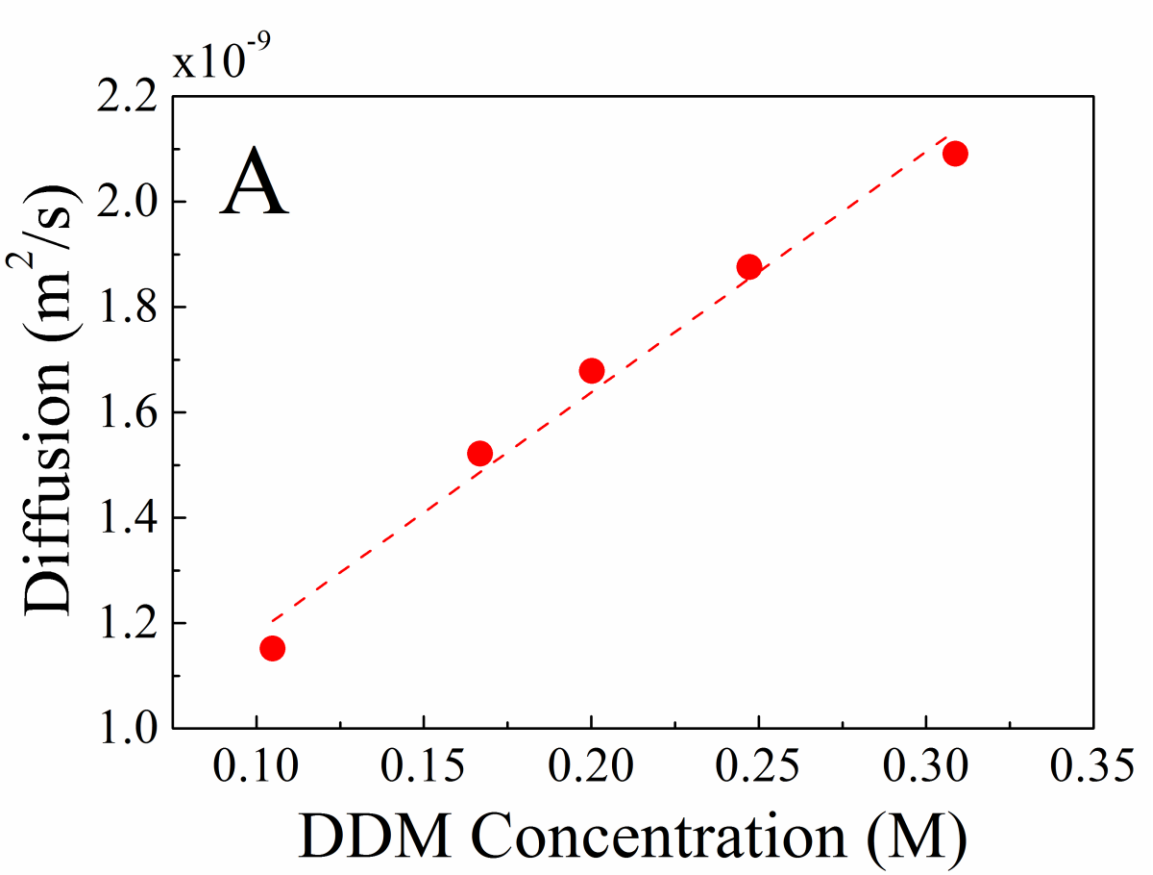

Figure 3-7. Measured diffusion of Grubbs catalyst as a function of substrate concentration. Diffusion of 3 mM Grubbs catalysts measured as a function of DDM concentration. The diffusion of the catalysts increases with increasing substrate concentration. The data presented are the average of three independent measurements with a maximum standard deviation of 3.03 $\times 10^{-10}$ m^2/s.

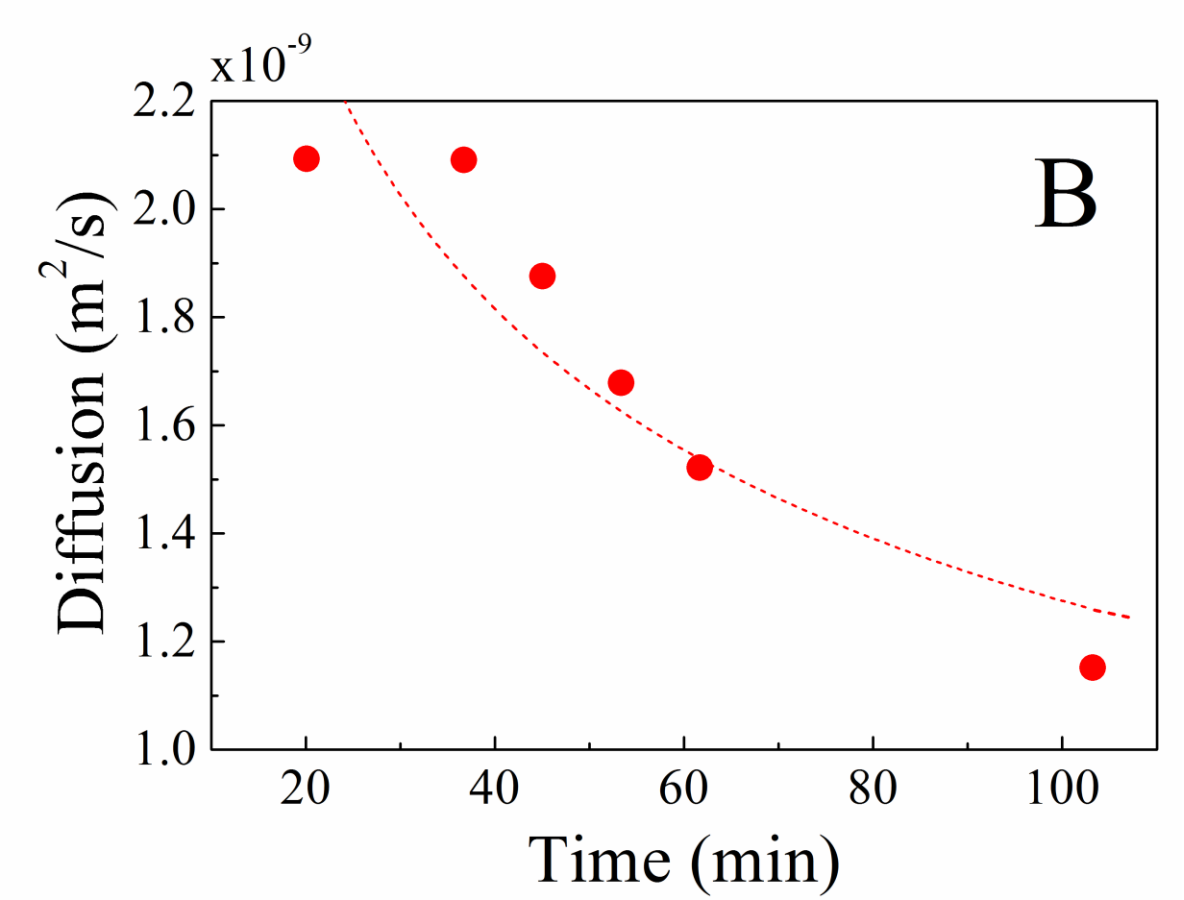

Figure 3-8. Measured diffusion of Grubbs catalyst as a function of time. Decrease in catalyst diffusion over time as the reaction proceeds towards completion in which the starting substrate concentration was 1 M. The data presented are the average of three independent measurements with a maximum standard deviation of 2.39×10^{-10} m^2/s.

3.2.6. Comparison of the diffusion of swimmers and tracers varying size

The diffusion values of both TMS and benzene increase monotonically with higher concentrations of substrate, a phenomenon that is consistent with previous observations on the advective displacement of particles by active microswimmers.[10-12] What makes the present system unique is that Grubbs catalyst is the smallest self-powered system to display dynamic coupling and control over tracer diffusion via catalytic turnover. Higher reaction rate resulted in an increased rate of net momentum transfer to the passive tracers thereby enhancing their overall diffusion. Miño et al. measured the tracer diffusion with increased number densities of microscopic swimmers (bacteria and self-propelled bimetallic rods) and found a linear dependence of the former on the total active flux of the system (defined as the product of number density and average ballistic speed of the swimmers).[11] Similarly, Kurtuldu et al. showed a linear relationship between the volume fraction of the active algal cells and diffusion of passive tracers suspended therein.[12] Both these systems show a direct dependence of tracer diffusivity on the total number of active events occurring in the system. Remarkably, even at the angström scale the diffusion of tracer molecules follows a similar trend, showing the generic influence of hydrodynamic coupling in transferring momentum around active swimmers and the scalability of this phenomenon down to the molecular level.

Our diffusion results can be used to draw a correlation between the behavior of active swimmers in a range of length scale and their effect on the surroundings. Following the definition proposed by Miño et al.[11], we calculated the active flux (J_A) in our system for Grubbs' molecular catalysts, where:

Equation 3- 3

$$J_A = \textbf{number density of active molecules} \times \textbf{ballistic speed } (\boldsymbol{U})$$

The ballistic speed *U* of the catalyst molecules at different substrate concentrations was obtained from their net change in diffusion and value of rotational diffusion coefficient using the following relation:

Equation 3-4 $$\Delta \boldsymbol{D} = \frac{\boldsymbol{U^2}}{\boldsymbol{6D_r}}$$

Here, ΔD is the change in diffusion of a swimmer and D_r is its rotational diffusion coefficient that is related to its radius R, which can be obtained from:

Equation 3-5 $$\Delta \boldsymbol{D} = \frac{\boldsymbol{kT}}{\boldsymbol{8\pi\eta R^3}}$$

In this equation, *k*, *T* and η are Boltzmann's constant, temperature and viscosity of the system, respectively. [25]

As shown in Figure 3-9, the diffusion coefficients of TMS, benzene and the Grubbs catalyst plotted against the active flux of the catalyst follow linear profiles. We also calculated the ballistic speed of the enzyme urease – another low Reynolds' number swimmer – at different concentrations of its substrate urea, using previously published data.[26] The behavior in the angstrom scale systems, are similar to that reported for systems containing active micron-scale swimmers, where the tracer diffusion (D_T) was found to vary linearly with the active flux (J_A) [11]. The relation between D_T and J_A can be defined as:

Equation 3- 6 $$\boldsymbol{D_{effective} = D_{tracer}^{brownian} + \beta \times J_A}$$

Here, $D_{tracer}^{brownian}$ corresponds to normal Brownian diffusion of the tracers and β defined as the interaction length scale, the physical significance of which remains to be established. We found that the interaction length scale decreases somewhat with increasing size of the swimmers (5.51

$\times 10^{-9}$ m^2/s for benzene, 5.36×10^{-9} m^2/s for TMS, and 4.74×10^{-9} m^2/s for Grubbs catalyst as seen in the inset bar graph of Figure 3-10.

The scalability in behavior of the active swimmers towards their surroundings can be assessed by comparing the interaction length scale values. The β values of bacteria and catalytic rods have been reported by Miño et al. to be 1.5 μm and 1.9 μm, respectively. For Grubbs molecular catalyst, we can consider the average β value (measured for three different tracers) to be 5.20 nm; that calculated for urease is 72 nm. Remarkably, the β values vary linearly with the dimension of the active swimmers (Figure 3-10), suggesting that they affect their surroundings similarly, irrespective of their mechanism of energy transduction and propulsion.

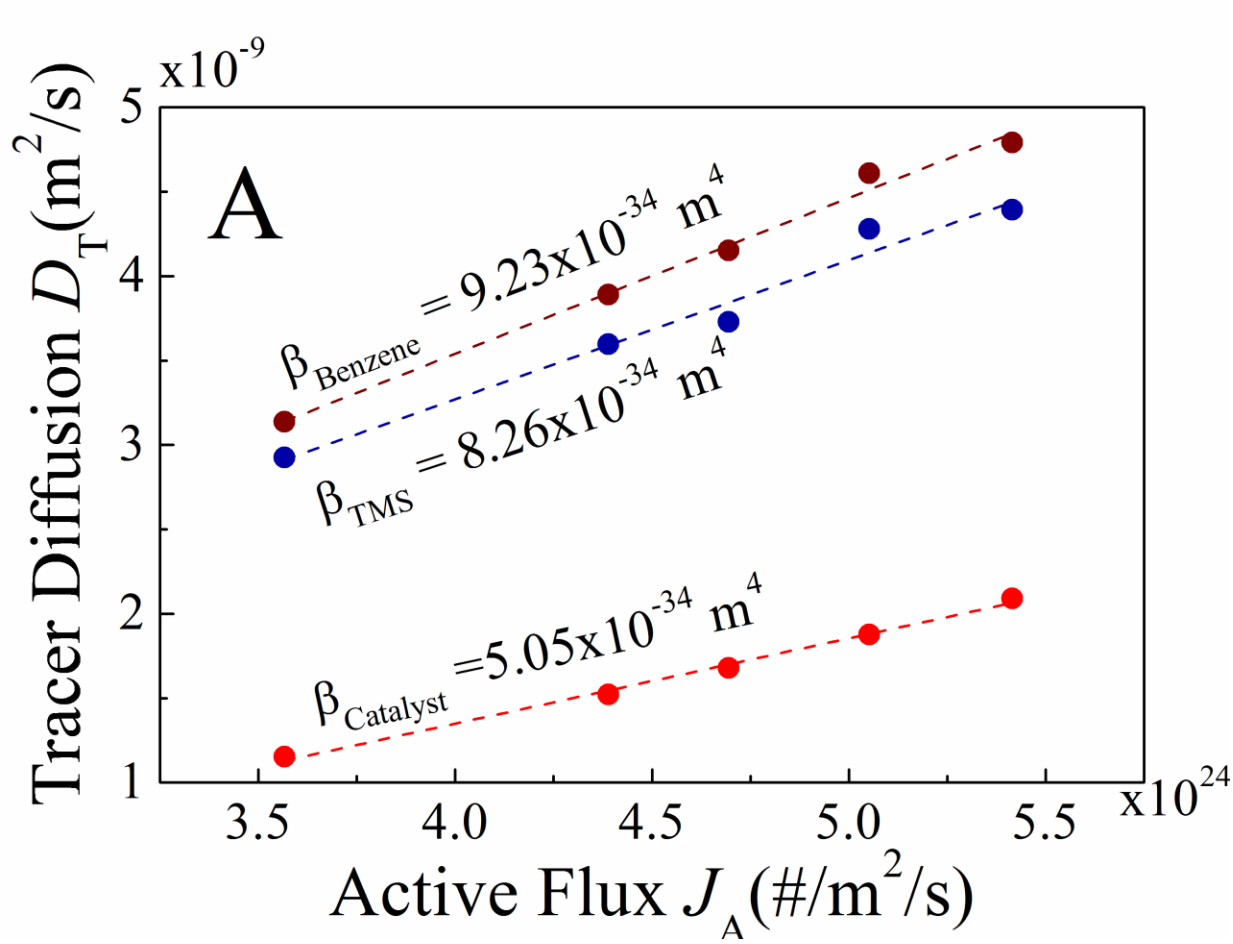

Figure 3-9. Generic behavior of active swimmers in transferring momentum to their surroundings. Change in tracer and catalyst diffusion as a function of total active flux of the system. The active flux was calculated using the number density of catalyst and ballistic speeds of swimmers at different substrate concentrations. For the angström-size tracers, the diffusion changed linearly with the active flux, similar to what was observed in systems with micron-scale swimmers.

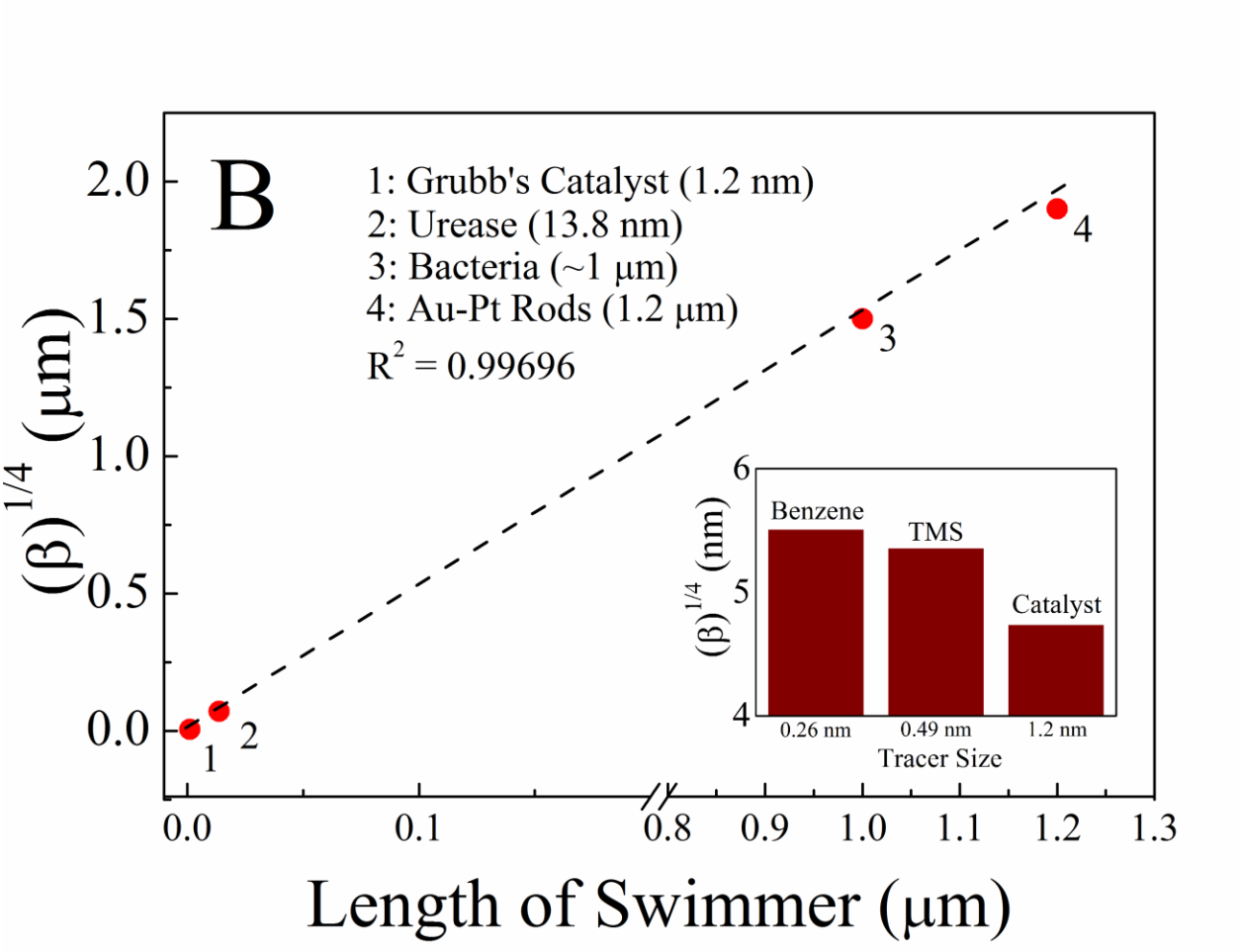

Figure 3-10. Generic behavior of active swimmers in transferring momentum to their surroundings. Variation of interaction length scales calculated (and taken from literature) for swimmers of different sizes. The results show that the active swimmers transfer momentum to their surroundings similarly over a wide range of swimmer dimensions. The inset shows how the interaction length scales calculated for different molecular tracers change with their size under the influence of the same molecular swimmer (Grubbs catalyst).

3.3. Experimental

3.3.1. NMR Measurements and Data Analysis

All ^{1}H-spectra were recorded on the HD-500 NMR spectrometer which was operated at 500.2 MHz. Measurements were taken using a liquid nitrogen cooled cryoprobe (5 mm CPPBBO) at 298 K and the data was processed using TopSpin v. 3.2. For samples containing active catalyst, 2D DOSY and 1D ^{1}H-NMR spectra were alternatively recorded for a period of 3 h. The former was used to monitor both tracer and catalyst diffusion, while the latter was used to record the consumption of DDM and reaction progress over time. In order to ensure there were enough points to monitor the decrease in diffusion during the course of the reaction, the diffusion of the tracers and of the catalyst were recorded separately.

3.3.2. ^{1}H Diffusion Ordered Spectroscopy (DOSY-NMR)

NMR parameters for the diffusion experiments were as follows: (1) Tracer diffusion of both TMS (0 ppm) and benzene (7.16 ppm) were recorded simultaneously using the longitudinal eddy current delay (LED) pulse sequence with bipolar gradient pulse pair and 2 spoil gradients: pulprog = ledbpgp2s, 16 slices, td = 4K, sw = 10 ppm, o1p = 4 ppm, ns/ds = 2/4, D1 = 10 sec, aq = 0.410 sec, δ (p30) = 1800 μs, Δ (D20) = 30 ms. (2) Slightly different parameters were used to record catalyst (2.31 ppm, mesityl groups of N-heterocyclic carbene ligand) diffusion: pulprog = ledbpgp2s, 16 slices, td = 2K, sw = 1 ppm, o1p = 2 ppm, ns/ds = 4/4, D1 = 3.65 sec, aq = 2 sec, δ (p30) = 3000 μs, Δ (D20) = 25 ms.

A delay (D21) of 5 ms was used for eddy current reduction. The maximum gradient strength produced in the z direction was 5.35 Gcm^{-1}. The duration of the magnetic field pulse gradients (δ) was optimized for each diffusion time (Δ) in order to obtain a 2% residual signal

with the maximum gradient strength. The pulse gradients were incremented from 2 to 95% of the maximum gradient strength in a linear ramp. The temperature was set and controlled to 298 K with a gas flow of 350 L h^{-1} in order to avoid any temperature fluctuations due to sample heating during the magnetic field pulse gradients.

3.3.3. ^{1}H Diffusion Ordered Spectroscopy (DOSY-NMR)

Substrate concentration was monitored by recording the disappearing DDM peak at 2.74 ppm (allylic hydrogens) using the terminal ethyl hydrogens (0.915 ppm) as an internal standard; parameters were: pulprog = zg30, ns/ds = 2/4, 90º pulse angle (10.13 μs), D1 = 17 sec to ensure quantitative results, aq = 0.454 sec, sw = 10 ppm, olp = 4 ppm. A polynomial fourth-order function was applied for base-line correction in order to achieve accurate quantitative measurements upon integration of signals of interest. The spectra were acquired without spinning the NMR tube in order to avoid artifacts, such as spinning side bands of the first or higher order. Chemical shifts are reported in ppm from TMS ($\delta = 0$).

3.3.4. Viscosity Measurements

The viscosity of experimental solutions was measured using a Rheometrics Fluids Spectrometer II (Rheosource Series, Patel Scientific) at 25.0 °C. The measurement involved shearing a thin film (0.3 mm) of liquid between two coaxial cylinders and sweeping shear rate from 50 to 350 s^{-1}. The solutions were all found to be Newtonian and for each measurement, averages of three consecutive experimental observations are reported in the manuscript. Also, time dependent viscosity measurement of the experimental solution (3 mM catalyst + 1 M DDM) showed that the viscosity of reacted mixture was approximately the same as that of the unreacted

solution, signifying that the conversion of reactant to product does not influence the solution viscosity at any point during the reaction. The measurements were done at a constant shear rate 200 s^{-1} and can be seen in section 3.2.3.

3.3.5. Active Flux Calculation for Grubbs Catalyst

Following the definition proposed by Miño et al.,[11] we calculate the active flux (J_A) in our system by estimating the number density of catalyst molecules (n_A in # m^{-3}) and ballistic speed of each catalyst molecule (u_A in ms^{-1}).

(1) The catalyst concentration in our system is 3×10^{-3} mols/L = 3 mols/m^3. Therefore, number density of swimmers is $n_A = 3\times6.023\times10^{23}$ $m^{-3} = 1.81\times10^{24}$ m^{-3}.

(2) To calculate the average ballistic speed of the catalyst molecule, we use the relation $\Delta D = \frac{u_A^2}{6D_r}$,[25] where ΔD is the change in diffusion of a catalyst and D_r is its rotation diffusion coefficient, which is related to its radius R as $D_r = \frac{kT}{8\pi\eta R^3}$.

(3) In this equation k, T and η are Boltzmann constant, temperature and viscosity of the system. For Grubbs catalyst, $R = 6\times10^{-10}$ m and therefore the rotational diffusion coefficient at room temperature ($\eta = 8.39\times10^{-4}$ Pa-s) is estimated to be $D_r = 9.03\times10^{8}$ s^{-1}.

Using this value and the measured diffusion of the catalysts at various substrate concentrations, the ballistic speeds of the catalyst molecules were calculated. The active fluxes at different substrate concentrations were then estimated by multiplying ballistic speeds of swimmers and their number density in the system (Table 3-1).

Table 3-1. Active flux calculations for different concentrations of DDM.

DDM (M)	Reaction Rate (M/s)	Catalyst Diffusion (m^2/s)	Change in Catalyst Diffusion (m^2/s)	Ballistic Speed u_A (ms^{-1})	Active Flux ($\#/m^2s$)
3.09E-01	2.37E-4	2.09E9	1.66E9	3.00	5.42E24
2.47E-01	1.23E-4	1.88E9	1.44E9	2.80	5.05E24
2.00E-01	9.44E-5	1.68E9	1.25E9	2.60	4.69E24
1.67E-01	6.68E-5	1.52E9	1.09E9	2.43	4.39E24
1.05E-01	2.48E-5	1.15E9	7.19E10	1.97	3.57E24

3.4. Conclusion

The experimental observations demonstrate transfer of momentum from the active catalyst molecules to the surrounding medium. As discussed previously,[22] the enthalpy change for the ring-closing metathesis of DDM is approximately +8 kcal/mol (endothermic) and therefore cannot contribute to the observed enhanced diffusion of the tracers. The most plausible mechanism involves reaction-generated advection caused by active force dipoles (catalyst molecules) "stirring" the solution.[17] Moreover, there are reports on the existence of nonlinear instabilities in fluids above some critical flow threshold, even when the system is expected to belinear and dominated by viscous drag.[27-28] The system with Grubbs catalyst may follow similar physics, wherein disturbances originating from the catalyst surface are propagated throughout the system, thereby changing its overall dynamics. Moreover, owing to the comparable dimensions of the solvent, catalyst and tracer molecules, the solvent may facilitate transfer of kinetic energy to the tracers, distributing the total momentum across the entire system immediately after the localized catalytic events.

In conclusion, we have demonstrated transfer of momentum from active, angström-sized catalysts to their immediate surroundings by monitoring the change in diffusion of molecular tracers present in a system undergoing catalytic substrate turnover. The diffusion enhancement is correlated with the total activity of the system, which has been previously observed in systems containing micron-scale swimmers. Interestingly, the enhancement is independent of the swimming mechanism, signifying the generic role of hydrodynamic coupling between the swimmers and their surroundings. Our observations are consistent with the recent prediction of long-range hydrodynamic effects due to active force dipoles "stirring" the medium.[17] This model also predicts a linear dependence of diffusion enhancement on substrate concentration as is

observed in our system. The results described open up a new area of mechanochemistry: intrinsic force generation by molecular-scale catalysts. The catalysis-induced force generation may be sufficient for the recently reported stochastic motion of the cytoplasm and for the convective transport of fluid in cells.[29, 30] Momentum transfer at the angström scale not only provides novel insights into the dynamics of low Reynolds number systems but offers opportunities for controlled mass and energy transfer, and mixing at the molecular scales by generation of in situ perturbations.

3.5. References

(1) Duan, W.; Liu, R.; Sen, A. Transition between Collective Behaviors of Micromotors in Response to Different Stimuli. *J. Am. Chem. Soc.* **2013**, *135*, 1280–1283.
(2) Sánchez, S.; Soler, L.; Katuri, J. Chemically Powered Micro- and Nanomotors. *Angew. Chem. Int. Ed.* **2015**, *54*, 1414–1444.
(3) Wang, J. Nanomachines Fundamentals and Applications. Wiley, Hoboken, 2013.
(4) Colberg, P. H.; Reigh, S. Y.; Robertson, B.; Kapral, R. Chemistry in Motion: Tiny Synthetic Motors. *Acc. Chem. Res.* **2014**, *47*, 3504–3511.
(5) Wang, W.; Duan, W.; Ahmed, S.; Sen, A.; Mallouk, T. E. From One to Many: Dynamic Assembly and Collective Behavior of Self-Propelled Colloidal Motors. *Acc. Chem. Res.* **2015**, *48*, 1938–1946.
(6) Solovev, A. A.; Sanchez, S.; Schmidt, O. G. Collective Behaviour of Self-Propelled Catalytic Micromotors. *Nanoscale* **2013**, *5*, 1284–1293.
(7) Xu, T.; Soto, F.; Gao, W.; Dong, R.; Garcia-Gradilla, V.; Magaña, E.; Zhang, X.; Wang, J. Reversible Swarming and Separation of Self-Propelled Chemically Powered Nanomotors under Acoustic Fields. *J. Am. Chem. Soc.* **2015**, *137*, 2163–2166.
(8) Saintillan, D.; Shelley, M. J. Emergence of Coherent Structures and Large-Scale Flows in Motile Suspensions. *J. R. Soc. Interface* **2012**, *9*, 571–585.
(9) Wu, X.-L.; Libchaber, A. Particle Diffusion in a Quasi-Two-Dimensional Bacterial Bath. *Phys. Rev. Lett.* **2000**, *84*, 3017–3020.
(10) Leptos, K. C.; Guasto, J. S.; Gollub, J. P.; Pesci, A. I.; Goldstein, R. E. Dynamics of Enhanced Tracer Diffusion in Suspensions of Swimming Eukaryotic Microorganisms. *Phys. Rev. Lett.* **2009**, *103*, 198103.
(11) Miño, G.; Mallouk, T. E.; Darnige, T.; Hoyos, M.; Dauchet, J.; Dunstan, J.; Soto, R.; Wang, Y.; Rousselet, A.; Clement, E. Enhanced Diffusion due to Active Swimmers at a Solid Surface. *Phys. Rev. Lett.* **2011**, *106*, 048102.
(12) Kurtuldu, H.; Guasto, J. S.; Johnson, K. A.; Gollub, J. P. Enhancement of Biomixing by Swimming Algal Cells in Two-Dimensional Films. *Proc. Natl. Acad. Sci. USA* **2011**, *108*, 10391–10395.
(13) Kim, M. J.; Breuer, K. S. Enhanced Diffusion due to Motile Bacteria. *Phys. Fluids* **2004**, *16*, L78–L81.
(14) Jepson, A.; Martinez, V. A.; Schwarz-Linek, J.; Morozov, A.; Poon, W. C. K. Enhanced Diffusion of Nonswimmers in a Three-Dimensional Bath of Motile Bacteria. *Phys. Rev. E* **2013**, *88*, 041002.
(15) Miño, G. L.; Dunstan, J.; Rousselet, A.; Clément, E.; Soto, R. Induced Diffusion of Tracers in a Bacterial Suspension: Theory and Experiments. *J. Fluid Mech.* **2013**, *729*, 423–444.
(16) Orozco, J.; Jurado-Sánchez, B.; Wagner, G.; Gao, W.; Vazquez-Duhalt, R.; Sattayasamitsathit, S.; Galarnyk, M.; Cortés, A.; Saintillan, D.; Wang, J. Bubble-Propelled Micromotors for Enhanced Transport of Passive Tracers. *Langmuir* **2014**, *30*, 5082–5087.
(17) Mikhailov, A. S.; Kapral, R. Hydrodynamic Collective Effects of Active Protein Machines in Solution and Lipid Bilayers. *Proc. Natl. Acad. Sci.* **2015**.
(18) Price, W. S. Pulsed-Field Gradient Nuclear Magnetic Resonance as a Tool for Studying Translational Diffusion: Part 1. Basic Theory. *Concepts Magn. Reson.* **1997**, *9*, 299–336.

(19) Price, W. S. Pulsed-Field Gradient Nuclear Magnetic Resonance as a Tool for Studying Translational Diffusion: Part II. Experimental Aspects. *Concepts Magn. Reson.* **1998**, *10*, 197–237.
(20) Price, K.; Lucas, L.; Larive, C. Analytical Applications of NMR Diffusion Measurements. *Anal. Bioanal. Chem.* **2004**, *378*, 1405–1407.
(21) Nicolay, K.; Braun, K. P. J.; Graaf, R. A. de; Dijkhuizen, R. M.; Kruiskamp, M. J. Diffusion NMR Spectroscopy. *NMR Biomed.* **2001**, *14*, 94–111.
(22) Pavlick, R. A.; Dey, K. K.; Sirjoosingh, A.; Benesi, A.; Sen, A. A Catalytically Driven Organometallic Molecular Motor. *Nanoscale* **2013**, *5*, 1301–1304.
(23) Colberg, P. H.; Kapral, R. Ångström-Scale Chemically Powered Motors. *EPL Europhys. Lett.* **2014**, *106*, 30004.
(24) Heitz, M. P.; Maroncelli, M. Rotation of Aromatic Solutes in Supercritical CO2: Are Rotation Times Anomalously Slow in the Near Critical Regime? *J. Phys. Chem. A* **1997**, *101*, 5852–5868.
(25) Golestanian, R.; Ajdari, A. Stochastic Low Reynolds Number Swimmers. *J. Phys. Condens. Matter* **2009**, *21*, 204104.
(26) Muddana, H. S.; Sengupta, S.; Mallouk, T. E.; Sen, A.; Butler, P. J. Substrate Catalysis Enhances Single-Enzyme Diffusion. *J. Am. Chem. Soc.* **2010**, *132*, 2110–2111.
(27) Pan, L.; Morozov, A.; Wagner, C.; Arratia, P. E. Nonlinear Elastic Instability in Channel Flows at Low Reynolds Numbers. *Phys. Rev. Lett.* **2013**, *110*, 174502.
(28) Almarcha, C.; Trevelyan, P. M. J.; Grosfils, P.; De Wit, A. Chemically Driven Hydrodynamic Instabilities. *Phys. Rev. Lett.* **2010**, *104*, 044501.
(29) Guo, M.; Ehrlicher, A. J.; Jensen, M. H.; Renz, M.; Moore, J. R.; Goldman, R. D.; Lippincott-Schwartz, J.; Mackintosh, F. C.; Weitz, D. A. Probing the Stochastic, Motor-Driven Properties of the Cytoplasm Using Force Spectrum Microscopy. *Cell* **2014**, *158*, 822–832.
(30) Parry, B. R.; Surovtsev, I. V.; Cabeen, M. T.; O'Hern, C. S.; Dufresne, E. R.; Jacobs-Wagner, C. The Bacterial Cytoplasm Has Glass-like Properties and Is Fluidized by Metabolic Activity. *Cell* **2014**, *156*, 183–194.

Chapter 4. Organometallic Polymerization Pumps

4.1. Introduction

Researchers have been actively studying motion at the nanoscale due to its potential applications in biology, chemistry, and physics. Our group and our collaborators have selected microscaled, reactive systems to serve as nanopumps, objects that are capable of generating enough force to create detectable movements in their immediate surroundings. We have studied a multitude of unique systems; examples of nanopumps include depolymerizable poly(phthalaldehyde) [1], a UV-triggered photoacid [2], rechargeable host-guest azobenzene hydrogels [3], and most recently, enzyme-powered nanocapsules[4].

Thus far, however, no studies have been performed using organometallic pumps. What makes organometallic catalysts particularly interesting is the size of the catalyst – the catalyst can be measured in angstroms, making it the smallest pump studied thus far. A second point of interest in using organometallic catalysts to power nanoscale pumping is that numerous organometallic catalysts, which are well-studied and understood, exist. Different reaction mechanisms exist can be harnessed to power pumps in different environments, using various fuels/substrates, and using different mechanistic triggers.

In this study, we observe the pumping of a solid-supported Grubbs' catalyst in the presence of two substrates, norbornene (NB) and diethyl diallymalonate (DDM). Grubbs' catalyst is an excellent choice for many reasons: the catalyst is well-studied [5], relatively air-stable within the time constraints of the experiment, can catalyze reactions at room temperature, can be used to catalyze a wide range of reactions with different substrates, and has already been effectively used to power the motion of micron-sized Janus particles [6].

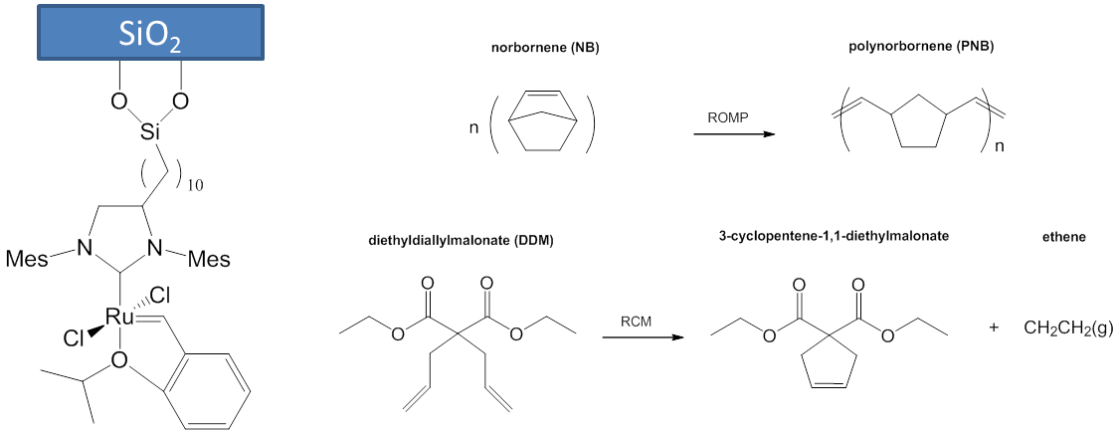

Figure 4-1. A representation of the anchored Grubbs' catalyst and the norbornene and diethyl diallylmalonate reactions the catalyst catalyzes.

4.2. Results and Discussion

In our experiments, we have observed that Grubbs' pumps react *differently* when exposed to norbornene or DDM. In the presence of norbornene, the pumps pull fluid inwards while in the presence DDM, the pumps push fluid outwards.

Norbornene, ROMP. In the presence of Grubbs' catalyst, norbornene undergoes ring opening metathesis (ROMP), forming polynorbornene. Norbornane, a fully saturated analog of norbornene, can be used as a control substrate to determine whether or not enhanced diffusion around the pumps occurs in the presence of polymerizing norbornene. The control shows that there is no observable directional flow in regards to the pump (Figure 4-2). In contrast, in the presence of the substrate norbornene, there is a strong flow of towards the pump over time (Figure 4-3). The direction of the flow towards the pump is characteristic for several concentrations of norbornene (0.01M, 0.10M, 0.25M). Without taking viscosity into account, the average velocity of the silica tracers ranges from 0.90 – 0.10 μm/second (Table 4-1).

DDM, RCM. In the presence of Grubbs' catalyst, DDM undergoes ring closing metathesis (RCM), forming two products – 3-cyclopentene-1-dimethylmalonate and ethene. (Figure 4-1). Ethene is a gas, but is highly soluble in organic solvents, so no bubble formation is observed for the duration of the experiments. The control for the DDM reaction – beads in TCE – again shows no specific movement towards the pump, similar to the behavior observed in the norbornane control (Figure 4-4).

In the presence of DDM, however, directional movement of the tracer particles is observed. However, unlike the case for norbornene, silica particles move *away* from the pump in the presence of DDM (Figure 4-5). The velocity of the tracers is significantly slower (at 0.04 μm/seconds), but the directionality of the silica tracers is still clearly discernable (Table 4-1).

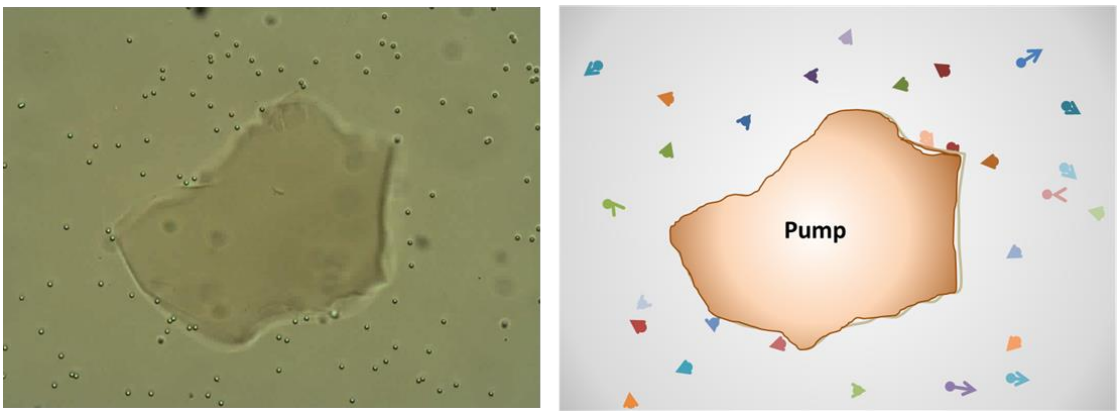

Figure 4-2. Pumps in the presence of 0.25 M Norbornane in trichloroethane (CONTROL). (Left) Top-down microscope image of pump in medium, 20x magnification. (Right) Schematic of the same pump with thirty tracers tracked over four minutes. The starting points of each tracer are marked by a circle and the end points are denoted by an arrowhead.

Figure 4-3. Pumps in the presence of 0.25 M Norbornene in trichloroethane. (Left) Top-down microscope image of pump in medium, 20x magnification. (Right) Schematic of the same pump with thirty tracers tracked over four minutes. The starting points of each tracer are marked by a circle and the end points are denoted by an arrowhead.

Table 4-1. Average velocity of tracked silica tracers.

Entry	Substrate	Substrate concentration (M)	Average velocity (μm/second)
1	Norbornane (control)	0.01M	No directional movement, only Brownian motion observed
2	Norbornene	0.01 M	0.09 ± 0.02
3	Norbornene	0.10 M	0.09 ± 0.02
4	Norbornene	0.25 M	0.10 ± 0.02
5	None (control)	N.A.	No directional movement, only Brownian motion observed
6	Diethyl diallyl malonate	0.25 M	0.04 ± 0.01

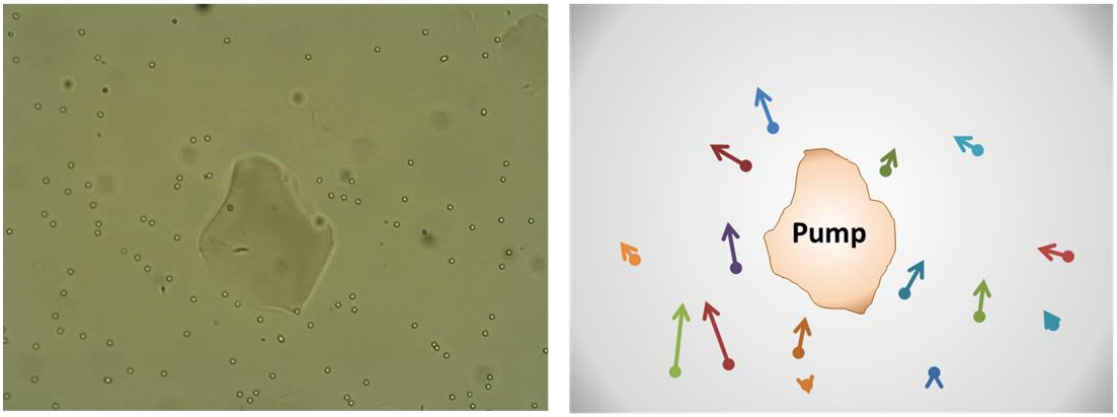

Figure 4-4. Pumps in trichloroethane (CONTROL). (Left) Top-down microscope image of pump in medium, 20x magnification. (Right) Schematic of the same pump with tracers tracked over eleven minutes. The starting points of each tracer are marked by a circle and the end points are denoted by an arrowhead.

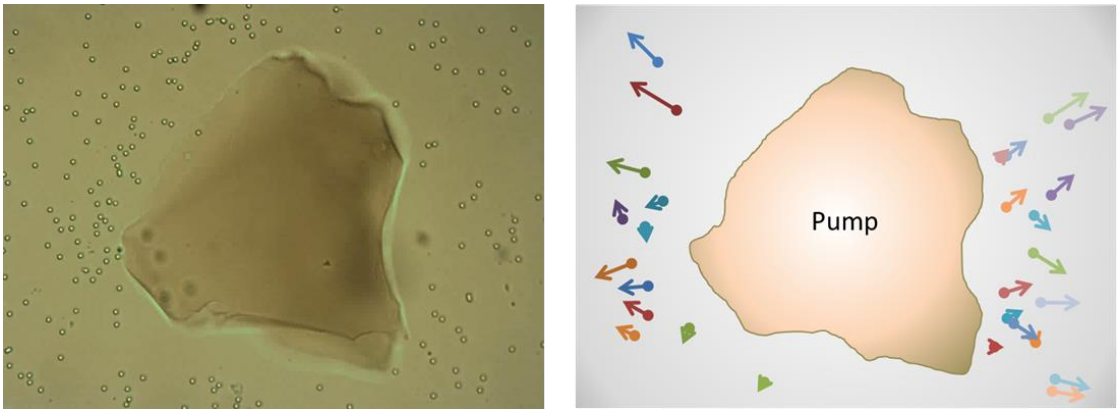

Figure 4-5. Pumps in the presence of 0.25 M Diethyl diallylmalonate in trichloroethane. (Left) Top-down microscope image of pump in medium, 20x magnification. (Right) Schematic of the same pump with thirty tracers tracked over 23 minutes. The starting points of each tracer are marked by a circle and the end points are denoted by an arrowhead.

Possible mechanisms. In the case of norbornene, flow appears to be driven by the substrate gradient. In ROMP, norbornene is continually inserted into the growing polynorbornene chain at the metal center of the catalyst. The product – the polymer chain – remains anchored to the catalytic pump for the duration of the reaction. The catalyst continues to consume norbornene, forming a substrate gradient around the pump. At the surface of the pump, the concentration of norbornene is lower than it is further away from the pump. This pushes the fluid/silica tracers inwards. The polymerization of norbornene is highly exothermic (-50 kJ/mol), so we did consider temperature to be a possible cause of the flow.

The reaction mechanism of DDM differs from that of norbornene; the resulting flows appear to be propelled by a density gradient formed by production of product ethene. Ethene, one of the two products formed by the RCM of DDM, is significantly less dense than the surrounding liquor. Additionally, ethene, is a gas that slowly desorbs from solution over time, and likely is responsible for driving the slow, outwards flow of fluid from the catalyst surface. Also, neither product produced in the DDM RCM reaction are anchored to the pump surface like polynorbornene. The DDM reaction is endothermic (8 kJ/mol), so flow should be directed outwards.

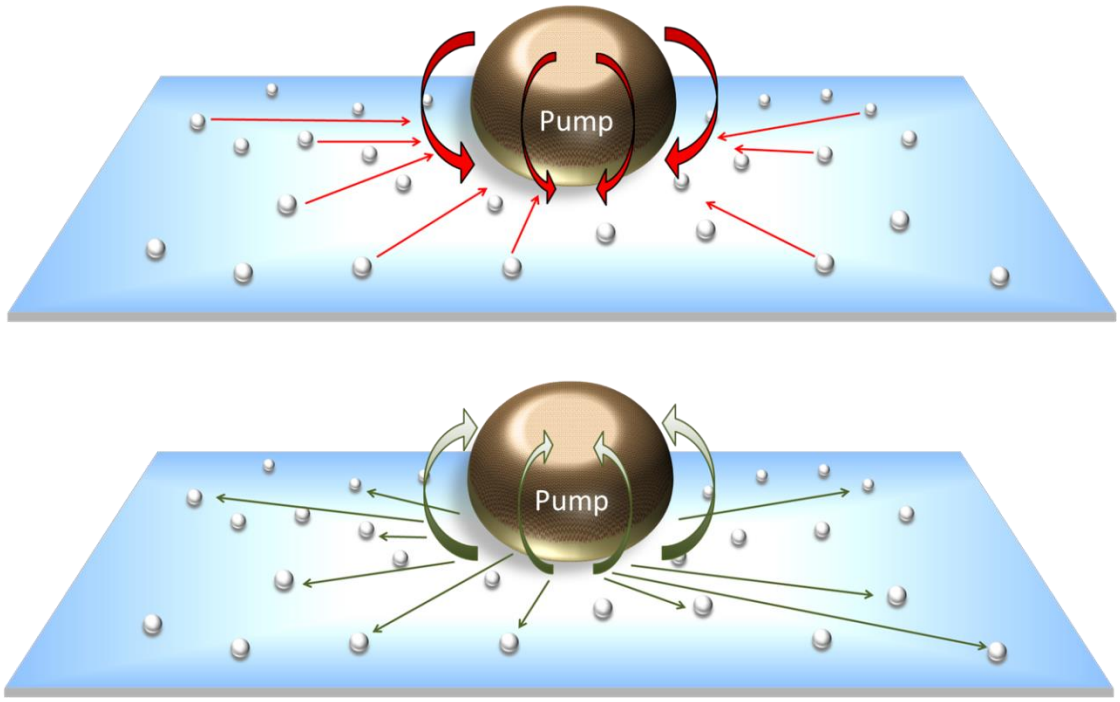

Figure 4-6. Density-driven flows. (Top) Representative of pumps in the presence of norbornene. (Bottom) Representative of pumps in the presence of diethyl diallyl malonate.

4.3. Materials and Methods

Norbornene (NB), norbornane, diethyl diallylmalonate (DDM), 1,1,2-trichloroethane (TCE), and octylhexyltrichlorosilane were purchased from Sigma-Aldrich and used without further purification. Circular cover glass slides (25 mm x 1 mm), used in the experiment, were also purchased from Sigma-Aldrich. Pumps were provided by Materia, Inc. The pumps were composed of silicon dioxide beads with covalently attached second generation Grubbs' catalyst. Manufacturer ICP-MS analysis shows that the catalyst is well-bound to the surface; there is no detectable leaching of ruthenium (<5 ppb, ICP-MS limit of detection). The catalyst loading of the beads is 0.06 mmol/g.

Glass slide silanization. Cover glass slides were first thoroughly cleaned in order to ensure complete silanization of the slide surface. The slides were washed with dichloromethane and water, multiple times, before being placed in piranha solution. The slides were carefully and thoroughly washed with water, and dried in a vacuum oven at 50°C overnight. Dried slides were then placed vials with 4:1 dry toluene: octylhexyltrichlorosilane. The vials were capped, and the slides were allowed to silanize for at overnight. Silanized slides were then washed with toluene and acetone, dried in an oven, and stored in a sealed container until use in microscope experiments.

Microscope experiments. All experiments were conducting using a sealable, custom-made metal microscope slide in which all components exposed to the sample were resistant to organic solvent (Figure 4-7). Fresh glass slides were used for each experiment to prevent sample-to-sample contamination. The threaded spacer was also thoroughly washed with acetone and well-dried before each experiment.

A dilute solution of catalytic beads in trichloroethane was prepared; the beads were allowed to swell for a period of 15 minutes. Firstly, TCE solutions of substrate (norbornene, norbonane, or DDM) and silica tracers (3 μm) were prepared and pipetted into the reaction chamber. Next, pump solution was added gently to the solution, in order to prevent excessive disturbance in the sample. The total sample volume was typically 0.4 mL; larger volumes of solvent tended to result in unwanted convective flows, while smaller volumes were much more sensitive to evaporative effects. The reaction chamber was immediately closed and placed on the microscope stage. The sample was allowed to sit for 10 to 15 minutes to allow silica tracers to settle to the bottom of the slide. Video of the pumps were recorded for a period of 1 to 2 hours. Better video is generally captured within the first 30 minutes of the recording; later into the experiment, the solvent has usually evaporated significantly. The microscope was focused specifically on the tracers on the bottom of the reaction chamber.

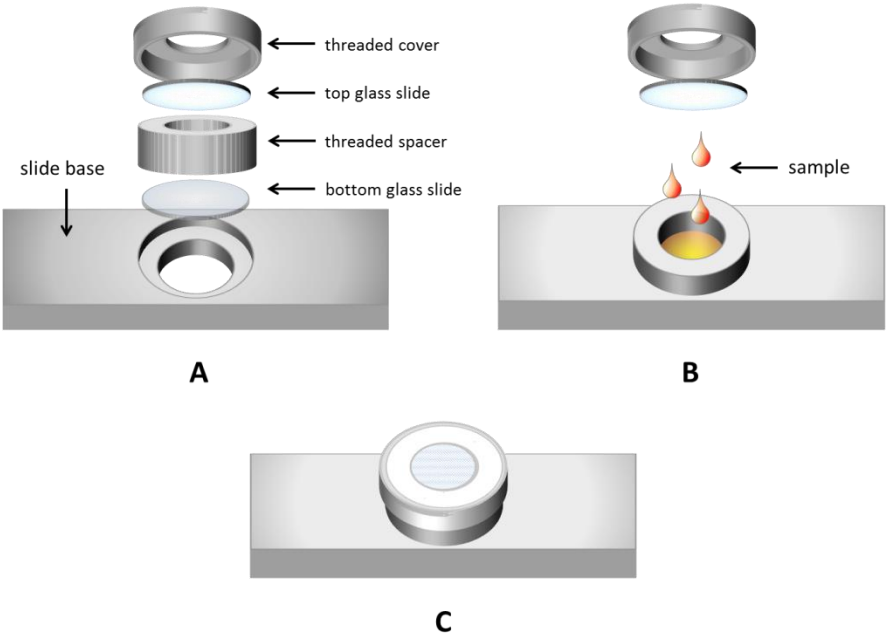

Figure 4-7. A graphical representation of custom-made reaction chamber for pumps in organic media. (A) Components of the custom-made reaction chamber. (B) After the slide base, bottom glass slide, and threaded spacer are assembled, the components of the reaction are added to the reaction chamber. The bottom glass slide is silanized before use. (C) After the addition of the sample, the top glass slide is placed on top of the threaded spacer, and the threaded cover is screwed on. The sample is then ready for analysis.

4.4. Conclusion

We have demonstrated that angström-sized catalysts are capable of driving observable flows in organic solvent. Additionally, we are able to control the direction of the fluid flow by changing the substrate in the reaction. Because of the wide variety of solid-supported, organometallic catalysts available, we can unearth numerous new pumps for future study.

References

(1) DiLauro, A. M.; Zhang, H.; Baker, M. S.; Wong, F.; Sen, A.; Phillips, S. T. Accessibility of Responsive End-Caps in Films Composed of Stimuli-Responsive, Depolymerizable Poly(phthalaldehydes). *Macromolecules* **2013**, *46*, 7257–7265.

(2) Yadav, V.; Zhang, H.; Pavlick, R.; Sen, A. Triggered "On/Off" Micropumps and Colloidal Photodiode. *J. Am. Chem. Soc.* **2012**, *134*, 15688–15691.

(3) Patra, D.; Zhang, H.; Sengupta, S.; Sen, A. Dual Stimuli-Responsive, Rechargeable Micropumps via "Host–Guest" Interactions. *ACS Nano* **2013**, *7*, 7674–7679.

(4) Sengupta, S.; Patra, D.; Ortiz-Rivera, I.; Agrawal, A.; Shklyaev, S.; Dey, K. K.; Córdova-Figueroa, U.; Mallouk, T. E.; Sen, A. Self-Powered Enzyme Micropumps. *Nat Chem* **2014**, *6*, 415–422.

(5) Sanford, M. S.; Love, J. A.; Grubbs, R. H. Mechanism and Activity of Ruthenium Olefin Metathesis Catalysts. *J. Am. Chem. Soc.* **2001**, *123*, 6543–6554.

(6) Pavlick, R. A.; Dey, K. K.; Sirjoosingh, A.; Benesi, A.; Sen, A. A Catalytically Driven Organometallic Molecular Motor. *Nanoscale* **2013**, *5*, 1301–1304.

Chapter 5. Biomass Synthesizing Renewable Monomer Intermediates Using a Recyclable Hydriodic Acid System

5.1. Introduction

Approximately 5 – 7% of all crude oil, about 560 million barrels annually, is used to make monomeric building blocks – primarily olefins – for plastics.[1] The rising costs of petroleum/natural gas, exacerbated by decreasing supplies and increasing regional instability in the Middle East, have re-emphasized the need for investment in alternative sources of raw materials. In effect, a growing number of researchers in both academia and industry have turned to using biomass as a possible supplemental/replacement feedstock source.[2-7]

The primary drawback of using carbohydrates and their derivatives to synthesize alkanes/alkenes is that they are highly functionalized. Biomass conversion, therefore, typically requires several catalytic steps to remove undesired hydroxyl groups.[8-11] Hydriodic acid has been used as a biomass reductant, and can stereoselectively produces iodoalkanes, which can, in turn be used to make olefins. However, the acid often degrades during the reaction, producing iodine, which must be extracted from the final product. Pure HI can be used to convert sorbitol directly into 2-iodohexane, at a molar ratio of 85:1 (HI: sorbitol). However, the reaction would produce a substantial amount of molecular iodine. In order to prevent this, systems with (1) red phosphorus or (2) hypophosphorous acid/hypophosphoric acid – which serve to reduce the hydriodic acid -- have been used in conjunction with the HI. However, in case (1), red phosphorus is a solid, and reacts very slowly with the iodine. In case (2), the use of large amounts of phosphoric acid and water suppress the production of 2-iodohexane, instead producing branched alkanes.

In 2010, Yang developed a hydriodic acid/metal catalyst system capable which addressed this problem (Scheme 5-1 & Figure 5-1).[12] This HI/metal catalyst system is able to simultaneously (1) reduce sugars and carbohydrates (such as fructose and lignocellulose) to much less-functionalized biofuels and (2) reduce molecular iodine byproduct to hydriodic acid under relatively mild conditions (temperature 120 – 160°C, pressure 100 – 300 psi). This is a biphasic system, therefore, it is possible to extract the product with solvent, and allow the catalytic layer to be recycled. Additionally, this is an extremely flexible system which has several levers – changes in acid concentration, starting substrate, catalyst, pressure, and temperature can all drastically change resulting product and product yield (Figure 5-2).[13-15]

To produce iodalkanes, linear short-chain sugars also known as polyols, were used as starting substrates. Of particular interest were the syntheses of 2-iodopropane, 2-iodobutane, and 2-iodohexane from their corresponding sugars (glycerol, erythritol, and sorbitol/mannitol). The market for olefinic monomers is large and growing; the polypropylene market, alone, is valued at $65 billion, while the linear low density polyethylene (LLDPE) market – a polymer which uses alpha-olefin monomers such as 1-butene and 1-hexene – is valued at $17 billion.

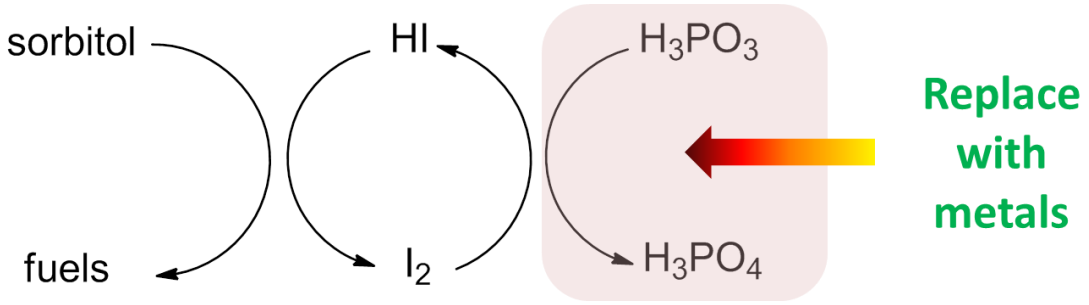

Scheme 5-1. Regeneration of hydiodic acid can be achieved by using metal catalysts or phosphoric acids.

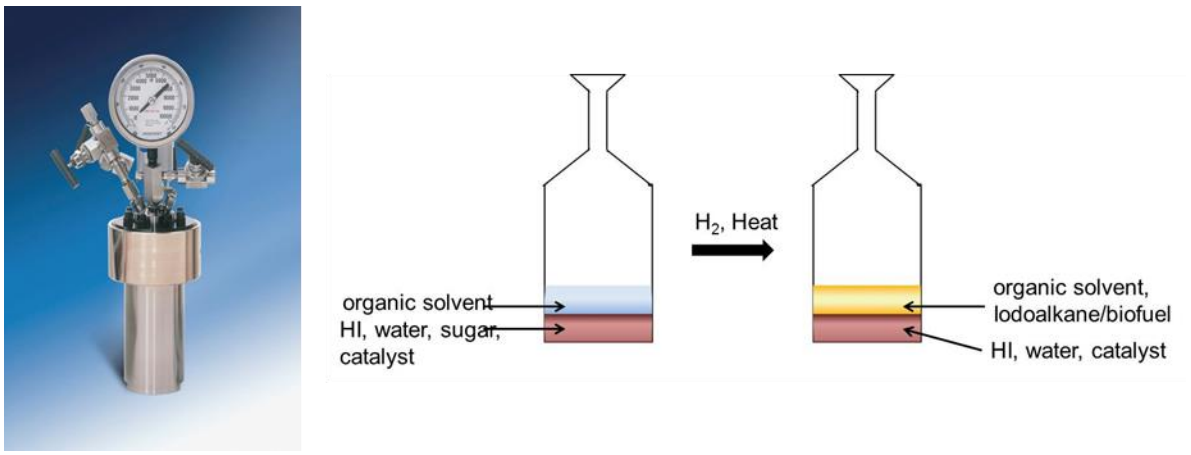

Figure 5-1. Biphasic reaction components.

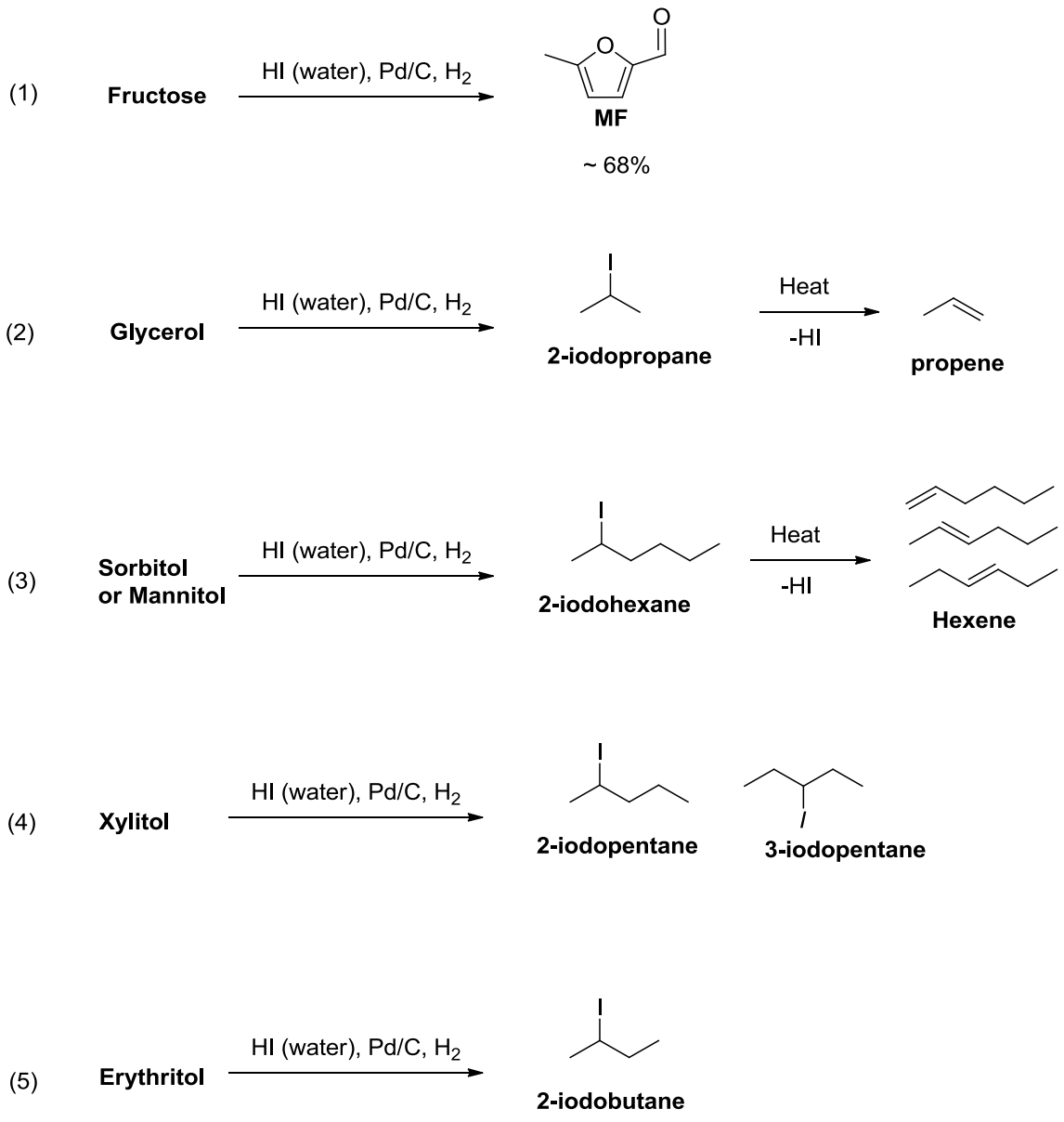

Figure 5-2. Examples of various products that can be produced from sugars using the catalytic HI and Pd/C biphasic system.

5.2. Results and Discussion

Acid concentration and water content. The acid has a strong influence on the reaction rate – the higher the amount of acid in the reaction, the greater the yield. Conversely, the less acid present in the reaction, the more slowly the reaction proceeds. At 0.05 mmol of Pd/C, 300 psi H_2, and 120°C, it appears that 30 mmol of acid can quantitatively convert sorbitol to 2-iodohexane.

Table 5-1. Effects of HI concentration on yield and reaction rate. Conditions: sorbitol (1 mmol), 5% palladium on carbon (20 mg), temperature at 120°C, 0.2 mL H_2O, 2 mL extractant – either toluene or benzene - added.

Entry	HI (mmol)	Time	Yield
1	5	5	25%
2	15	8	45 – 54%
3	30	8	83 – 98%

In the presence of even slight increases of water content – for example if 0.4 mL H_2O, instead of 0.2 mL H_2O is used, the product yield drops drastically. Dumesic *et al.* did use this technique to suppress the production of 2-iodohexane and increase the production of a branched hydrocarbon which was to be used for biofuels.

Table 5-2. Effects of HI concentration on yield and reaction rate. Conditions: sorbitol (1 mmol), hydriodic acid (15 mmol), rhodium (I) chloride (4 mg), 2 mL chlorobenzene, 3 hours.

Entry	Water (mL)	Temp (°C)	Yield
1	0.2	120	60%
2	0.4	140	41%

The same catalytic layer recycled for the reaction several times. However, the acidic layer is continually diluted because of the water produced by the dehydration of the sorbitol, resulting in continually decreasing yields after each reaction cycle.

Catalyst concentration. Increasing the amount of catalyst boosts yields significantly. It appears that rhodium and Pd/C actually have similar catalytic efficiency at least for initial trials.

Table 5-3. Influence of catalyst amount. Conditions: sorbitol (1 mmol), 5% palladium on carbon (20 mg), temperature at 120°C, 0.2 mL H_2O, 2 mL extractant – either toluene or benzene - added. Note that $RhCl_3$ (4 mg) = 0.015 mmol metal, Pd/C (20 mg) = 0.005 mmol metal, and Pd/S = 0.025 mmol metal.

Entry	Catalyst (mg)	Time (hours)	Yield
1	$RhCl_3$ (4)	6	60%
2	Pd/C (20)	3	28%
3	Pd/C (90)	3	58 – 65%

Hydrogen pressure. Hydrogen pressure is essential in the reaction – when different gases are used – such as CO or helium - the reaction rate drops significantly. For example, in with only helium (600 psi), no 2-iodohexane is produced. In contrast, at 600 psi H_2, a 95% yield of 2-iodohexane can be achieved. With an increasing amount of hydrogen pressure, higher yields of 2-iodohexane are produced.

Table 5-4. Effects of Hydrogen Pressure. Conditions: sorbitol (1 mmol), 5% palladium on carbon, temperature at 120°C, 0.2 mL H_2O, 2 mL extractant – either toluene or benzene - added.

Entry	Pd/C (mg)	H_2 (psi)	Time (hours)	Yield
1	20	600	3	0%
2	30	300	3	34%
3	From 3	600	11	95%

Increasing hydrogen pressure appears to be a much "greener" alternative when compared to using longer heating times, higher temperature, or more catalyst/acid.

Using different polyols and studying recyclability. In order to generate iodoalkanes of varying chain length, different polyols were reacted under the same conditions: 1 mmol of substrate, Pd/C (20 mg), 12 hour cycle, 120°C, 0.2 mL H_2O, and 2 mL HI(aq). Reaction efficiency was highly dependent upon polyol chain length – the longer the chain, the lower the

conversion, and the less recyclable the reaction became over time. Additionally, for xylitol (5C) and sorbitol/mannitol (6C), more polyiodic products were produced – the organic layer was typically brown-colored, after the reactions. In contrast, for glycerol (3C) and erythritol (4C), the organic layer remained relatively clear initially after extraction.

Table 5-5. Reaction of different polyols. Conditions: 1 mmol of substrate, Pd/C (20 mg), 12 hour cycle, 120°C, 0.2 mL H_2O, and 2 mL HI(aq). The catalytic layer from entry 1 is recycled in 1a; 1a is used once more for entry 1b. Entries 2–2b and 3–3b are similarly used.

Entry	Substrate	Time (hours)	Product	Yield
1		12		71%
1a	glycerol	12	2-iodopropane	64%
1b		12		84%
2		12		76%
2a	erythritol	12	2-iodobutane	54%
2b		12		
3		12		55%
3a	xylitol	12	iodopentane (2- and 3-)	48%
3b		12		28%

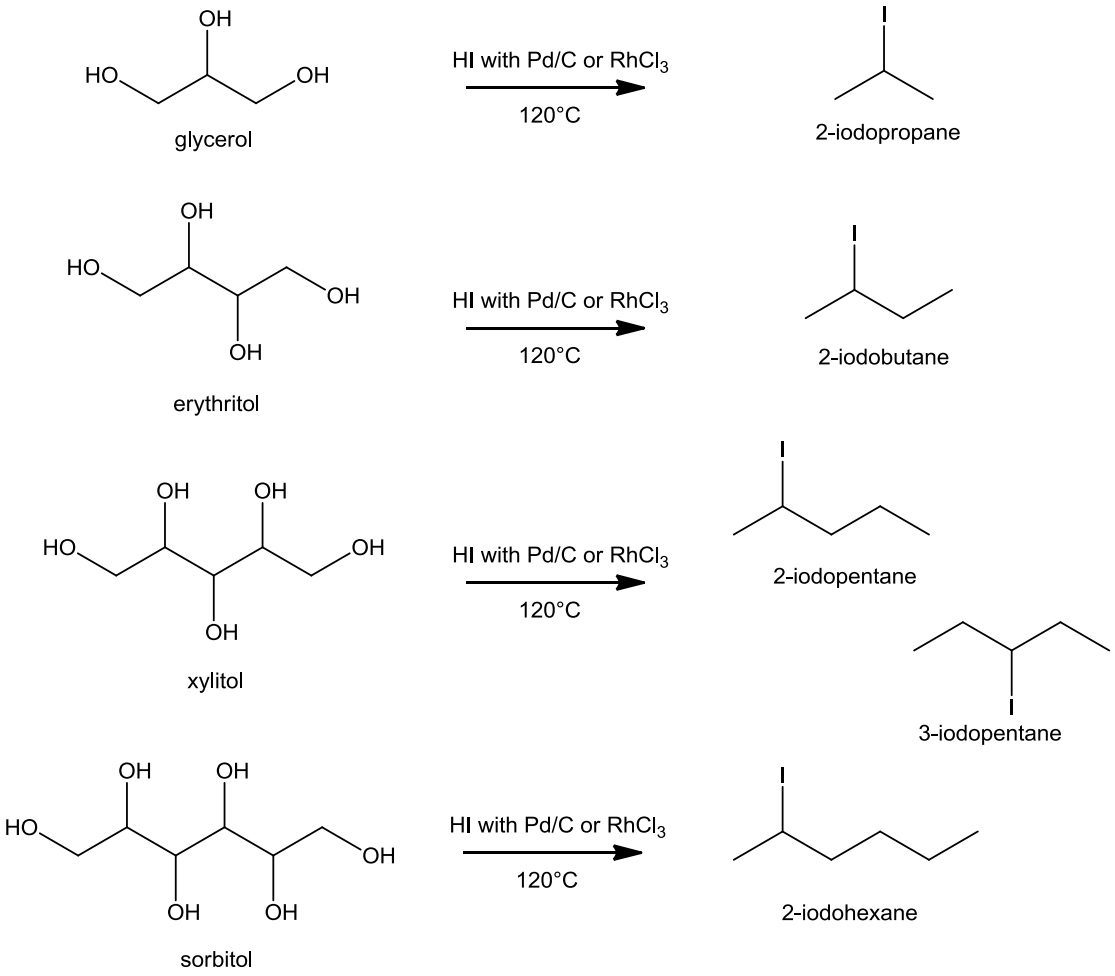

Figure 5-3. Polyol conversion. All polyols produce 2-iodoalkanes with the exception of xylitol, which produces both 2- and 3-iodopentane.

5.3. Experimental

5.3.1. Biphasic Reaction.

This is a biphasic reaction system, composed of both an organic layer and a recyclable aqeuous layer, and is conducted under positive hydrogen pressure (300 – 600 psi). The organic layer, which is typically an aromatic solvent (benzene, toluene, chlorobenzene) is used solely as an extractant. The aqueous layer is composed of the hydriodic acid, the catalyst of choice, water, and sugar. In most cases, sorbitol is used as the test substrate. Increasing the amounts of any of the reactants – hydroidic acid, catalyst ($RhCl_3$, Pd/C), and hydrogen pressure – all increase the reaction yield and reaction rate. This is quite logical based on Le Chatelier's principle (i.e. higher concentration of reactants give yield more product). It is to be noted that despite variations in the reaction conditions, 2-iodoalkanes (with the exception of xylitol) are solely produced from the polyols, thereby, supplanting the need for any further purification.

5.3.2. Materials and Instrumentation.

Palladium on carbon (Pd/C, 5% wt Pd, 51.98% H_2O) was purchased from Johnson Matthey; rhodium chloride ($RhCl_3$, 40% wt Rh) was purchased from Pressure Chemical Company. Hydriodic acid (57% wt HI, <1.5% hypophosphorous acid) and all sugars – glycerol, erythritol, xylitol, and sorbitol – were purchased from Sigma-Aldrich. All chemicals were used without further purification. Gas chromatography (GC) and NMR analyses were performed samples. GC analysis was performed on an Agilent 5890 Series II GC using a RTX-5 split capillary column (Restek) connected to an FID detector. The GC column specifications are as follows: 5% diphenyl/95% dimethyl polysiloxane, 30 m, 0.25 mm i.d. (internal diameter), 0.5μm d.f. (film thickness). ^{1}H NMR (300 MHz) and ^{13}C NMR (75 MHz) spectra were recorded using a Bruker 300-DPX spectrometer.

5.3.2. Sample preparation and analysis.

A glass liner was loaded with catalyst (0.003 – 0.020 mmol), sugar (1 mmol), HI (2 mL), and chlorobenzene (2 mL). As the reaction proceeds, the chlorobenzene layer serves as an extractant. The glass liner was placed in a high-pressure Parr Autoclave and pressurized with the appropriate amount of hydrogen gas (300 or 600 psi). GC analysis was performed on the chlorobenzene layer (extractant) to determine the amount of polyol converted into iodoalkane; 0.4 mL of the extractant (containing the iodoalkane), 11 uL nitromethane (internal standard, 0.2049 mmol), and 1 mL of chlorobenzene. Approximately 1 uL of sample was injected into the GC, and run at a rate of 10°C/min; good separation was achieved between the solvent and iodoalkane.

5.4. Conclusion

Thus far, in this work, we have demonstrated that the HI/metal catalyst biphasic system can be used to convert sugar alcohols into iodoalkanes in realtively high and pure yields. There is still a significant amount of work that needs to be performed to explore the recyclability of the catalytic acid layer. Preserving the efficacy of the catalytic layer requires the fulfillment of two objectives: (i) using a catalyst that can regenerate the hydriodic acid and (ii) removing water generated during the reaction. For objective (i) rhodium chloride and palladium on carbon have already been proved to be somewhat effective in ensuring the recycling of HI over the course of multiple reactions. However, it would be monetarily advantageous if we were able to find a cheaper , preferably non-precious metal catalyst. Cheaper resins or tungsten oxide catalysts can be investigated. For objective (ii), the catalytic layer can be re-concented via vaccum. However, this method is relatively cumbersome, because the catalytic layer must be removed. An alternate method which has yet to be explored is to use the gas-water shift reaction to convert the unwanted water into hydrogen and carbon dioxide, thereby ensuring that the acid stays concentrated and also keeps the system a single-pot reaction.

5.5 References

(1) U.S. Energy Information Administration. http://www.eia.gov/.
(2) Chatterjee, C.; Pong, F.; Sen, A. Chemical Conversion Pathways for Carbohydrates. *Green Chem.* **2015**, *17*, 40–71.
(3) Gallezot, P. Catalytic Conversion of Biomass: Challenges and Issues. *ChemSusChem* **2008**, *1*, 734–737.
(4) Perlack, R. D.; Wright, L. L.; Turhollow, A. F.; Graham, R. L.; Stokes, B. J.; Erbach, D. C. *Biomass as Feedstock for a Bioenergy and Bioproducts Industry: The Technical Feasibility of a Billion-Ton Annual Supply*; Report DOE/GO-102995-2135; U.S. Department of Energy and U.S. Department of Agriculture: Oak Ridge, TN, 2005.
(5) Bozell, J. J.; Holladay, J. E.; Johnson, D.; White, J. F. *Top Value Added Chemicals from Biomass. Vol. II: Results of Screening for Potential Candidates from Biorefinery Lignin*; 2007.
(6) Klaas, M. R.; Schoene, H. Direct, High-Yield Conversions of Cellulose into Biofuel and Platform Chemicals-on the Way to a Sustainable Biobased Economy. *ChemSusChem* **2009**, *2*, 127–128.
(7) Climent, M. J.; Corma, A.; Iborra, S. Conversion of Biomass Platform Molecules into Fuel Additives and Liquid Hydrocarbon Fuels. *Green Chem* **2014**, *16*, 516–547.
(8) Huber, G. W.; Chheda, J. N.; Barrett, C. J.; Dumesic, J. A. Production of Liquid Alkanes by Aqueous-Phase Processing of Biomass-Derived Carbohydrates. *Sci. Wash. DC U. S.* **2005**, *308*, 1446–1450.
(9) Chheda, J. N.; Huber, G. W.; Dumesic, J. A. Liquid-Phase Catalytic Processing of Biomass-Derived Oxygenated Hydrocarbons to Fuels and Chemicals. *Angew. Chem. Int. Ed.* **2007**, *46*, 7164–7183.
(10) West, R. M.; Liu, Z. Y.; Peter, M.; Dumesic, J. A. Liquid Alkanes with Targeted Molecular Weights from Biomass-Derived Carbohydrates. *ChemSusChem* **2008**, *1*, 417–424.
(11) Gürbüz, E. I.; Gallo, J. M. R.; Alonso, D. M.; Wettstein, S. G.; Lim, W. Y.; Dumesic, J. A. Conversion of Hemicellulose into Furfural Using Solid Acid Catalysts in Γ-Valerolactone. *Angew. Chem. Int. Ed.* **2013**, *52*, 1270–1274.
(12) Sen, A.; Yang, W. One-Step Catalytic Conversion of Biomass-Derived Carbohydrates to Liquid Fuels. US8674150 B2.
(13) Yang, W.; Sen, A. Direct Catalytic Synthesis of 5-Methylfurfural from Biomass-Derived Carbohydrates. *ChemSusChem* **2011**, *4*, 349–352.
(14) Grochowski, M. R.; Yang, W.; Sen, A. Mechanistic Study of a One-Step Catalytic Conversion of Fructose to 2,5-Dimethyltetrahydrofuran. *Chem. – Eur. J.* **2012**, *18*, 12363–12371.
(15) Yang, W.; Grochowski, M. R.; Sen, A. Selective Reduction of Biomass by Hydriodic Acid and Its In-Situ Regeneration from Iodine by Metal/Hydrogen. *ChemSusChem* **2012**, *5*, 1218–1222.

Appendix A. Polymerization Catalysts

A.1. Catalyst A cif file

Table 1. Crystal data and structure refinement for Catalyst A.

Identification code	fyp7s
Empirical formula	C29 H33 N2 O Pd
Formula weight	531.97
Temperature	293(2) K
Wavelength	0.71073 A
Crystal system, space group	?, ?
Unit cell dimensions	a = 23.108(3) A alpha = 90 deg. b = 8.3660(10) A beta = 90 deg. c = 26.211(3) A gamma = 90 deg.
Volume	5067.1(11) A^3
Z, Calculated density	8, 1.395 Mg/m^3
Absorption coefficient	0.756 mm^-1
F(000)	2200
Crystal size	0.32 x 0.18 x 0.10 mm
Theta range for data collection	1.55 to 28.31 deg.
Limiting indices	-29<=h<=29, -10<=k<=11, -34<=l<=34
Reflections collected / unique	44740 / 6223 [R(int) = 0.0293]
Completeness to theta = 28.31	98.6 %
Max. and min. transmission	0.9283 and 0.7940
Refinement method	Full-matrix least-squares on F^2
Data / restraints / parameters	6223 / 0 / 303
Goodness-of-fit on F^2	1.052
Final R indices [I>2sigma(I)]	R1 = 0.0350, wR2 = 0.0851
R indices (all data)	R1 = 0.0409, wR2 = 0.0881
Largest diff. peak and hole	0.826 and -0.861 e.A^-3

Table 2. Atomic coordinates (x 10^4) and equivalent isotropic displacement parameters (A^2 x 10^3) for fyp7s.
U(eq) is defined as one third of the trace of the orthogonalized Uij tensor.

	x	y	z	U(eq)
C(1)	5056(1)	3947(4)	709(1)	45(1)
C(2)	6429(1)	4753(2)	2165(1)	20(1)
C(3)	6618(1)	5267(2)	2670(1)	21(1)
C(4)	6244(1)	6182(3)	2980(1)	26(1)
C(5)	6411(1)	6661(3)	3458(1)	32(1)
C(6)	6958(1)	6233(3)	3645(1)	34(1)
C(7)	7326(1)	5325(3)	3356(1)	28(1)
C(8)	7167(1)	4828(3)	2858(1)	22(1)
C(9)	7546(1)	3882(3)	2549(1)	24(1)
C(10)	7376(1)	3422(3)	2078(1)	23(1)
C(11)	6823(1)	3842(2)	1868(1)	20(1)
C(12)	6700(1)	3233(2)	1373(1)	21(1)
C(13)	6260(1)	2600(2)	603(1)	20(1)
C(14)	6473(1)	3451(3)	183(1)	21(1)
C(15)	6470(1)	2686(3)	-288(1)	29(1)
C(16)	6252(1)	1158(3)	-344(1)	35(1)
C(17)	6043(1)	353(3)	76(1)	34(1)
C(18)	6047(1)	1041(3)	557(1)	27(1)
C(19)	5823(1)	132(3)	1020(1)	35(1)
C(20)	6289(2)	-1026(4)	1207(1)	58(1)
C(21)	5264(2)	-752(7)	918(2)	103(2)
C(22)	6708(1)	5135(3)	241(1)	26(1)
C(23)	6574(2)	6201(3)	-212(1)	48(1)
C(24)	7359(1)	5122(4)	333(2)	54(1)
C(25)	4369(1)	6252(3)	1445(1)	28(1)
C(26)	3876(1)	6784(3)	1688(1)	31(1)
C(27)	3777(1)	6335(3)	2184(1)	32(1)
C(28)	4182(1)	5390(3)	2426(1)	37(1)
C(29)	4673(1)	4922(3)	2165(1)	32(1)
N(1)	6238(1)	3385(2)	1093(1)	20(1)
N(2)	4766(1)	5327(2)	1674(1)	24(1)
O(1)	5918(1)	5136(2)	2023(1)	26(1)
Pd(1)	5508(1)	4450(1)	1349(1)	22(1)

Table 3. Bond lengths [A] and angles [deg] for fyp7s.

C(1)-Pd(1)	2.020(2)
C(1)-H(1A)	0.9600
C(1)-H(1B)	0.9600
C(1)-H(1C)	0.9600
C(2)-O(1)	1.280(3)
C(2)-C(11)	1.419(3)
C(2)-C(3)	1.457(3)
C(3)-C(8)	1.410(3)
C(3)-C(4)	1.411(3)
C(4)-C(5)	1.371(3)
C(4)-H(4)	0.9300
C(5)-C(6)	1.401(4)
C(5)-H(5)	0.9300
C(6)-C(7)	1.369(4)
C(6)-H(6)	0.9300
C(7)-C(8)	1.418(3)
C(7)-H(7)	0.9300
C(8)-C(9)	1.431(3)
C(9)-C(10)	1.353(3)
C(9)-H(9)	0.9300
C(10)-C(11)	1.436(3)
C(10)-H(10)	0.9300
C(11)-C(12)	1.423(3)
C(12)-N(1)	1.300(3)
C(12)-H(12A)	0.9700
C(12)-H(12B)	0.9700
C(13)-C(14)	1.398(3)
C(13)-C(18)	1.400(3)
C(13)-N(1)	1.444(3)
C(14)-C(15)	1.392(3)
C(14)-C(22)	1.518(3)
C(15)-C(16)	1.381(4)
C(15)-H(15)	0.9300
C(16)-C(17)	1.377(4)
C(16)-H(16)	0.9300
C(17)-C(18)	1.387(3)
C(17)-H(17)	0.9300
C(18)-C(19)	1.522(3)
C(19)-C(21)	1.513(4)
C(19)-C(20)	1.528(4)
C(19)-H(19)	0.9800
C(20)-H(20A)	0.9600
C(20)-H(20B)	0.9600
C(20)-H(20C)	0.9600
C(21)-H(21A)	0.9600
C(21)-H(21B)	0.9600
C(21)-H(21C)	0.9600
C(22)-C(23)	1.517(3)
C(22)-C(24)	1.523(4)
C(22)-H(22)	0.9800
C(23)-H(23A)	0.9600
C(23)-H(23B)	0.9600
C(23)-H(23C)	0.9600

C(24)-H(24A)	0.9600
C(24)-H(24B)	0.9600
C(24)-H(24C)	0.9600
C(25)-N(2)	1.343(3)
C(25)-C(26)	1.379(3)
C(25)-H(25)	0.9300
C(26)-C(27)	1.374(4)
C(26)-H(26)	0.9300
C(27)-C(28)	1.379(4)
C(27)-H(27)	0.9300
C(28)-C(29)	1.382(4)
C(28)-H(28)	0.9300
C(29)-N(2)	1.347(3)
C(29)-H(29)	0.9300
N(1)-Pd(1)	2.0236(17)
N(2)-Pd(1)	2.0491(19)
O(1)-Pd(1)	2.0848(15)

Pd(1)-C(1)-H(1A)	109.5
Pd(1)-C(1)-H(1B)	109.5
H(1A)-C(1)-H(1B)	109.5
Pd(1)-C(1)-H(1C)	109.5
H(1A)-C(1)-H(1C)	109.5
H(1B)-C(1)-H(1C)	109.5
O(1)-C(2)-C(11)	124.4(2)
O(1)-C(2)-C(3)	117.82(19)
C(11)-C(2)-C(3)	117.77(19)
C(8)-C(3)-C(4)	119.3(2)
C(8)-C(3)-C(2)	120.62(19)
C(4)-C(3)-C(2)	120.0(2)
C(5)-C(4)-C(3)	120.9(2)
C(5)-C(4)-H(4)	119.6
C(3)-C(4)-H(4)	119.6
C(4)-C(5)-C(6)	119.9(2)
C(4)-C(5)-H(5)	120.1
C(6)-C(5)-H(5)	120.1
C(7)-C(6)-C(5)	120.6(2)
C(7)-C(6)-H(6)	119.7
C(5)-C(6)-H(6)	119.7
C(6)-C(7)-C(8)	120.7(2)
C(6)-C(7)-H(7)	119.6
C(8)-C(7)-H(7)	119.6
C(3)-C(8)-C(7)	118.6(2)
C(3)-C(8)-C(9)	119.80(19)
C(7)-C(8)-C(9)	121.6(2)
C(10)-C(9)-C(8)	119.8(2)
C(10)-C(9)-H(9)	120.1
C(8)-C(9)-H(9)	120.1
C(9)-C(10)-C(11)	122.6(2)
C(9)-C(10)-H(10)	118.7
C(11)-C(10)-H(10)	118.7
C(2)-C(11)-C(12)	124.44(19)
C(2)-C(11)-C(10)	119.43(19)
C(12)-C(11)-C(10)	116.07(19)
N(1)-C(12)-C(11)	130.00(19)
N(1)-C(12)-H(12A)	104.8

C(11)-C(12)-H(12A)	104.8
N(1)-C(12)-H(12B)	104.8
C(11)-C(12)-H(12B)	104.8
H(12A)-C(12)-H(12B)	105.8
C(14)-C(13)-C(18)	122.0(2)
C(14)-C(13)-N(1)	118.73(18)
C(18)-C(13)-N(1)	119.16(19)
C(15)-C(14)-C(13)	117.6(2)
C(15)-C(14)-C(22)	121.1(2)
C(13)-C(14)-C(22)	121.35(19)
C(16)-C(15)-C(14)	121.4(2)
C(16)-C(15)-H(15)	119.3
C(14)-C(15)-H(15)	119.3
C(17)-C(16)-C(15)	119.8(2)
C(17)-C(16)-H(16)	120.1
C(15)-C(16)-H(16)	120.1
C(16)-C(17)-C(18)	121.4(2)
C(16)-C(17)-H(17)	119.3
C(18)-C(17)-H(17)	119.3
C(17)-C(18)-C(13)	117.8(2)
C(17)-C(18)-C(19)	121.0(2)
C(13)-C(18)-C(19)	121.1(2)
C(21)-C(19)-C(18)	113.2(3)
C(21)-C(19)-C(20)	110.4(3)
C(18)-C(19)-C(20)	109.5(2)
C(21)-C(19)-H(19)	107.9
C(18)-C(19)-H(19)	107.9
C(20)-C(19)-H(19)	107.9
C(19)-C(20)-H(20A)	109.5
C(19)-C(20)-H(20B)	109.5
H(20A)-C(20)-H(20B)	109.5
C(19)-C(20)-H(20C)	109.5
H(20A)-C(20)-H(20C)	109.5
H(20B)-C(20)-H(20C)	109.5
C(19)-C(21)-H(21A)	109.5
C(19)-C(21)-H(21B)	109.5
H(21A)-C(21)-H(21B)	109.5
C(19)-C(21)-H(21C)	109.5
H(21A)-C(21)-H(21C)	109.5
H(21B)-C(21)-H(21C)	109.5
C(23)-C(22)-C(14)	113.2(2)
C(23)-C(22)-C(24)	109.3(2)
C(14)-C(22)-C(24)	111.3(2)
C(23)-C(22)-H(22)	107.6
C(14)-C(22)-H(22)	107.6
C(24)-C(22)-H(22)	107.6
C(22)-C(23)-H(23A)	109.5
C(22)-C(23)-H(23B)	109.5
H(23A)-C(23)-H(23B)	109.5
C(22)-C(23)-H(23C)	109.5
H(23A)-C(23)-H(23C)	109.5
H(23B)-C(23)-H(23C)	109.5
C(22)-C(24)-H(24A)	109.5
C(22)-C(24)-H(24B)	109.5
H(24A)-C(24)-H(24B)	109.5
C(22)-C(24)-H(24C)	109.5

H(24A)-C(24)-H(24C)	109.5
H(24B)-C(24)-H(24C)	109.5
N(2)-C(25)-C(26)	123.0(2)
N(2)-C(25)-H(25)	118.5
C(26)-C(25)-H(25)	118.5
C(27)-C(26)-C(25)	119.1(2)
C(27)-C(26)-H(26)	120.4
C(25)-C(26)-H(26)	120.4
C(26)-C(27)-C(28)	118.6(2)
C(26)-C(27)-H(27)	120.7
C(28)-C(27)-H(27)	120.7
C(27)-C(28)-C(29)	119.4(2)
C(27)-C(28)-H(28)	120.3
C(29)-C(28)-H(28)	120.3
N(2)-C(29)-C(28)	122.3(2)
N(2)-C(29)-H(29)	118.9
C(28)-C(29)-H(29)	118.9
C(12)-N(1)-C(13)	115.33(17)
C(12)-N(1)-Pd(1)	122.71(14)
C(13)-N(1)-Pd(1)	121.69(13)
C(25)-N(2)-C(29)	117.6(2)
C(25)-N(2)-Pd(1)	126.28(16)
C(29)-N(2)-Pd(1)	116.15(16)
C(2)-O(1)-Pd(1)	126.76(14)
C(1)-Pd(1)-N(1)	93.68(9)
C(1)-Pd(1)-N(2)	89.29(9)
N(1)-Pd(1)-N(2)	173.27(7)
C(1)-Pd(1)-O(1)	174.68(9)
N(1)-Pd(1)-O(1)	91.30(6)
N(2)-Pd(1)-O(1)	85.96(7)

A.2. Catalyst C cif file

Table 1. Crystal data and structure refinement for fyp13m.

Identification code	fyp13m
Empirical formula	C30 H34 N2 O2 Pd
Formula weight	560.99
Temperature	293(2) K
Wavelength	0.71073 A
Crystal system, space group	?, ?
Unit cell dimensions	a = 9.3297(14) A alpha = 101.590(2) deg. b = 10.5642(16) A beta = 91.832(2) deg. c = 14.770(2) A gamma = 104.375(2) deg.
Volume	1376.3(3) A^3
Z, Calculated density	2, 1.354 Mg/m^3
Absorption coefficient	0.702 mm^-1
F(000)	580
Crystal size	? x ? x ? mm
Theta range for data collection	2.04 to 28.37 deg.
Limiting indices	-12<=h<=12, -14<=k<=13, -19<=l<=19
Reflections collected / unique	13323 / 6703 [R(int) = 0.0236]
Completeness to theta = 28.37	97.3 %
Refinement method	Full-matrix least-squares on F^2
Data / restraints / parameters	6703 / 0 / 322
Goodness-of-fit on F^2	1.142
Final R indices [I>2sigma(I)]	R1 = 0.0456, wR2 = 0.0954
R indices (all data)	R1 = 0.0526, wR2 = 0.0985
Largest diff. peak and hole	0.875 and -1.033 e.A^-3

Table 2. Atomic coordinates (x 10^4) and equivalent isotropic displacement parameters (A^2 x 10^3) for fyp13m.
U(eq) is defined as one third of the trace of the orthogonalized Uij tensor.

	x	y	z	U(eq)
Pd(1)	6696(1)	7807(1)	3547(1)	28(1)
O(1)	4827(2)	6483(2)	3870(1)	35(1)
O(2)	3361(2)	6025(2)	5264(2)	45(1)
N(1)	6486(3)	6708(2)	2246(2)	32(1)
N(2)	6736(3)	8999(2)	4823(2)	32(1)
C(1)	8618(4)	9067(4)	3355(2)	51(1)
C(2)	4033(3)	5391(3)	3366(2)	31(1)
C(3)	4273(3)	4942(3)	2416(2)	35(1)
C(4)	3313(4)	3734(3)	1877(2)	46(1)
C(5)	2191(4)	2984(3)	2241(3)	50(1)
C(6)	1926(3)	3355(3)	3190(3)	43(1)
C(7)	2832(3)	4552(3)	3765(2)	35(1)
C(8)	2507(3)	4863(3)	4708(2)	38(1)
C(9)	1361(4)	4017(4)	5043(3)	50(1)
C(10)	500(4)	2854(4)	4459(3)	59(1)
C(11)	761(4)	2534(4)	3556(3)	56(1)
C(12)	5414(3)	5625(3)	1946(2)	35(1)
C(13)	7474(3)	7131(3)	1567(2)	36(1)
C(14)	8716(3)	6623(3)	1438(2)	41(1)
C(15)	9650(4)	7047(4)	785(2)	58(1)
C(16)	9374(5)	7964(4)	297(3)	65(1)
C(17)	8169(5)	8475(4)	455(2)	59(1)
C(18)	7198(4)	8084(4)	1100(2)	46(1)
C(19)	5864(5)	8655(4)	1292(3)	60(1)
C(20)	4544(5)	7891(5)	597(4)	85(2)
C(22)	9052(4)	5666(4)	1999(2)	46(1)
C(25)	6910(3)	10329(3)	4932(2)	39(1)
C(26)	6841(4)	11149(3)	5761(3)	48(1)
C(27)	6605(4)	10598(4)	6535(3)	54(1)
C(28)	6426(4)	9245(4)	6433(2)	49(1)
C(29)	6486(3)	8474(3)	5571(2)	38(1)
C(30)	3100(4)	6278(4)	6218(2)	56(1)
C(24)	10673(5)	6034(5)	2362(4)	96(2)
C(23)	8568(6)	4212(4)	1480(3)	78(1)
C(21)	6218(7)	10154(5)	1328(4)	95(2)

Table 3. Bond lengths [A] and angles [deg] for fyp13m.

Pd(1)-N(1)	2.012(2)
Pd(1)-C(1)	2.017(3)
Pd(1)-N(2)	2.040(2)
Pd(1)-O(1)	2.0820(19)
O(1)-C(2)	1.276(3)
O(2)-C(8)	1.373(4)
O(2)-C(30)	1.421(4)
N(1)-C(12)	1.306(4)
N(1)-C(13)	1.445(4)
N(2)-C(29)	1.335(4)
N(2)-C(25)	1.349(4)
C(1)-H(1A)	0.9600
C(1)-H(1B)	0.9600
C(1)-H(1C)	0.9600
C(2)-C(3)	1.432(4)
C(2)-C(7)	1.465(4)
C(3)-C(12)	1.415(4)
C(3)-C(4)	1.430(4)
C(4)-C(5)	1.344(5)
C(4)-H(4)	0.9300
C(5)-C(6)	1.424(5)
C(5)-H(5)	0.9300
C(6)-C(11)	1.408(5)
C(6)-C(7)	1.424(4)
C(7)-C(8)	1.425(4)
C(8)-C(9)	1.387(4)
C(9)-C(10)	1.392(5)
C(9)-H(9)	0.9300
C(10)-C(11)	1.355(6)
C(10)-H(10)	0.9300
C(11)-H(11)	0.9300
C(12)-H(12)	0.9300
C(13)-C(14)	1.396(4)
C(13)-C(18)	1.398(4)
C(14)-C(15)	1.387(5)
C(14)-C(22)	1.512(5)
C(15)-C(16)	1.384(6)
C(15)-H(15)	0.9300
C(16)-C(17)	1.370(6)
C(16)-H(16)	0.9300
C(17)-C(18)	1.387(5)
C(17)-H(17)	0.9300
C(18)-C(19)	1.523(5)
C(19)-C(20)	1.521(6)
C(19)-C(21)	1.525(6)
C(19)-H(19)	0.9800
C(20)-H(20A)	0.9600
C(20)-H(20B)	0.9600
C(20)-H(20C)	0.9600
C(22)-C(24)	1.516(5)
C(22)-C(23)	1.520(5)
C(22)-H(22)	0.9800
C(25)-C(26)	1.364(5)

C(25)-H(25)	0.9300
C(26)-C(27)	1.382(5)
C(26)-H(26)	0.9300
C(27)-C(28)	1.374(5)
C(27)-H(27)	0.9300
C(28)-C(29)	1.377(4)
C(28)-H(28)	0.9300
C(29)-H(29)	0.9300
C(30)-H(30A)	0.9600
C(30)-H(30B)	0.9600
C(30)-H(30C)	0.9600
C(24)-H(24A)	0.9600
C(24)-H(24B)	0.9600
C(24)-H(24C)	0.9600
C(23)-H(23A)	0.9600
C(23)-H(23B)	0.9600
C(23)-H(23C)	0.9600
C(21)-H(21A)	0.9600
C(21)-H(21B)	0.9600
C(21)-H(21C)	0.9600

N(1)-Pd(1)-C(1)	93.04(12)
N(1)-Pd(1)-N(2)	174.01(9)
C(1)-Pd(1)-N(2)	88.66(12)
N(1)-Pd(1)-O(1)	90.75(9)
C(1)-Pd(1)-O(1)	173.98(12)
N(2)-Pd(1)-O(1)	88.05(8)
C(2)-O(1)-Pd(1)	128.79(18)
C(8)-O(2)-C(30)	117.2(3)
C(12)-N(1)-C(13)	115.9(2)
C(12)-N(1)-Pd(1)	122.8(2)
C(13)-N(1)-Pd(1)	121.15(19)
C(29)-N(2)-C(25)	117.6(3)
C(29)-N(2)-Pd(1)	120.85(19)
C(25)-N(2)-Pd(1)	121.4(2)
Pd(1)-C(1)-H(1A)	109.5
Pd(1)-C(1)-H(1B)	109.5
H(1A)-C(1)-H(1B)	109.5
Pd(1)-C(1)-H(1C)	109.5
H(1A)-C(1)-H(1C)	109.5
H(1B)-C(1)-H(1C)	109.5
O(1)-C(2)-C(3)	122.4(3)
O(1)-C(2)-C(7)	119.5(3)
C(3)-C(2)-C(7)	118.1(3)
C(12)-C(3)-C(4)	115.7(3)
C(12)-C(3)-C(2)	124.5(3)
C(4)-C(3)-C(2)	119.8(3)
C(5)-C(4)-C(3)	121.8(3)
C(5)-C(4)-H(4)	119.1
C(3)-C(4)-H(4)	119.1
C(4)-C(5)-C(6)	121.0(3)
C(4)-C(5)-H(5)	119.5
C(6)-C(5)-H(5)	119.5
C(11)-C(6)-C(5)	119.7(3)
C(11)-C(6)-C(7)	120.1(3)
C(5)-C(6)-C(7)	120.2(3)

C(6)-C(7)-C(8)	117.2(3)
C(6)-C(7)-C(2)	119.0(3)
C(8)-C(7)-C(2)	123.7(3)
O(2)-C(8)-C(9)	121.6(3)
O(2)-C(8)-C(7)	117.6(3)
C(9)-C(8)-C(7)	120.7(3)
C(8)-C(9)-C(10)	120.3(3)
C(8)-C(9)-H(9)	119.8
C(10)-C(9)-H(9)	119.8
C(11)-C(10)-C(9)	120.7(3)
C(11)-C(10)-H(10)	119.7
C(9)-C(10)-H(10)	119.7
C(10)-C(11)-C(6)	120.8(3)
C(10)-C(11)-H(11)	119.6
C(6)-C(11)-H(11)	119.6
N(1)-C(12)-C(3)	130.6(3)
N(1)-C(12)-H(12)	114.7
C(3)-C(12)-H(12)	114.7
C(14)-C(13)-C(18)	122.3(3)
C(14)-C(13)-N(1)	118.6(3)
C(18)-C(13)-N(1)	119.0(3)
C(15)-C(14)-C(13)	117.5(3)
C(15)-C(14)-C(22)	121.0(3)
C(13)-C(14)-C(22)	121.5(3)
C(16)-C(15)-C(14)	121.0(4)
C(16)-C(15)-H(15)	119.5
C(14)-C(15)-H(15)	119.5
C(17)-C(16)-C(15)	120.3(3)
C(17)-C(16)-H(16)	119.8
C(15)-C(16)-H(16)	119.8
C(16)-C(17)-C(18)	121.1(4)
C(16)-C(17)-H(17)	119.4
C(18)-C(17)-H(17)	119.4
C(17)-C(18)-C(13)	117.7(3)
C(17)-C(18)-C(19)	121.7(3)
C(13)-C(18)-C(19)	120.6(3)
C(20)-C(19)-C(18)	111.1(3)
C(20)-C(19)-C(21)	111.3(4)
C(18)-C(19)-C(21)	112.8(4)
C(20)-C(19)-H(19)	107.1
C(18)-C(19)-H(19)	107.1
C(21)-C(19)-H(19)	107.1
C(19)-C(20)-H(20A)	109.5
C(19)-C(20)-H(20B)	109.5
H(20A)-C(20)-H(20B)	109.5
C(19)-C(20)-H(20C)	109.5
H(20A)-C(20)-H(20C)	109.5
H(20B)-C(20)-H(20C)	109.5
C(14)-C(22)-C(24)	112.4(3)
C(14)-C(22)-C(23)	113.1(3)
C(24)-C(22)-C(23)	110.3(3)
C(14)-C(22)-H(22)	106.9
C(24)-C(22)-H(22)	106.9
C(23)-C(22)-H(22)	106.9
N(2)-C(25)-C(26)	123.3(3)
N(2)-C(25)-H(25)	118.3

C(26)-C(25)-H(25)	118.3
C(25)-C(26)-C(27)	118.6(3)
C(25)-C(26)-H(26)	120.7
C(27)-C(26)-H(26)	120.7
C(28)-C(27)-C(26)	118.6(3)
C(28)-C(27)-H(27)	120.7
C(26)-C(27)-H(27)	120.7
C(27)-C(28)-C(29)	119.6(3)
C(27)-C(28)-H(28)	120.2
C(29)-C(28)-H(28)	120.2
N(2)-C(29)-C(28)	122.2(3)
N(2)-C(29)-H(29)	118.9
C(28)-C(29)-H(29)	118.9
O(2)-C(30)-H(30A)	109.5
O(2)-C(30)-H(30B)	109.5
H(30A)-C(30)-H(30B)	109.5
O(2)-C(30)-H(30C)	109.5
H(30A)-C(30)-H(30C)	109.5
H(30B)-C(30)-H(30C)	109.5
C(22)-C(24)-H(24A)	109.5
C(22)-C(24)-H(24B)	109.5
H(24A)-C(24)-H(24B)	109.5
C(22)-C(24)-H(24C)	109.5
H(24A)-C(24)-H(24C)	109.5
H(24B)-C(24)-H(24C)	109.5
C(22)-C(23)-H(23A)	109.5
C(22)-C(23)-H(23B)	109.5
H(23A)-C(23)-H(23B)	109.5
C(22)-C(23)-H(23C)	109.5
H(23A)-C(23)-H(23C)	109.5
H(23B)-C(23)-H(23C)	109.5
C(19)-C(21)-H(21A)	109.5
C(19)-C(21)-H(21B)	109.5
H(21A)-C(21)-H(21B)	109.5
C(19)-C(21)-H(21C)	109.5
H(21A)-C(21)-H(21C)	109.5
H(21B)-C(21)-H(21C)	109.5

Symmetry transformations used to generate equivalent atoms:

Table 4. Anisotropic displacement parameters (A^2 x 10^3) for fyp13m. The anisotropic displacement factor exponent takes the form: -2 pi^2 [h^2 a*^2 U11 + ... + 2 h k a* b* U12]

	U11	U22	U33	U23	U13	U12
Pd(1)	29(1)	23(1)	31(1)	6(1)	2(1)	1(1)
O(1)	37(1)	24(1)	39(1)	5(1)	6(1)	1(1)
O(2)	47(1)	40(1)	45(1)	14(1)	12(1)	3(1)
N(1)	31(1)	32(1)	33(1)	9(1)	1(1)	6(1)
N(2)	31(1)	24(1)	40(1)	6(1)	0(1)	4(1)
C(1)	45(2)	48(2)	47(2)	5(2)	7(2)	-10(2)
C(2)	26(1)	27(1)	43(2)	12(1)	0(1)	7(1)
C(3)	32(2)	28(1)	43(2)	5(1)	-6(1)	5(1)
C(4)	42(2)	40(2)	48(2)	2(2)	-4(1)	2(1)
C(5)	42(2)	34(2)	62(2)	3(2)	-11(2)	-6(1)
C(6)	32(2)	29(2)	65(2)	16(2)	-6(1)	0(1)
C(7)	28(1)	26(1)	52(2)	14(1)	0(1)	6(1)
C(8)	30(2)	34(2)	53(2)	20(1)	5(1)	10(1)
C(9)	38(2)	52(2)	64(2)	29(2)	16(2)	9(2)
C(10)	38(2)	51(2)	90(3)	34(2)	12(2)	-1(2)
C(11)	35(2)	40(2)	86(3)	20(2)	-2(2)	-10(1)
C(12)	35(2)	35(2)	34(1)	6(1)	-1(1)	9(1)
C(13)	36(2)	38(2)	29(1)	7(1)	3(1)	3(1)
C(14)	38(2)	47(2)	34(2)	6(1)	1(1)	7(1)
C(15)	45(2)	83(3)	45(2)	12(2)	12(2)	14(2)
C(16)	64(3)	82(3)	44(2)	20(2)	18(2)	1(2)
C(17)	76(3)	62(2)	43(2)	26(2)	9(2)	10(2)
C(18)	52(2)	50(2)	36(2)	15(2)	3(1)	11(2)
C(19)	74(3)	69(3)	55(2)	30(2)	12(2)	36(2)
C(20)	66(3)	110(4)	99(4)	45(3)	5(3)	41(3)
C(22)	43(2)	54(2)	44(2)	8(2)	4(1)	18(2)
C(25)	30(2)	29(2)	55(2)	9(1)	-4(1)	4(1)
C(26)	36(2)	31(2)	69(2)	-2(2)	2(2)	9(1)
C(27)	45(2)	50(2)	52(2)	-14(2)	5(2)	10(2)
C(28)	47(2)	56(2)	41(2)	7(2)	4(2)	10(2)
C(29)	41(2)	33(2)	41(2)	9(1)	2(1)	10(1)
C(30)	51(2)	71(3)	47(2)	18(2)	16(2)	9(2)
C(24)	64(3)	87(4)	137(5)	32(3)	-41(3)	17(3)
C(23)	96(4)	56(3)	76(3)	3(2)	-5(3)	22(2)
C(21)	135(5)	79(3)	94(4)	36(3)	15(4)	54(4)

A.3. 2D NMR of Catalyst B

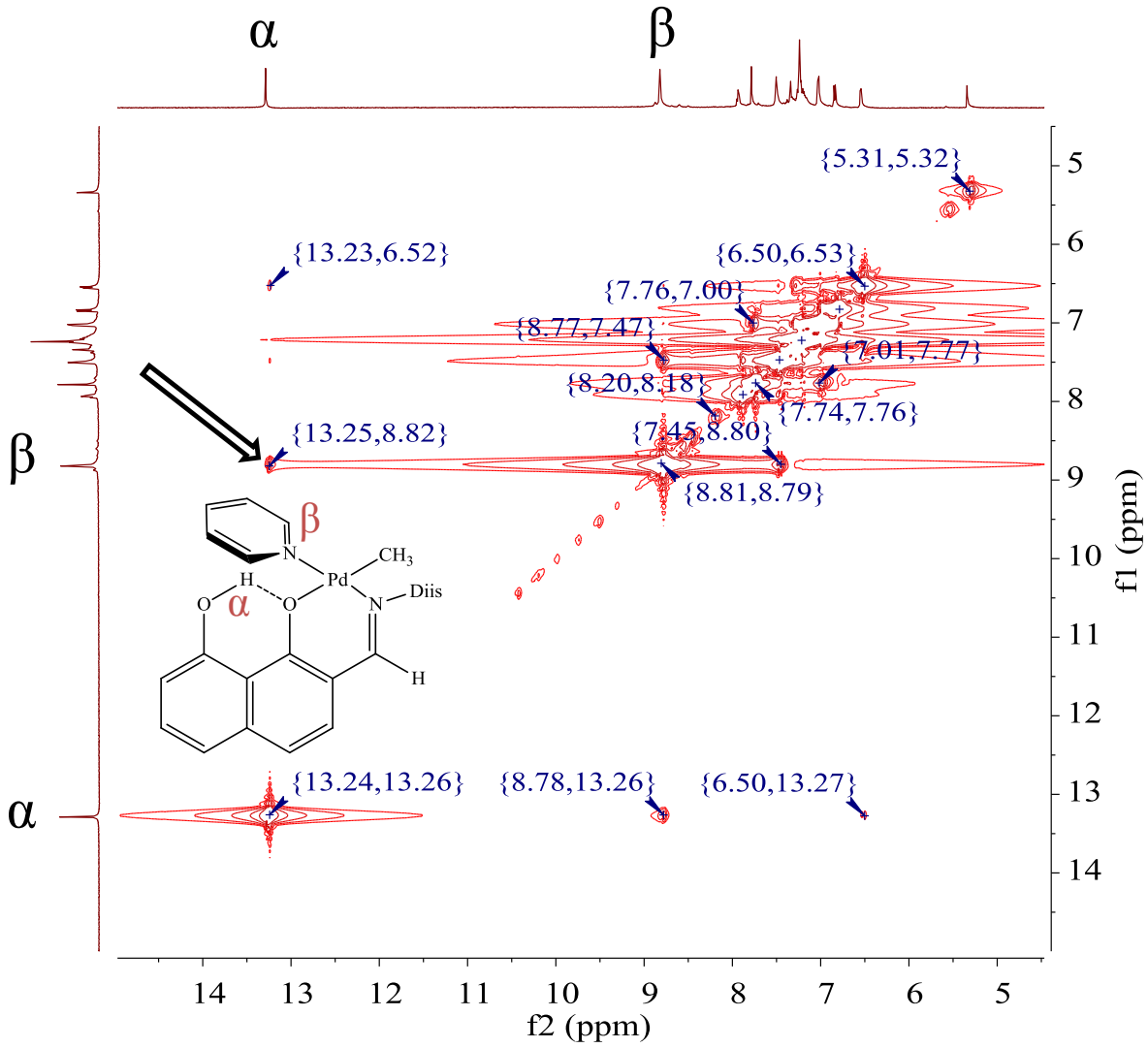

Figure A-1. ^{1}H-^{1}H 2D NOESY spectrum of Catalyst B. Sample conditions: CD_2Cl_2, 298 K, 600 MHz. Acquisition parameters: 16 scans, 2 second relaxation delay, 1 k x 0.25 k (f1 x f2) points acquired, 1.5 second mixing time. Interaction between the phenolic hydrogen (α), pyridine hydrogens on the 2,6 positions (β) is shown by the arrow at (13.25 ppm, 8.82 ppm).

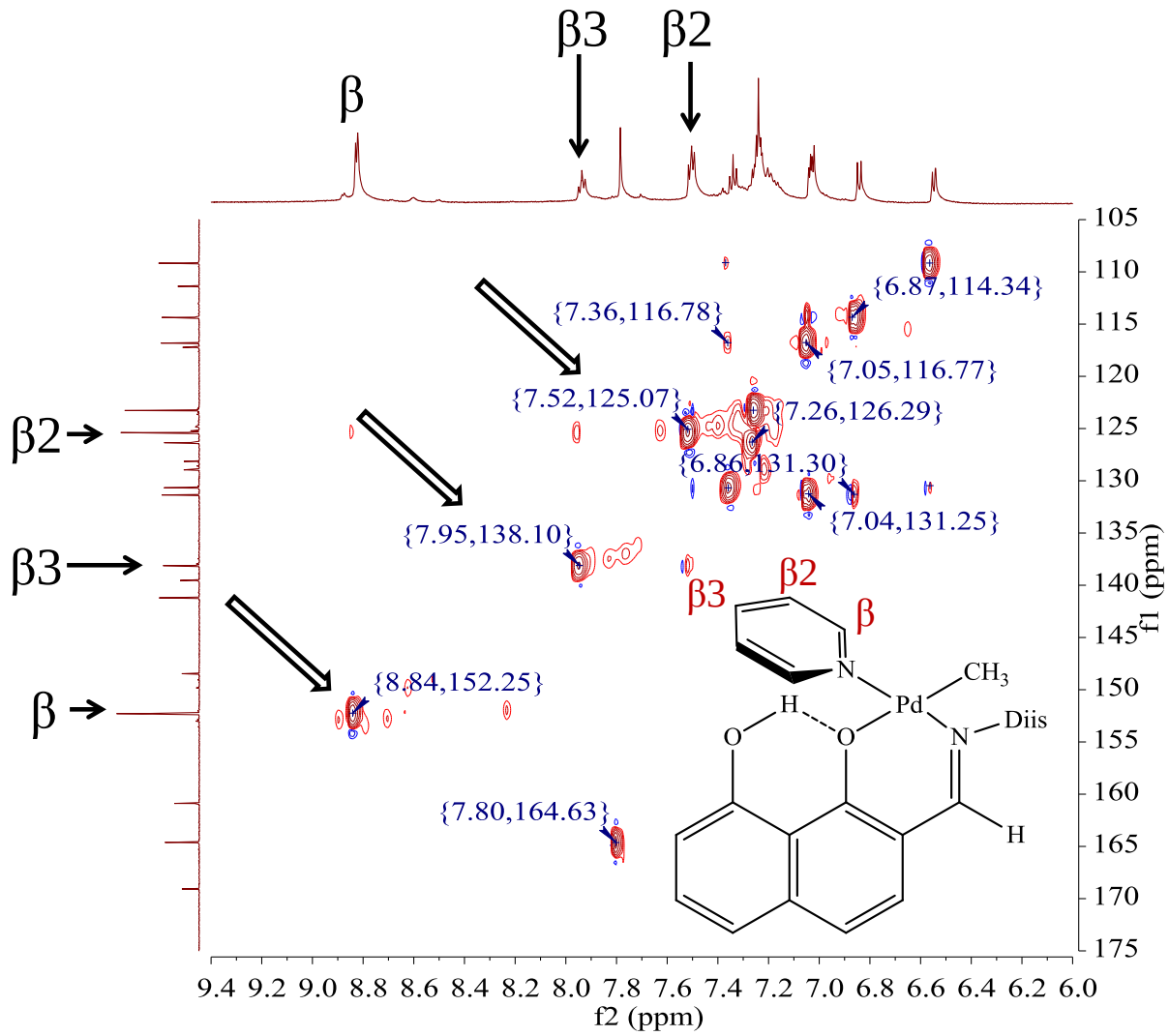

Figure A-2. 2D HSQC ^{13}C-^{1}H spectrum of Catalyst B, aromatic region. Sample conditions: CD_2Cl_2, 298 K, 600 MHz. Acquisition parameters: 8 scans, 1.5 second relaxation delay, 2 k x 0.5 k (f1 x f2) points acquired. The crosspeaks in the spectrum above indicate one bond ^{13}C-^{1}H interactions for the pyridine moiety: (8.84 ppm, 152.5 ppm), (7.95 ppm, 138.10 ppm), and (7.52 ppm, 125.07 ppm).

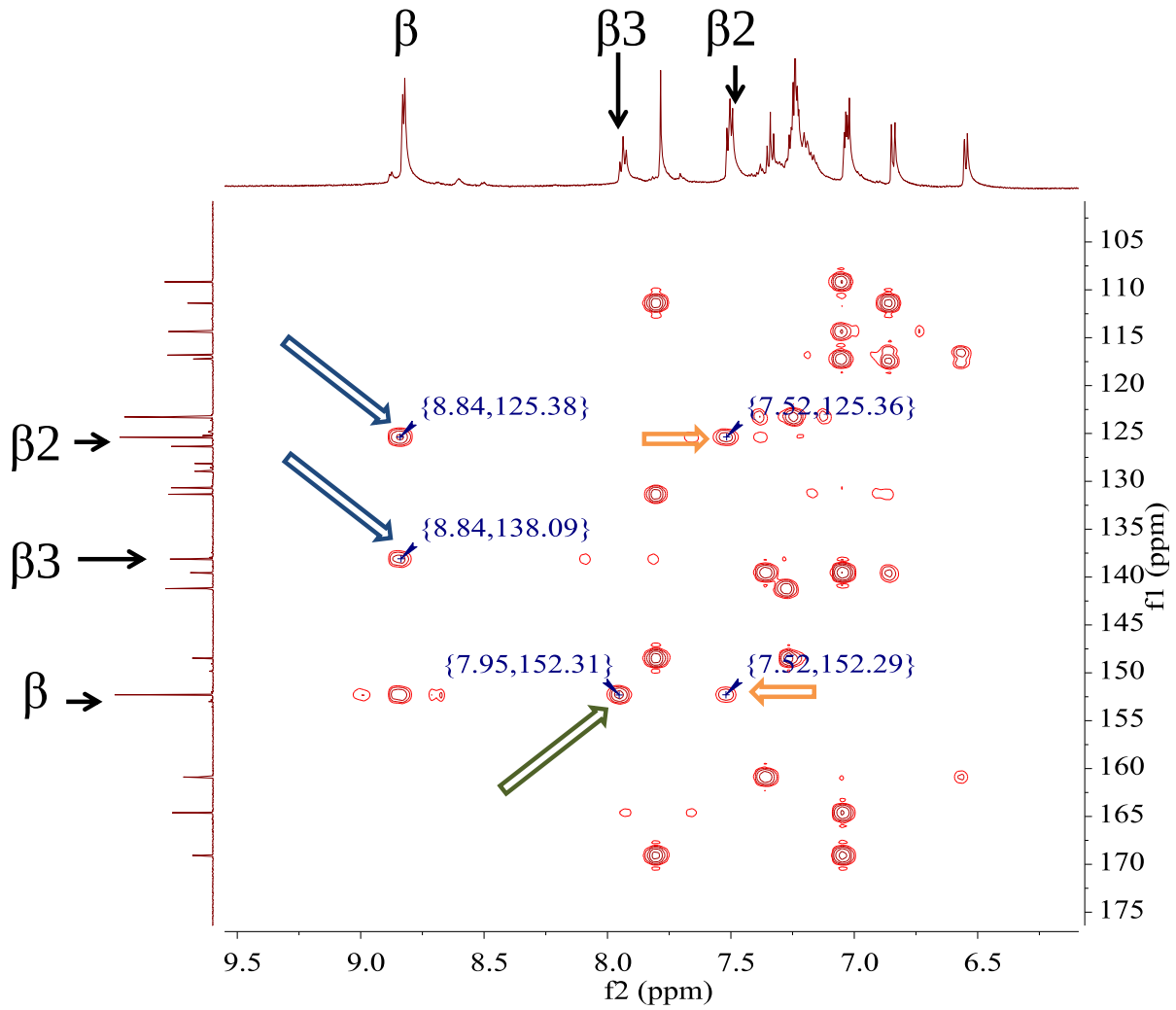

Figure A-3. 2D HMBC ^{13}C-^{1}H spectrum of Catalyst B. Sample conditions: CD_2Cl_2, 298 K, 600 MHz. Acquisition parameters: 8 scans, 1.5 second relaxation delay, 2 k x 0.5 k (f1 x f2) points acquired. Multiple bond correlations between pyridine carbons and hydrogens are indicated by arrows. Blue arrows indicate ^{13}C-^{1}H interactions of the β hydrogen (8.84 ppm); green indicates those of the β3 hydrogen (7.95 ppm); and yellow indicates those of the β2 hydrogen (7.52 ppm).

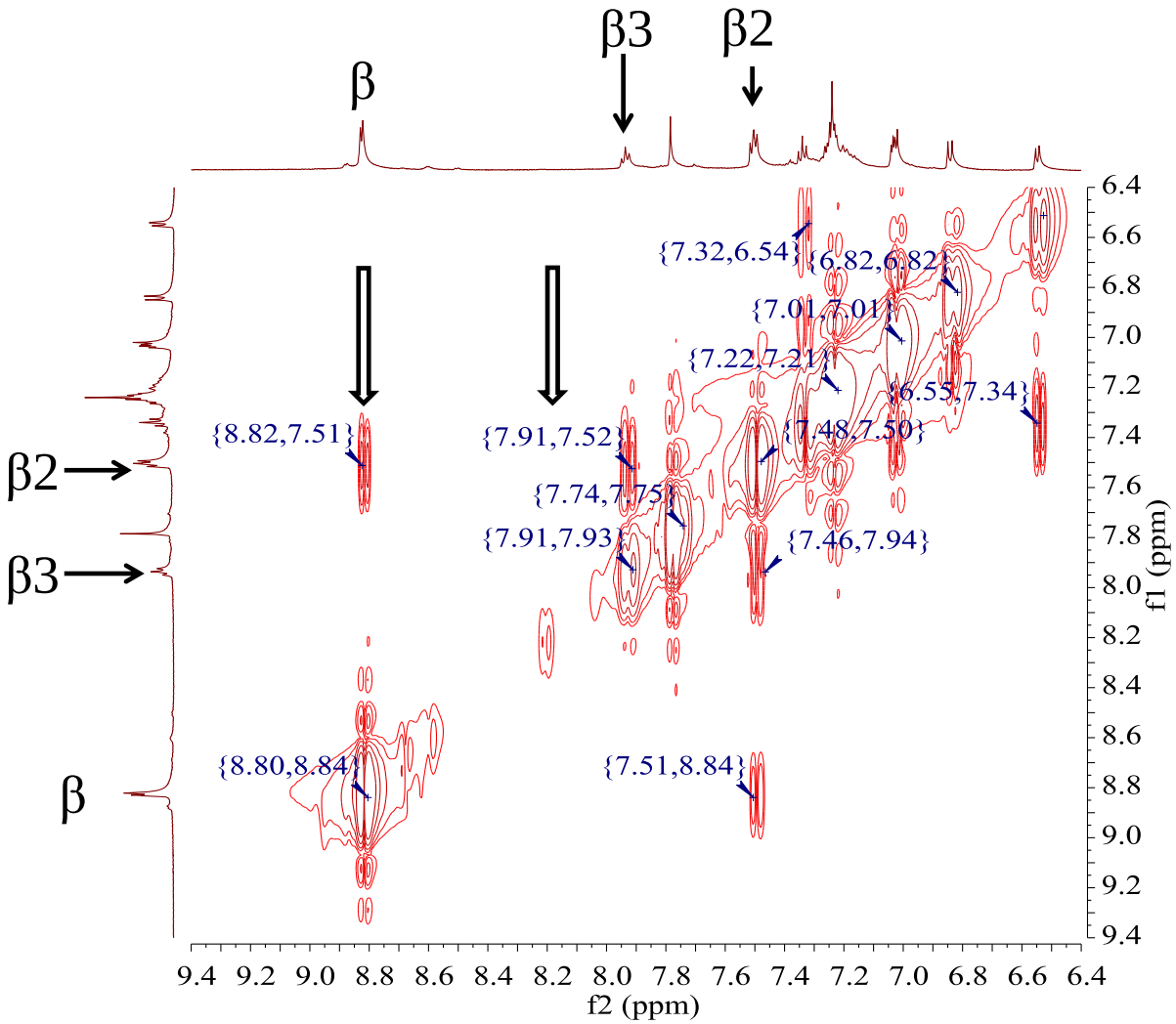

Figure A-4. 2D COSY ^{1}H-^{1}H spectrum of Catalyst B, aromatic region. Sample conditions: CD_2Cl_2, 298 K, 600 MHz. Acquisition parameters: 8 scans, 2 second relaxation delay, 1 k x 0.25 k (f1 x f2) points acquired. There are ^{1}H-^{1}H interactions between the pyridine hydrogens at (8.82 ppm, 7.51 ppm) and (7.91 ppm, 7.52 ppm).

Appendix B. NMR spectra

B.1. DOSY NMR data

Picosecond fluorescence anisotropy decay measurements of the soluble, poly-aromatic fluorophore 9,10-bis(phenylethnyl)anthracene (PEA) was measured in an active solution of Grubbs catalyst (3 mM) in presence of 0.5 M DDM dissolved in $CDCl_3$. Rotational dynamics allows one to determine changes in the local viscosity around a probe solute, correlated by the Stokes-Debye-Einstein relation

$$\tau_{rot} = \frac{\eta V_p}{k_B T} fC$$

Here η is the viscosity, V_p the volume of the probe solute, and $k_B T$ is Boltzmann's constant times the absolute temperature. The factor *f* accounts for the shape of the solute and *C* allows for possible variation of the hydrodynamic boundary conditions. Since all the experiments performed involved the same probe (PEA) at a constant temperature, any change in the rotation time is expected to be directly proportional to changes in the local viscosity. Time-resolved emission was collected at magic angle, parallel, and perpendicular polarization relative to the excitation, and simultaneously fit with the observed instrumental response function (25 ps FWHM) using an iterative re-convolution algorithm, as described in detail in ref. 24 from Chapter 2. In these fits the initial anisotropy was fixed at the value 0.38. For each of three conditions: only PEA, PEA with Grubbs catalyst, and PEA with Grubbs catalyst and DDM, six independent measurements were taken producing the average results shown in table below. Within the uncertainty of the experiment, the local viscosity does not change significantly in the presence of the catalyst or the catalytic reaction. (See Figure B-1)

Sample	Index	τ (ns)	r(t) (ps)	r_0	χ^2		Δτ (ns)	Δr(t) (ps)
PEA	A	3.351	92.53	0.38	1.298	Mean, *x* =	**3.316**	**93.395**
	B	3.601	94.00	0.38	1.096	Sample standard deviation, *s* =	0.147	0.903
	1	3.231	93.43	0.38	1.052	Sample size, *n* =	6	6
	2	3.235	94.02	0.38	1.106	Standard uncertainty, *u* =	0.060	0.368
	3	3.236	92.08	0.38	1.125	Degrees of freedom, *df* =	5	5
	4	3.240	94.31	0.38	1.026	95% *t*-value, *t* =	2.571	2.571
						95% Confidence deviation, *Cd* =	**0.155**	**0.947**
Grubbs & PEA	A	2.307	97.35	0.38	1.230	Mean, *x* =	**2.270**	**95.734**
	B	2.422	95.16	0.38	1.174	Sample standard deviation, *s* =	0.096	1.465
	1	2.203	94.21	0.38	1.217	Sample size, *n* =	5	5
	2	2.200	94.71	0.38	1.095	Standard uncertainty, *u* =	0.043	0.655
	3	2.218	97.24	0.38	1.164	Degrees of freedom, *df* =	4	4
	4	2.219	102.70	0.38	1.263	95% *t*-value, *t* =	2.776	2.776
						95% Confidence deviation, *Cd* =	**0.119**	**1.819**
RCM Substrate & PEA	A	3.371	109.80	0.38	1.506	Mean, *x* =	**3.239**	**109.500**
	B	3.485	112.40	0.38	1.060	Sample standard deviation, *s* =	0.074	0.640
	1	3.203	108.60	0.38	1.198	Sample size, *n* =	5	5
	2	3.208	109.80	0.38	1.057	Standard uncertainty, *u* =	0.033	0.286
	3	3.201	109.10	0.38	1.126	Degrees of freedom, *df* =	4	4
	4	3.214	110.20	0.38	1.107	95% *t*-value, *t* =	2.776	2.776
						95% Confidence deviation, *Cd* =	**0.092**	**0.795**

Figure B-1. Example of Rotational Diffusion Data Collected.

B.2. Additional Diffusion NMR data from the AV-3-850

B.2.1. Experimental Overview

Many sets of data were collected for the Grubbs Diffusion NMR study using the AV-3-850. While similar conclusions can be drawn from the data here as in the main text (e.g. more catalytic turnover results in a greater enhancement of diffusion), the conditions used here are different. All of the experiments are performed in tubes open to atmosphere, so the ethane formed is allowed to escape. A lower concentration of catalyst is used (generally 0.5 mM as opposed to 3 mM of Grubbs catalyst). Two sets of studies are performed here:

(1) Where the [catalyst] = 0.5 mM is held constant and the [DDM] is varied.

(2) Where the [DDM] = 1.5 M, and [catalyst] is varied.

B.2.2. Instrumentation and Experimental Conditions

Instrumentation. Several NMR instruments were used to collect the data for this study. The AV-3-850, equipped with a gradient probe, was specifically used to monitor the diffusion (D) of test and control samples. The DPX-300 and AV-360 were used to record the T1 relaxation times of the TMS and benzene spectators. TOPSPIN 2.1 was used for spectral analysis.

Sample preparation. Spectator diffusion was observed in two different sets of DDM samples: in the first set, (1) the catalyst concentration was held constant, at 0.5 mM, while [DDM] was varied; and in the second set, (2) the substrate concentration was held constant, at 1.5 M, while [catalyst] was varied. For set (1), the substrate concentrations were [DDM] = 0.5 M, 1.0 M, 1.5 M, 2.0 M, and 2.5 M, and for set (2) the catalyst concentrations were [catalyst] = 0.1 mM, 0.2 mM, 0.3 mM, 0.5 mM, and 0.75 mM. In order to formulate solutions accurately and easily, two sets of stock solutions were prepared: (i) substrate stock solutions and (ii) catalyst solutions. For (i) substrate stock solutions diethyl diallylmalonate (DDM), *d6*-benzene (C_6D_6), and tetramethylsilane (TMS) were combined. To prepare (ii) catalyst solutions, 10 mg of Grubbs' 2nd generation catalyst was dissolved in an appropriate amount of benzene. The catalyst solution (1.2 mL) was then immediately added to the DDM stock and well-shaken; the final solution of reactants always contained a 500 mM concentration of the two spectators (TMS and benzene). The solution (0.6 mL) was pipetted into an NMR tube for immediate testing. In order to prevent ethene over-pressurization, a small hole was poked in the NMR cap. Control samples – in which no reaction was on-going – were prepared in an identical fashion excepting the addition of catalyst.

DOSY NMR and kinetic studies. All NMR samples were allowed to equilibrate in the NMR for period of 15 minutes before spectra were recorded. For each sample, the diffusion constants of TMS (D_{TMS}) and C_6D_6 (D_{C6H6}) and [DDM] were recorded. In a typical experiment, D_{TMS}, D_{C6H6}, and [DDM] were all concurrently recorded by alternating diffusion and 1D pulse programs. Data was collected for two hours after equilibration. Long sampling times were required because the diffusion profile is different for each [DDM]/[catalyst] condition (See Figures B-2 and B-3). Diffusion parameters were as follows: p1 = 10.50 ms, rg = 4, O1 = 1300 Hz, sw = 10 ppm, aq = 2.00 s, D1 = 3.97 s, steps = 16, P30 (δ) = 1.00 ms, D20 (Δ) = 20.00 ms, ds = 2, ns = 4, total time = 6 min 36 seconds. Depending on the [DDM], the 90° pulse (p1) selected changes slightly. Conveniently, the 90° pulse (p1) selected was usually appropriate for both TMS and C_6H_6 peaks. For monitoring [DDM], 1D spectra were recorded using the following parameters: ns = 8, ns = 2, D1 = 6, aq = 2, total time = 1 min 19 sec. Both spectator peaks are sufficiently distanced from product/reactant peaks in the spectrum, ensuring that the diffusion constants can be extracted easily and that the values are accurate ($Si(CH_3)_4$ = 0 ppm, C_6H_6 = 6.0 ppm). Test and control samples were run in triplicate.

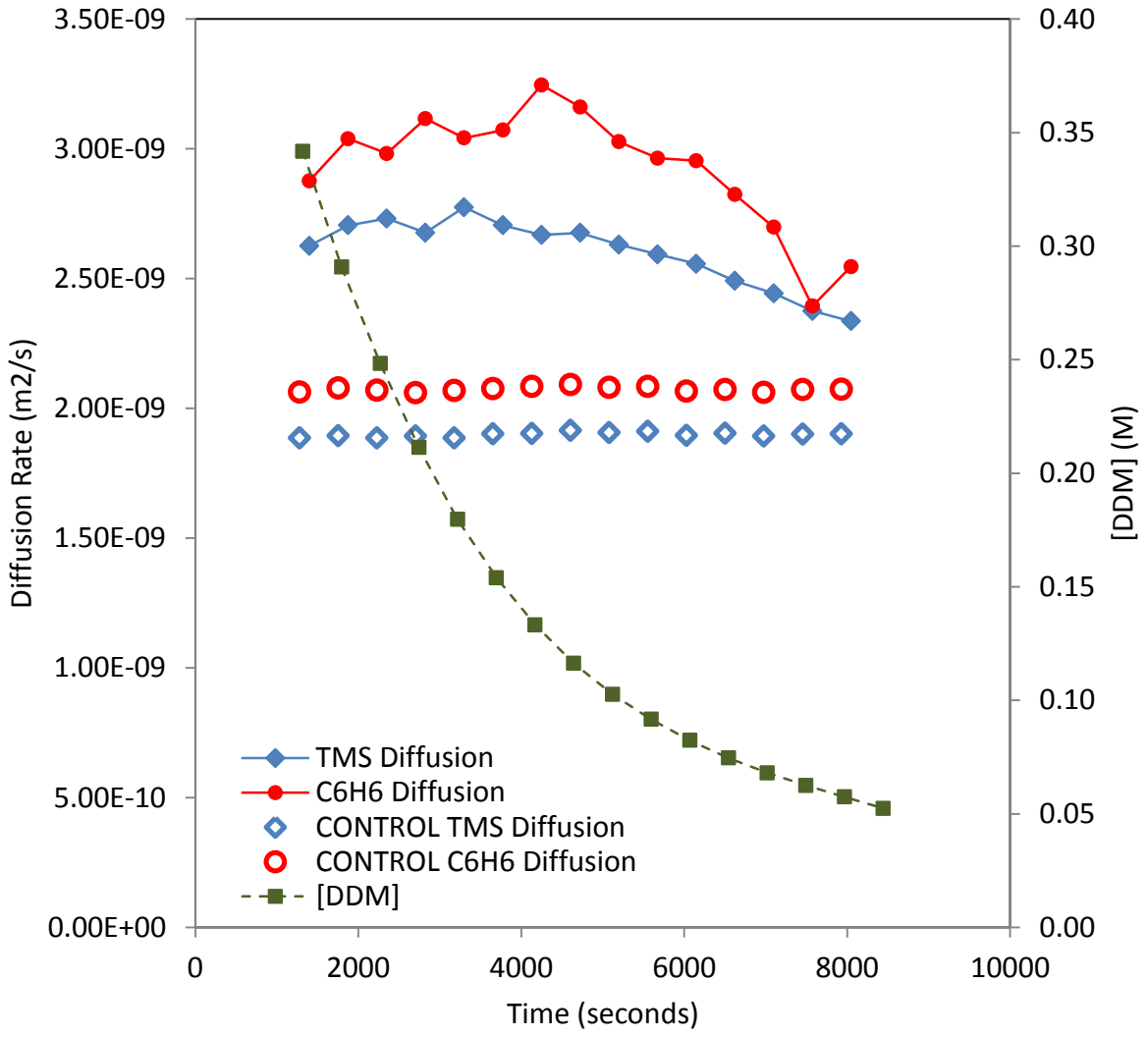

Figure B-2. Diffusion of TMS and C_6H_6 in during a RCM reaction, [DDM] = 0.5 M. The diffusion of TMS (500 mM) and C_6H_6 (500 mM) are observed in a solution of 0.5 M DDM/C_6D_6 at 0.5 mM catalyst loading.

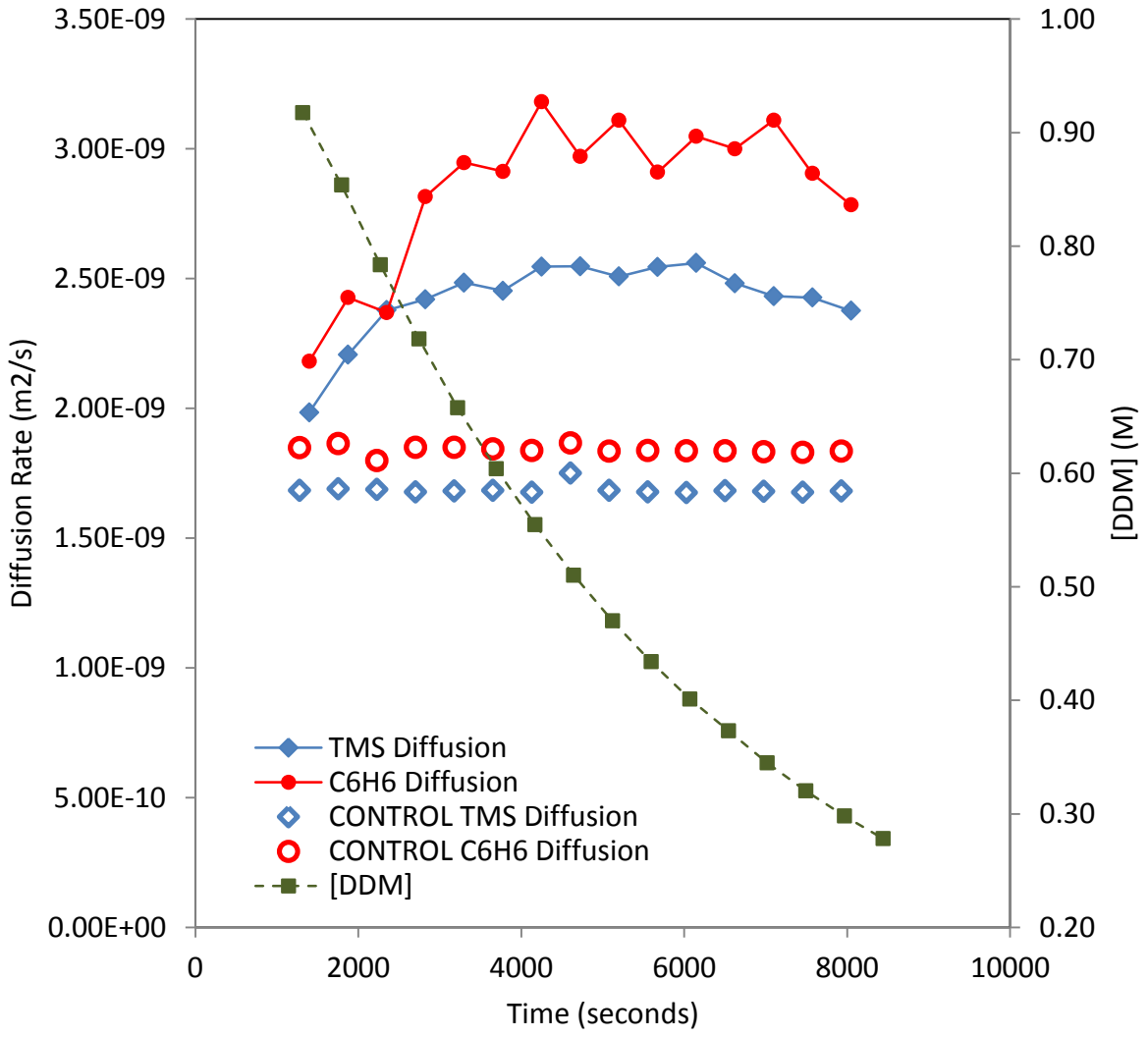

Figure B-3. Diffusion of TMS and C_6H_6 in during a RCM reaction, [DDM] = 1.0 M. The diffusion of TMS (500 mM) and C_6H_6 (500 mM) are observed in a solution of 1.0 M DDM/C_6D_6 at 0.5 mM catalyst loading.

B.2.3. Results and Discussion

To analyze how the substrate turnover by molecular catalysts influences the dynamics of the surroundings, the diffusion of TMS and benzene – both spectators molecules – was measured in a C_6D_6 suspension of Grubbs' catalyst. We employed DOSY-NMR to measure the diffusion coefficients of the tracers over a range of reaction rates by changing both the substrate and catalyst concentrations. Using the aforementioned conditions, excellent reproducibility in results are achieved, as seen in Figure B-4 and Tables B-2 & B-3 of three overlapped, individual trials. The diffusion values denoted in Tables B-2 & B-3 are the averaged numbers extracted at the times which the diffusion plateaus as seen in Figures B-2 & B-3.

In order to compare samples which have different [DDM], the rate and the viscosity of each sample is taken into account (see Figure B-5 and Table B-1, respectively, for values). The viscosity-corrected values are displayed in Figure B-6. In Figure B-7, the diffusion of samples with varied amounts of catalyst (and therefore different rates) is compared. In either case, the relationship between reaction rate and diffusion is monotonic.

The effect of ethylene on diffusion was also investigated (Figure B-8); the presence of ethylene itself has no effect on the diffusion of the tracers in solution.

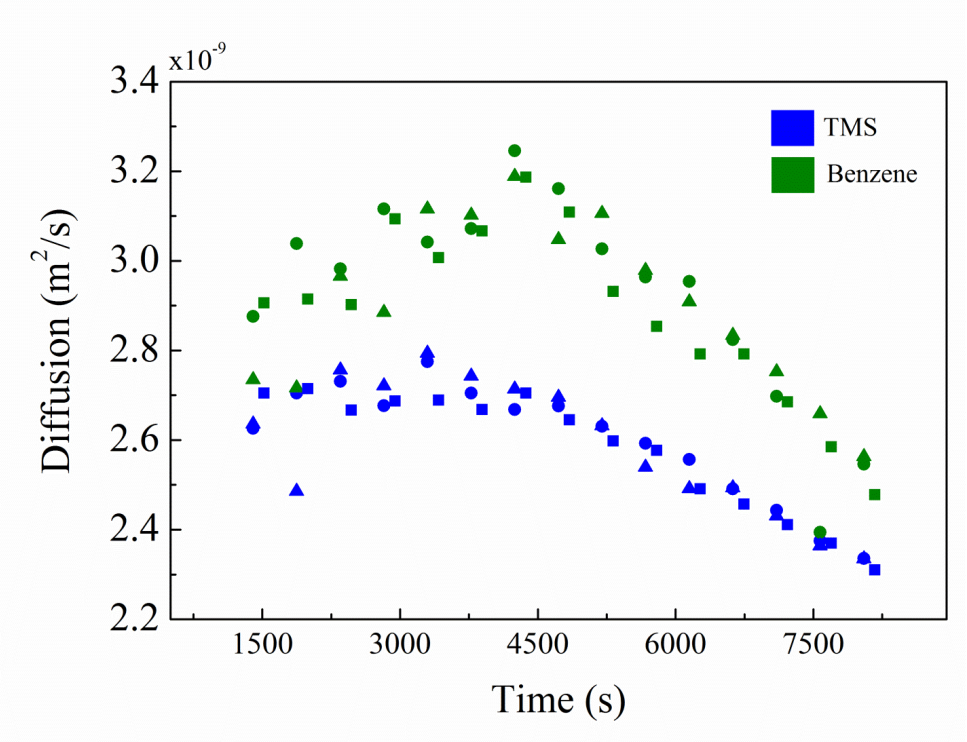

Figure B-4. **Time dependent change in the diffusion of the tracers (TMS and benzene) in a solution of 0.5 M DDM and 0.5 mM Grubbs' catalyst.** The results are consistent as can be observed from three independent measurements shown in the figure. The rates are measured from the rate of DDM consumption obtained from the 1D ^{1}H-NMR data, for a particular period of time after the start of the reaction.

Table B-1. D_{TMS} and D_{C6H6} vs. changing [DDM]. All samples contained 0.5 mM Grubbs' catalyst, 500 mM TMS, 500 mM C_6H_6, and C_6D_6. Substrate concentrations were varied as such: [DDM] = 0.5M, 1.0M, 1.5M, 2.0M, 3.0M.

TMS							
Entry	[DDM] (M)	D_{TMS} (m^2/s)	SD	Control D (m^2/s)	Control SD	ΔD (%)	absolute ΔD (m^2/s)
1	0.50	1.90E-09	8.91E-12	2.71E-09	4.95E-11	43%	8.11E-10
2	1.00	1.69E-09	1.83E-11	2.50E-09	3.95E-11	48%	8.10E-10
3	1.50	1.45E-09	4.79E-12	2.07E-09	1.05E-10	42%	6.12E-10
4	2.00	1.17E-09	5.04E-12	1.95E-09	1.14E-10	66%	7.76E-10
5	3.00	7.84E-10	5.66E-12	1.15E-09	2.32E-11	46%	3.63E-10
C6H6							
Entry	[DDM] (M)	D_{C6H6} (m^2/s)	SD	Control D (m^2/s)	Control SD	ΔD (%)	absolute ΔD (m^2/s)
6	0.50	2.07E-09	9.21E-12	3.00E-09	1.24E-10	45%	9.31E-10
7	1.00	1.84E-09	1.57E-11	2.99E-09	9.50E-11	63%	1.15E-09
8	1.50	1.61E-09	7.89E-12	2.65E-09	3.73E-11	65%	1.04E-09
9	2.00	1.32E-09	1.11E-11	2.61E-09	3.64E-11	98%	1.29E-09
10	3.00	9.27E-10	7.83E-12	1.52E-09	5.08E-11	63%	5.88E-10

Table B-2. D_{TMS} and D_{C6H6} vs. changing [DDM]. All samples contained 1.5 mM DDM, 500 mM TMS, 500 mM C_6H_6, and C_6D_6. Catalyst concentrations were varied as such: [catalyst] = 0.1 mM, 0.2 mM, 0.3 mM, 0.5 mM, 0.75 mM.

		TMS				C_6H_6			
Entry	[Grubbs] (mM)	D_{TMS} (m^2/s)	SD	ΔD (%)	absolute ΔD (m^2/s)	D_{C6H6} (m^2/s)	SD	ΔD (%)	absolute ΔD (m^2/s)
1	0	1.45E-09	4.79E-12	NA	NA	1.61E-09	7.89E-12	NA	NA
2	0.10	1.55E-09	2.47E-11	6%	9.40E-11	1.72E-09	2.47E-11	7%	1.10E-10
3	0.20	1.93E-09	3.08E-11	33%	4.79E-10	2.26E-09	4.73E-11	41%	6.53E-10
4	0.30	2.13E-09	2.32E-11	46%	6.72E-10	2.57E-09	1.74E-10	60%	9.59E-10
5	0.50	2.18E-09	5.64E-11	50%	7.23E-10	2.69E-09	1.07E-10	67%	1.08E-09
6	0.75	2.09E-09	5.09E-11	44%	6.41E-10	2.90E-09	7.58E-11	80%	1.29E-09

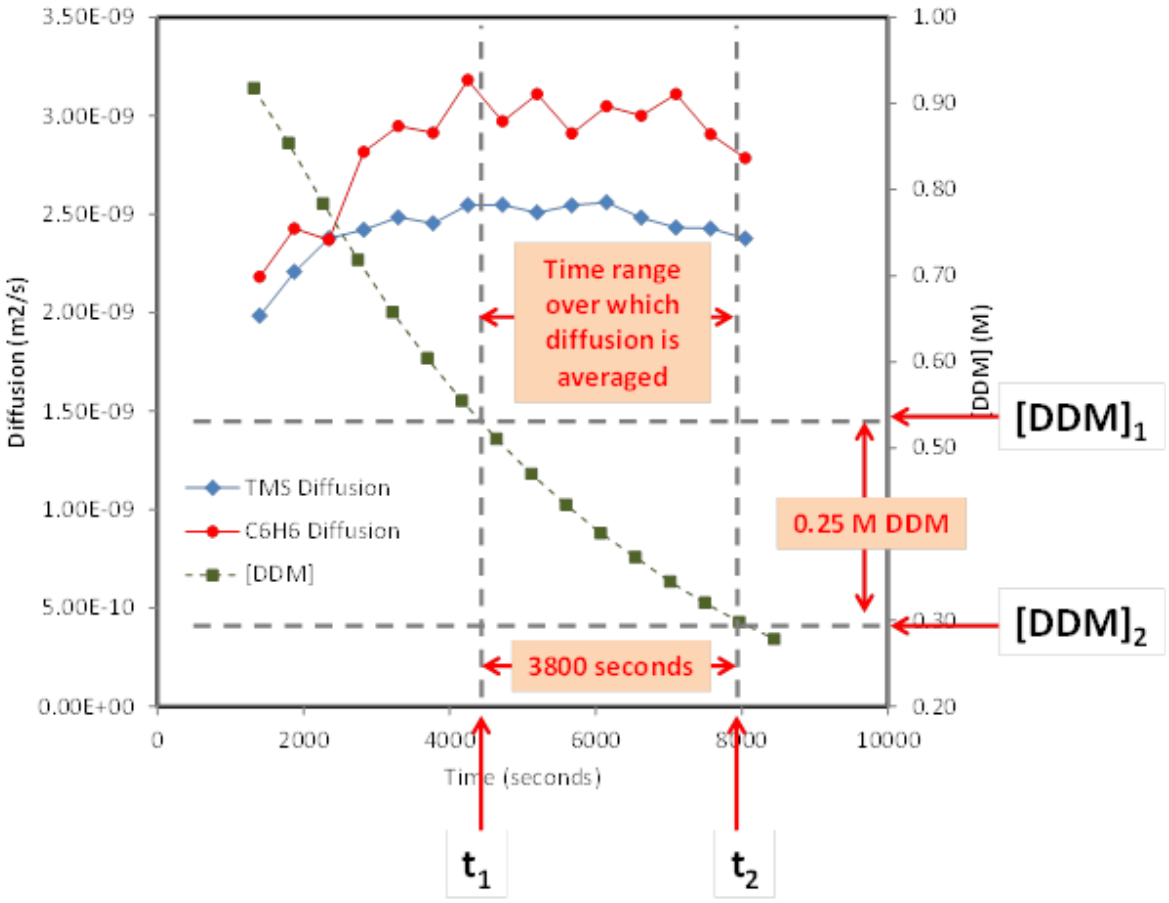

Figure B-5. Example figure of determining average reaction rate. Based on the profile of the diffusion speeds of the tracers, we select a range of time (t_1 to t_2) over which we calculate an average rate of the reaction. The values marked are: t_1 (initial time), t_2 (end time), [DDM]1 (substrate concentration at t_1), and $[DDM]_2$ (concentration time at t_2).

Rate is calculated as such:

$$rate = \frac{[DDM]_2 - [DDM]_1}{[catalyst] \cdot (t_2 - t_1)}$$

Rate is expressed in these units:

$$rate = \left(\frac{M\ substrate}{M\ catalyst \cdot \text{time}}\right)$$

$$D_{ave} = \frac{\sum_{t1}^{t2} D_{tracer}}{number\ of\ D_{tracer}\ entries}$$

Table B-3. Viscosity of solutions containing different amounts of [DDM].

[DDM](M)	η (Pa.s)
0.5	0.000620887
1	0.000856919
1.5	0.001085759
2	0.001295714
3	0.002225714
4.1 (Only DDM)	0.004948571

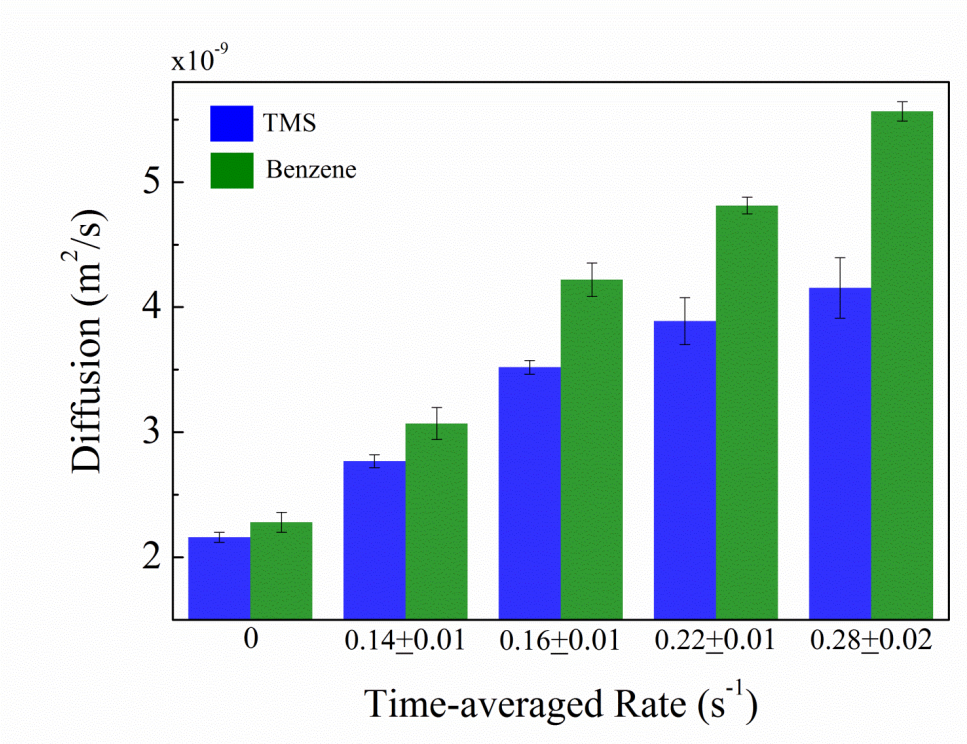

Figure B-6. Diffusion coefficients of TMS and benzene measured in a solution containing 0.5 mM Grubbs' catalyst and varied amount of DDM. The diffusion values are corrected for viscosity. With the increase in total reaction rate, the diffusion of the tracers enhanced significantly showing increased momentum transfer from the catalysts to the surroundings. Units of reaction rate are moles of substrate consumed per mole of the catalyst, per second.

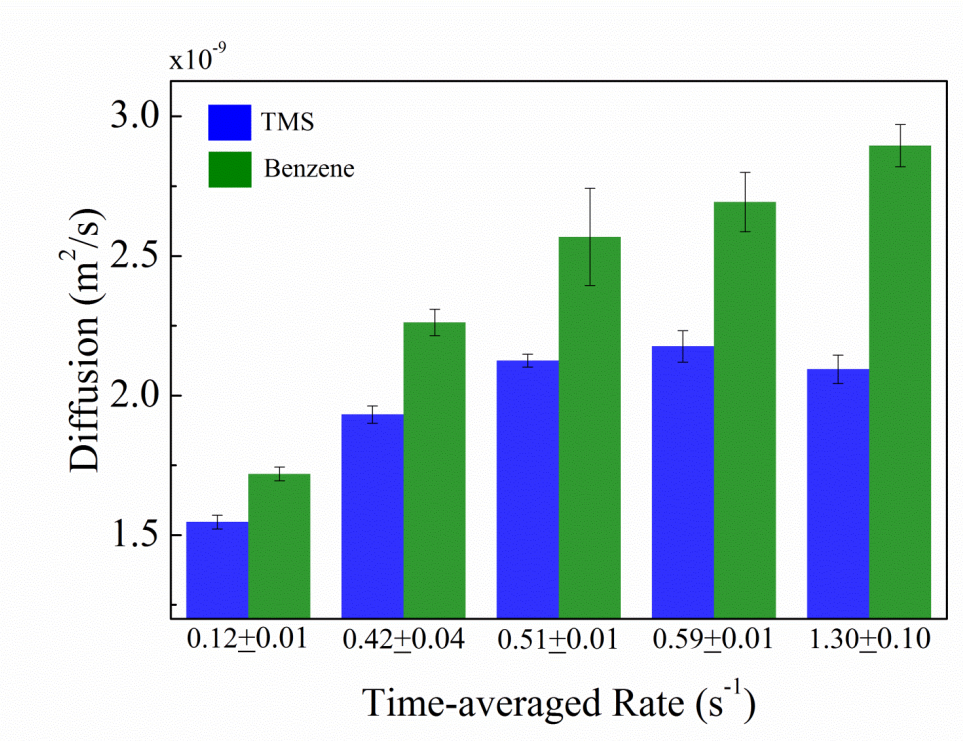

Figure B-7. Diffusion of tracers at different catalyst concentrations, keeping DDM concentration fixed at 1.5 M. With the increase in total reaction rate, the diffusion of the tracers increased significantly showing substantial momentum transfer from the catalytic sites to the surroundings.

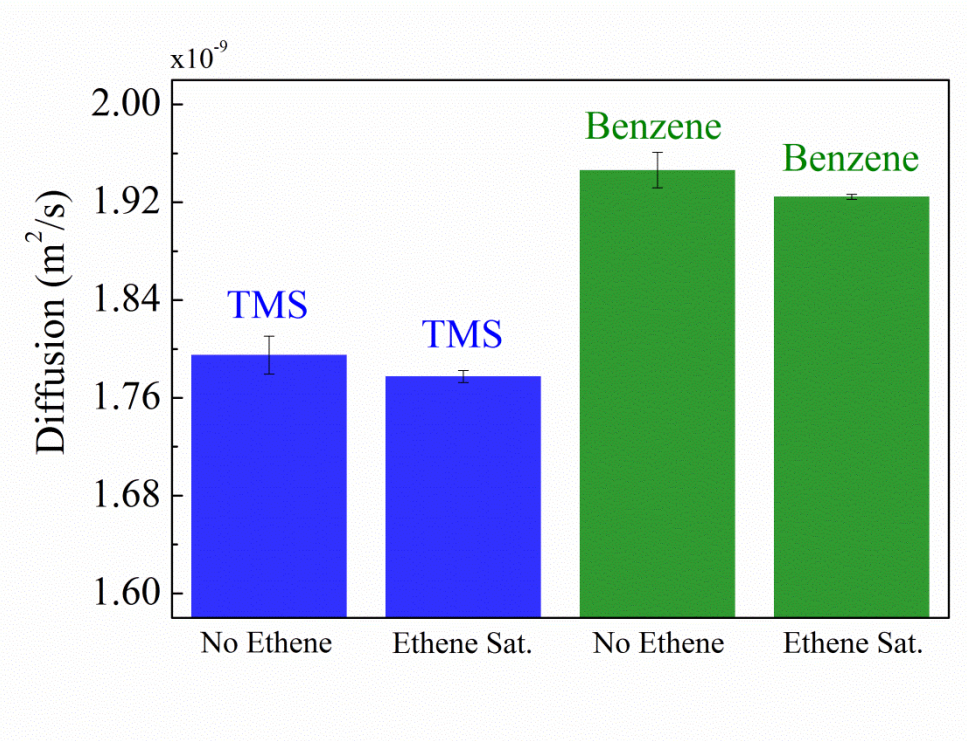

Figure B-8. **Tracer diffusion in measured in normal and ethylene saturated solvents (deuterated benzene).** The data clearly show the negligible effect of ethylene dissolved in the solvent over the diffusion of the tracers. The viscosity of the solvent changed negligibly in the presence of ethylene.

VITA

Frances Pong graduated from Wellesley College in 2005 with a B.A. in Chemistry. While at Wellesley under the guidance of Professor Nolan Flynn, she synthesized and extensively studied the behavior of *N*-isopropylacrylamide hydrogels embedded with in situ gold nanoparticles. Immediately after graduating, she joined Cabot Corporation as a research associate and worked on developing shelf-stable aqueous and solvent particle dispersions for high end applications such as UV inks and displays. In 2009, she joined the Chemistry Ph.D. program at Pennsylvania State University under the supervision of Professor Ayusman Sen. Her research interests include organometallic polymerization catalysts, biomass conversion, and studying the behavior of synthetic and biological nanomotors/nanopumps. In addition to her research responsibilities, Frances also serves as the Sen lab's group manager and as a member of the Chemistry Department's safety council, which discusses and communicates safety policy.